SAPIENZA

University of Rome

Department of Molecular Medicine

Mechanisms of response of Mesothelial Cells to viral infections: role of epigenetic HDAC1/2 regulation

FLAVIA TRIONFETTI

XXXV cycle

PhD PROGRAMME IN LIFE SCIENCES

TUTOR:

Prof. Raffaele Strippoli

COORDINATOR:

Prof. Francesca Cutruzzolà

'Io sono tra quelli che pensano che la scienza abbia una grande bellezza. Uno scienziato nel suo laboratorio non è solo un tecnico: è anche un bambino posto di fronte a fenomeni naturali che lo impressionano come un racconto di fiabe'

'Niente nella vita va temuto, dev'essere solamente compreso. Ora è tempo di comprendere di più, così possiamo temere di meno'

Marie Curie

INDEX

ABSTRACT

The main focus of this doctoral thesis is the analysis of the response of mesothelial cells (MCs) to viral infections. As a cellular model we used first primary MCs from patients undergoing peritoneal dialysis (PD). In mammals, the recognition of pathogen infection occurs trough pathogen recognition receptors (PRRs), and among them, Toll-like receptor (TLR) family plays an important role. TLR3 is one of the TLRs associated to the recognition of viral infection and its role in MC plasticity has not been fully clarified yet.

Here, we first analysed the TLRs pattern expression in primary MCs from dialyzed patients. We found that they express a specific subset composed by TRL1, TLR2, TLR3 and TLR5. We then, characterized the effects of TLR3 stimulation with Poly(I:C). We observed changes in MC cellular plasticity indicating the occurrence of bona fide mesothelial to mesenchymal transition (MMT), characterized by the acquisition of a spindle-like morphology, loss of epithelial markers and induction of mesenchymal markers, including the EMT master gene Snail. Moreover, Poly(I:C) stimulation promoted the induction of a pro-inflammatory response as shown by secretion of inflammatory cytokines and chemokines such as IL-1β, TNFα, IL-6, CXCL8 and CXCL10.

Epigenetic reprogramming is a potentially relevant mechanism governing these changes in MC cell plasticity. Here, we analysed the impact of histone deacetylase (HDAC) inhibition using MS-275, an HDAC1/2 pharmacological inhibitor.

Quantitative mass spectrometry analysis revealed several pathways altered by MS-275 treatment, including mesenchymal genes, actin cytoskeleton, extracellular matrix, and type-I interferon response regulation. Results obtained by proteomic analysis were then validated by Western blot analysis. Thus, we confirmed the role of MS-275 in promoting the expression of epithelial markers and in the downregulation of the IFNβ-driven response in Poly(I:C) stimulated MCs, which was linked to STAT1 tyrosine phosphorylation.

To directly analyse the effects of viral infections on MCs, we then evaluated the response of a pleura mesothelial cell line, MeT5A cells, to SARS-CoV-2 infection. First, we found that MCs express the specific receptors/coreceptors ACE2, TMPRSS2, NRP1 and ADAM17. Moreover, MeT5A were found responsive to SARS-CoV-2 infection. MeT5A cells reacted to viral stimulation through a specific cytokine expression profile characterized by the predominance of an anti-inflammatory over a pro-inflammatory phenotype.

Next, we evaluated the role of HDAC1/2 inhibition in SARS-CoV-2 infection. Treatment with MS-275 favoured SARS-CoV-2 infection and productive replication in MeT5A cells. We provided two different mechanisms by which HDAC1/2 inhibition can cause viral spreading in MCs. We found that MS-275 treatment both induced ACE2 and TMPPRSS2 expression and impaired interferon type-I response to SARS-CoV-2 infection.

Mechanistically, treatment with MS-275 increased the H3 histone acetylation at ACE2 and TMPRSS2 promoter regions.

Last, to find direct evidence of COVID-19 infection in mesothelium, we analysed 4 pleural autoptic samples of COVID-19 patients comparing them with 4 non COVID-

19 -infected patients. Immunohistochemical analysis of samples from COVID-19 patients demonstrated a specific alteration of pleura characterized by disruption of the MC monolayer and invasion of the sub-mesothelial stroma by spindle-like MCs, but not evidence of direct MC infection by SARS-CoV-2.

Overall, in this study we provided a characterization of changes in MC plasticity upon exposure to virus-related stimuli. Moreover, our data raise a concern on the use of class I HDACs pharmacological inhibitors such as MS-275 and derivatives in immunocompromised patients since they can potentiate SARS-CoV-2 infectivity.

INTRODUCTION

1. The peritoneal membrane

Peritoneum is a serosal membrane that forms the lining of the abdominal cavity (*1, 6, 7*). Peritoneum is generally less than 1 mm thick with a coverage surface area of 1-2 m^2 in adults. Peritoneum originates during the gastrulation process from mesoderm (*8-10*), and it is the largest of the three serosal cavities of the human body (peritoneum, pleura and pericardium) (*11-13*).
Peritoneum is composed of two different layers: parietal and visceral layer. Parietal peritoneum lines the internal surface of abdominal wall, while visceral peritoneum invaginates to cover the majority of the abdominal viscera. The two layers form a virtual space called peritoneal cavity, visible on cross section imaging when filled with abnormal fluid or gas (*4*). (**Fig1**)
The peritoneal cavity is filled by 50-100 ml volume of interstitial fluid in adults. This peritoneum fluid has lubrification properties and facilitates peristaltic movements.
The peritoneal fluid has a pH of 7.5–8.0 and is composed by water, solutes, electrolytes, proteins, antimicrobial peptides and antibodies (*7-11, 13*). The cellular fraction is composed mainly of recirculating leukocytes and detached mesothelial cells (see below).

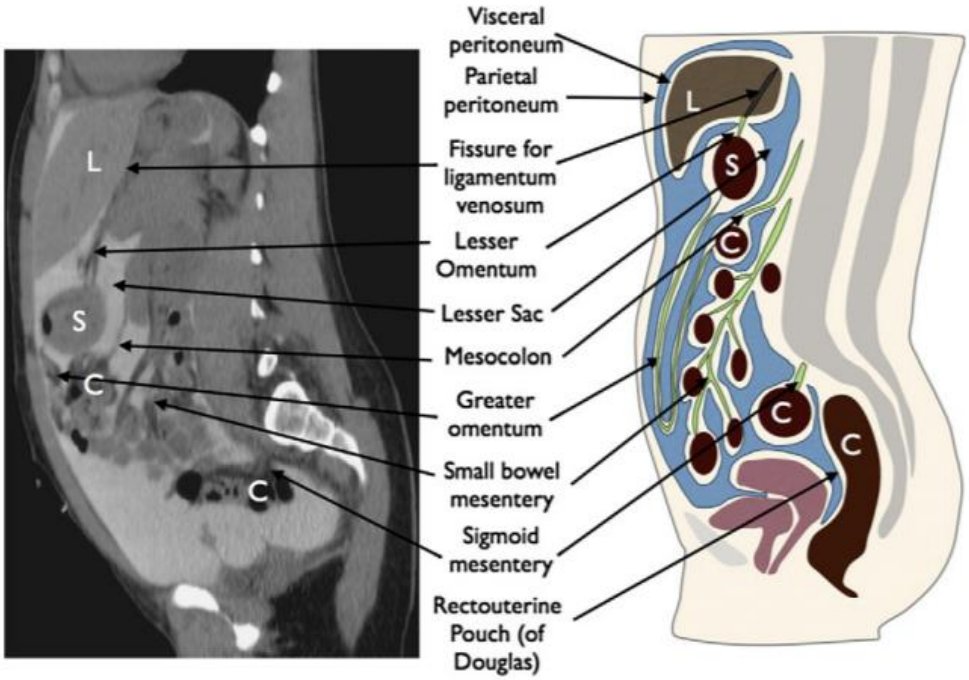

Figure 1 Sagittal computed tomography peritoneogram with contrast medium correlated with schematic diagram resuming the peritoneal cavity. C, colon; S, stomach; L, liver. Adapter from R. R. Patel & Planche (*4*).

1.1 Cellular components: mesothelial cells and other cellular components

The **peritoneal membrane** is composed by a continuous monolayer of mesothelial cells (MCs), placed upon a basal lamina, that lines a submesothelial zone composed by connective tissue (*13, 14*). The submesothelial region, also called submesothelial compact zone is formed by bundles of Collagen fibers and other extracellular matrix (ECM) proteins with few fibroblasts, mast cells, macrophages, vessels and a dense network of capillaries (*5, 6*). (**Fig 2**)

The whole **mesothelium** is formed by ~ 1 x 10^9 of flattened MCs, with around 25 μm in diameter.

MCs originate from mesoderm during the gastrulation, and their differentiation is controlled by the transcription factor Wilms Tumor1(WT1), which is commonly used for lineage tracing experiments (*15-17*). Despite their mesodermal origin, MCs have a cobblestone-like morphology and actually coexpress in basal conditions epithelial and mesenchymal markers (*3, 18, 19*).

MCs express tight and adherent junction-related molecules such as ZO-1, Occludin, Claudins and E-cadherin, which is expressed both in plasma membrane and in cytoplasm (*20*). Moreover, these cells express epithelial intermediate filament proteins such as Cytokeratins (8–18) that play an important role in maintaining cellular structural integrity. At the same time, MCs constitutively express also mesenchymal intermediate filaments such as Vimentin and Desmin (*3, 21, 22*). MCs have a system of vesicles and vacuoles used for micropinocytosis, but also multivesicular bodies and large vacuoles can be found (*10, 22*). MCs apical surface is covered with microvilli and sporadic cilia; physiological and pathological condition can change number and shape of microvilli (*22-24*). MCs secrete various molecules forming a film named Glycocalyx, composed of Lipoproteins, Phospholipids (such as Phosphatidylcholine) and Glycosaminoglycans, predominantly Hyaluronan (HA) (*25*), that can combine with proteins (Proteoglycans) and with lipids (Glycolipids). Glycocalyx production facilitate the movements between the visceral and parietal layers (*6*). Moreover, production of cytokines and chemokines by MCs regulate tissue homeostasis as well as leukocyte trafficking and immune responses (*1, 26*).

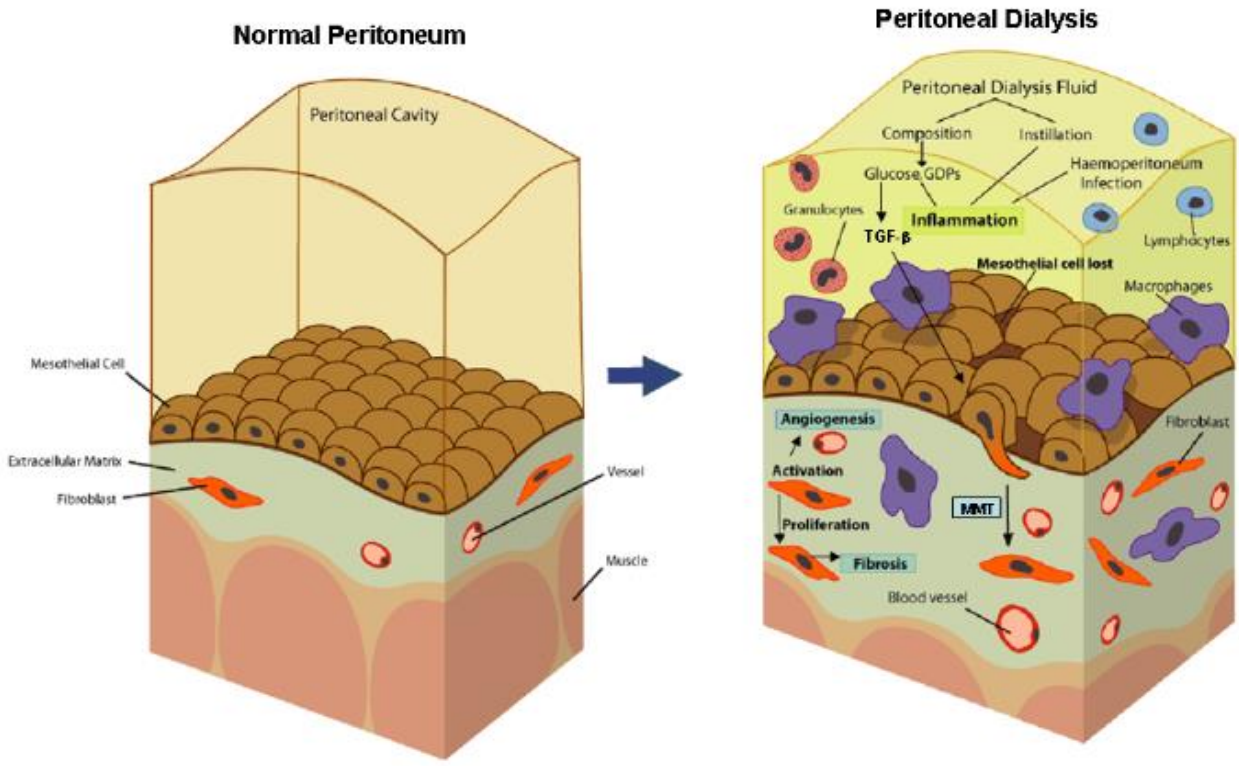

Figure 2 Schematic illustration of normal peritoneum vs dialyzed peritoneum. Right image shows a normal peritoneun without fibrosis, angiogenesis or MMT (3D image). Left image shows a PD peritoneum with MCs exposed to PD fluids. Both glucose (GDPs and AGEs) from Aguilera et al (*27*)

The structural integrity of mesothelium depends on cell-cell and cell-ECM interactions (*10, 11, 14, 22, 24*).
Tight and adherent junctions, as well as gap junctions and desmosomes allow MCs to directly communicate to each other, while interaction and communication between cell and ECM depends on focal adhesion and hemidesmosome formation. (**Fig3**)
Proteins that compose **tight junctions** are transmembrane proteins (Occludin, Claudins, Tricellulin and Junctional Adhesion Molecules (JAM)); cytoplasmatic proteins Zonula Occludens 1/3 (ZO-1/3), that bind Actin cytoskeleton (*28-31*). Tight junctions have a role in polarity maintenance and mediate water, ions and solute diffusion through peritoneum (*22, 31, 32*).
Adherens junctions are composed of the Nectin-Afadin complex and the classical E-Cadherin-Catenin complex (*33*). E-cadherin is a transmembrane protein; in extracellular space it interacts with other Cadherins, while in the intracellular space it binds p120-catenin, β-catenin and α-catenin, linking them Actin cytoskeleton (*30, 34-36*).
Adherens junctions have a role in cells contacts formation and maintenance, intracellular signals transfer, transcriptional regulation and cytoskeleton organization (*33, 35, 36*).
Gap junctions have a channel shape. They are composed by transmembrane proteins, which connect the cytoplasm of two adjacent MCs and allow the diffusion of molecules and ions (*37*).

Desmosomes form a "patch" between the lateral MC membranes on opposite cells and bind intermediate filaments to the plasma membrane (*30*).

Focal Adhesions are multiprotein structures that form the link between intracellular actin cytoskeleton and the ECM. Focal adhesion principal components are αβ Integrin heterodimers which is a superfamily of cell adhesion receptors that recognize ECM and cell-surface ligands (*38, 39*) (see below). Integrins can be activated from the extracellular space by multivalent ligands, such as ECM components and cells surface specific ligands (outside-in signaling) or from cytosol by the regulated binding of proteins to the cytoplasmic tails (inside-out signaling)(*40*). In either case. their activation triggers focal adhesion formation by aggregation and recruiting the structural proteins, such as Talin, Vinculin, α-Actinin and Zyxin, which link other focal adhesion proteins and actin cytoskeleton. This process regulates actin cytoskeleton polymerization and stress fibers formation (*41, 42*).

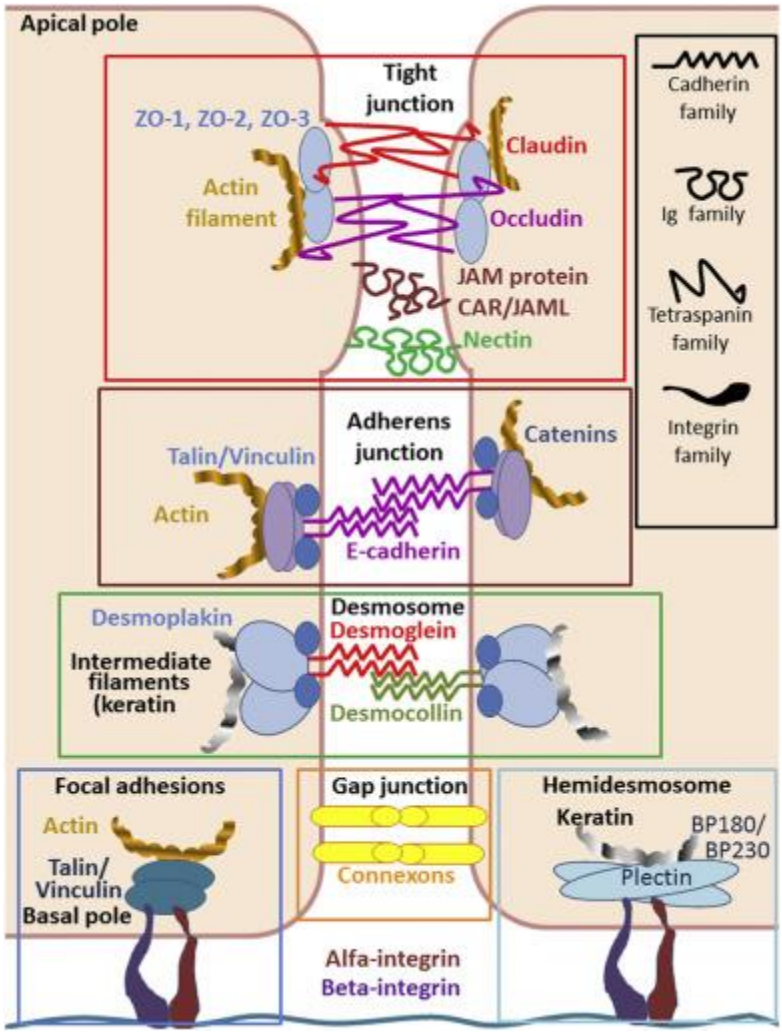

Figure 3 Schematic representation of the principal cell-cell junctions (Tight junction, Adherens junctions, Desmosoms, and Gap junctions). Adapted from Shilova et al (*2*).

1.2 Functions of the peritoneum

1.2.1 Water and solute transport

The transport of solutes and water between the plasma contained in the peritoneal capillaries and the fluid in the peritoneal cavity faces three different barriers: a) the capillary endothelium, b) the peritoneal interstitial space, and c) the mesothelium.

a) The capillary wall appears to be the major resistance site, limiting solute and water exchange. The capillarity endothelium can be functionally described by a three-pore model: i) large pores determine the crossing of macromolecules (proteins and immunoglobulins); ii) small pores are crossed by half of the removed water and by low molecular weight solutes (urea and creatinine); iii) ultrasmall pores, corresponding to aquaporin-1 (AQP1), allow the water transport (*5, 43*).
b) The interstitium constitutes the peritoneal barrier and can modify the transport of solutes.
c) The mesothelium operates as a semipermeable membrane involved in the fluid, particulates, solutes and cell transport through the serosal cavities *via* pinocytic vesicles, intracellular junctions and stomata (cavities at the junction between MC) (*10, 22, 44*). The luminal surface of MCs is covered by an elevate number of microvilli that increases the surface area for the solutes transport and absorption (*22, 24*). Furthermore, the glycocalyx can bind fluids, mediating adsorption (*22*)(**Fig 4**).

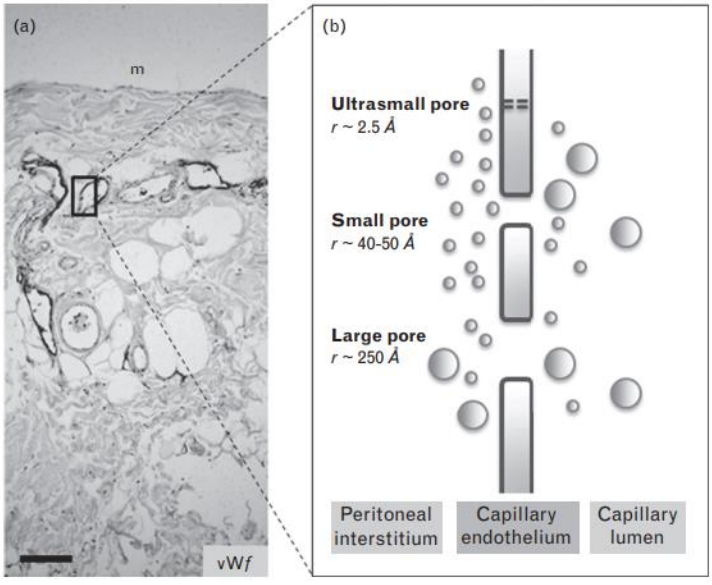

Figure 4 (a) Cross-section of the human parietal peritoneum stained for the von Willebrand factor (vWf). m, mesothelium; bar, 100 mm. (b) Structure of the peritoneal membrane and the three-pore model. A˚, angstrom (1010 m); r, functional radius. Adapted from Morelle et al (*5*)

1.2.2 Peritoneal Dialysis (PD)

Dialysis is a process allowing to remove from the blood excess of fluid, solutes, toxins, wastes and end-products of nitrogen metabolism (urea, creatinine, uric acid) and to replace bicarbonate deficit, when kidneys lose their capacity to perform these activities (*45*). Dialysis is mediated by the passing of different molecules in solution through of a semipermeable membrane along an electrochemical concentration gradient (*46*). Dialysis treatments are used in end-stage renal disease (ESRD) patients as renal replacement therapies (RRT) and consist in hemodialysis (HD) and peritoneal dialysis (PD).

During Hemodialysis, blood flows in a extracorporeal circuit across a semipermeable synthetic membrane that remove small solute, toxins and water (*47*).

During PD the peritoneum is used as a semipermeable membrane to transfer extra fluids and waste products from the blood to the dialysate (*5*). PD is preceded by the implantation of a permanent plastic catheter on the abdominal cavity of the patient. The dialysis solution (PD solution composition will be discussed below) is contained in a plastic bag. It can be transferred through catheter into abdomen. Importantly, PD patients can perform their daily activities when the process is ongoing. After several hours (according to patient-specific protocols), the patient can remove the filled solution with excess fluid and dispose it. The patient can restart all the steps with a bag containing fresh dialysate (exchange). The dwell time corresponds to the interval between two subsequent exchanges (*48*) (**Fig 5**).

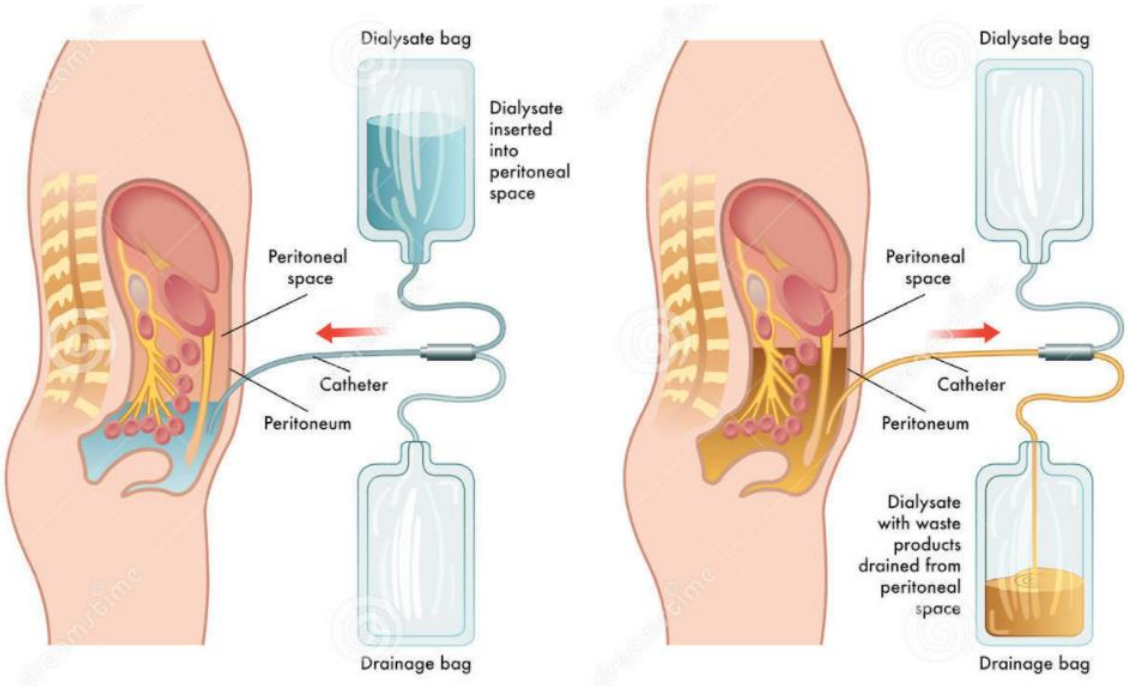

Figure 5 Peritoneal dialysis medical illustration procedure. Adapted from (https://www.dreamstime.com/)

Overall, PD treatment is simpler and cheaper than HD, but with comparable efficacy. PD patients can perform their treatment at home through two different regimens: continuous ambulatory peritoneal dialysis (CAPD), consisting in three or four daily exchange of 30/40 minutes with a dwell time of 4/6 hours during the day e 8/10 hours during the night (*48*); or automated peritoneal dialysis (APD), consisting in the infusion and drainage of PD solution 3/5 times during the night while patient sleeps (*48, 49*).
However, the PD practice may have several disadvantages and complications: 1) daily treatments; 2) fatigue; 3) infection of skin around catheter exit site; 4) peritonitis; 5) hemoperitoneum; 6) hernias; 7) loss of amino acids and albumin and high absorption of glucose, leading to hypertriglyceridemia or weight gain; 8) a gradual thickening and scarring of the peritoneum (*5, 48-50*).

1.2.3 Immunity and inflammation

MCs play a pivotal role in the development of serosal inflammation during infections because they synthesize mediators of inflammation such as prostaglandins and prostacyclin, cytokines and chemokines, intracellular adhesion molecules, growth factors, nitric oxide (NO), reactive nitrogen, oxygen species, anti-oxidant enzymes, ECM proteins, and products of coagulation cascade (*10, 21, 22, 24, 26*). Invading microorganisms induce the first phase of peritoneal inflammation, activating resident macrophages and MCs.
Infection with Gram positive bacteria such as Staphylococcal spp. or with cell-free components such as LPS or zymosan, mimicking Gram negative or fungal infection, respectively, promotes a first wave of polymorphonuclear neutrophils recruited by chemoattractants of bacterial origin and by chemokines such as CXCL1 and CXCL8 produced mainly by MCs and omental fibroblasts. Neutrophils can use high endothelial venules present in FALCs to enter the peritoneal cavity under the guidance of CXCL1 (*51*). Neutrophil influx causes an initial inflammatory response due to the accumulation of neutrophil-secreted proteases and reactive oxygen species. Once they entered the peritoneum, neutrophils undergo NETosis, which consists in the release of necrotic cell DNA forming a net of aggregated neutrophils able to trap and sequester microorganisms in FALCs, thus limiting their spreading (*52*).
Peritoneal macrophages and mast cells may recognize a bacterial infection producing vasoactive substances (e.g. prostaglandins and histamine) that induce a vasodilatation with an increase of peritoneal blood vessels permeability and an increment of synthesis of fibrin, complement, opsonins, immunoglobulins, and clotting factors. Peritoneal macrophages are also involved in the release of a series of inflammatory mediators, in particular IFN-1-γ, TGFβ1, IL-1β, and TNFα, which stimulate the inflammatory cascade promoting chemokine secretion, chemotaxis and leukocyte recruitment (*24*). The cross-talk between macrophages and MCs plays a role in the amplification of the inflammatory response through production of pro-inflammatory cytokines (*53, 54*). TNFα, IFN-1-γ and IL-1β, produced by peritoneal macrophages, may activate MCs that in turn release numerous cytokines and chemokines: monocyte chemotactic protein-1 (MCP-1/CCL2), RANTES/CCL5 (*55*), IL-8/CXCL8 (*55-58*), IL-6 (*55, 57*), macrophage colony-

stimulating factor (M-CSF), granulocyte-CSF (G-CSF) (*59*), IL-1α, and IL-1β (*53, 55, 59*). MCs also express adhesion molecules such as intercellular adhesion molecule-1 (ICAM-1), vascular cellular adhesion molecule-1 (VCAM-1) and N-cadherin, Integrins such as α1-, α2- and α4-β1 Integrins facilitating leukocyte recruitment (*26, 60*). The cytokines and chemokines induced by MCs may bypass the submesothelial interstitium to activate resident macrophages, fibroblasts, endothelial cells lining the capillaries, and to amplify leukocyte recruitment from the bloodstream facilitating their transmigration across the mesothelium (*53, 54, 61-63*).

1.2.4 Defensive barrier and Adhesiveness

MCs secrete a film of fluid, called **glycocalyx**, which covers the MC surface; it protects the cells from abrasions and invasive organisms, facilitates cell-cell contacts, tissue hydration and remodelling. The glycocalyx is composed of lipoproteins, phospholipids (as phosphatidylcholine) and glycosaminoglycans, predominantly hyaluronan (HA) (*25*), that can combine with proteins (proteoglycans) and with lipids (glycolipids) (*24, 44*). Phosphatidylcholine is the principal component of lamella bodies and cellular surfactant and plays a role as a lubricant between surfaces (*10, 22, 64*). HA forms the hyaluronan-dependent pericellular matrix "coats" around microvilli (*65, 66*) to facilitate cell protection, mediate cell differentiation, and hamper the formation of adhesions(*67*). The production of HA increases during peritoneal damage (*68*). Peritoneum provides a hurdle against foreign microorganisms and damage and creates a **non-adhesive** slippery interface to facilitate the movements of abdominal organs. **Intrabdominal adhesions** are a complication that frequently occurs with peritoneal surgery due to the unavoidable disruption of this fragile mesothelial layer (*69*).

2. Mesothelial to mesenchymal transition (MMT) of MCs and peritoneal fibrosis

Epithelial to mesenchymal transition (EMT) is a dedifferentiation process implicated in many physio-pathologic processes. During EMT, epithelial cells lose their interaction with adjacent cells mediated by cell-cell junctions, their apical-basal polarity and their function as a permeability barrier, while they acquire mesenchymal features, such as front-rear polarity, invasiveness, migratory capacity, resistance to apoptosis, increased release of ECM molecules, and reorganization of cytoskeleton and cell shape. All these changes are accompanied by a down-regulation of epithelial genes and an up-regulation of mesenchymal genes (*30, 70, 71*).

EMT can be found under physiological and pathological conditions in diverse common biologic events, and it is in fact a main mechanism of cellular plasticity (*24*). EMT may classified in three major types:

1. **Type 1 EMT** occurs during the implantation, the embryonic gastrulation, the embryo formation, and the organ development; this type of EMT is associated with different rounds of EMT and MET.
2. **Type 2 EMT** is typically activated during inflammation, wound healing, tissue regeneration, and organ fibrosis. This type of EMT can be present as long as the inflammation persists, causing, in the worst situation, irreversible alterations of affected organ.
3. **Type 3 EMT** is present in cancer cells and it is a main mechanism of cell invasion and metastasis (*30, 70, 71*).

MCs originate from mesoderm and their origin explains why unlike 'true' epithelial cells, MCs coexpress both epithelial and mesenchymal markers in basal conditions. In particular, like an epithelial cell, they express Cytokeratin 8-18 and proteins of tight and adherens junctions, while, like a mesenchymal cell, they express constitutively the intermediate filaments Vimentin and Desmin (*7*). Because of its specificity, the EMT of MCs is generally described as a "**mesothelial to mesenchymal transition**" (**MMT**) (*3*).
MMT has a complex reprogramming in gene expression profile characterized by a series of sequential steps. The first event is the destabilization of intracellular junctions. In the tight junctions, a down-regulation of Claudins and Occludin expression, and a delocalization of ZO-1, are observed. Instead, the dissolution of adherens junctions is caused by a down-regulation of E-cadherin expression, associated with a concomitant increase of N-cadherin; this phenomenon is called "Cadherin switch" and leads to changes in cell adhesion and motility of the cells since E-cadherin mediates homotypic static adhesion, whereas N-cadherin may promote cell migration. The integrity of gap junctions and desmosomes also is lost in MMT. In addition, cells lose microvilli. Next, cells lose their apical-basal cell polarity, which is replaced by a front-back polarity, due to the reorganization of cortical actin cytoskeleton. In parallel, MCs acquire mesenchymal markers such as alpha-smooth muscle actin (α-SMA), PAI-1, and Fibroblast Specific Protein (FSP1) expression. Interestingly, the expression of WT1, the main MCs differentiation factor, is down-regulated (*17*), while Snail is induced (see below). Altogether these changes facilitate the increment of mobility. Finally, cells increase the expression of ECM molecules, such as FN-1 and Collagen, and of Matrix Metalloproteinases MMP2 and MMP9, involved in the degradation of membrane basement (*3, 7, 21, 30*). (**Fig 6)**
The transcription factors Snail, Twist and Zinc-finger E-box binding (ZEB) are the master regulators of MMT progression, and they downregulate the expression of epithelial markers while inducing mesenchymal markers.
Snail is the main transcriptional repressor of E-cadherin and it binds the promoter region of E-cadherin through E-box sequences (*24*). In addition, Snail down-regulates other epithelial markers such as Claudins, Occludin, Desmoplakin, Plakophilin, Mucin Muc-1 and Cytokeratin-18.
Differently from 'true' epithelial cells, such as hepatocytes of mammary epithelium, transdifferentiated MCs tend to maintain their "mesenchymal" state, even once the pro-fibrotic stimuli have been removed (*7*).

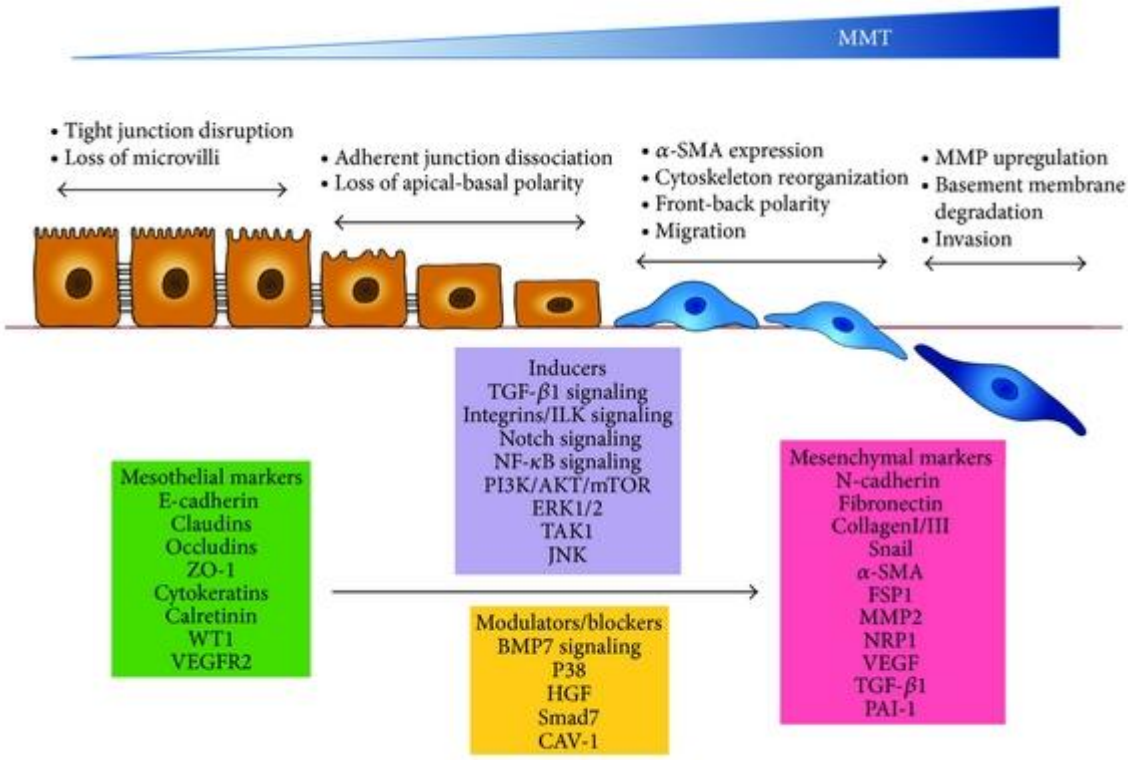

Figure 6 Schematic representation of the crucial events during MMT. MCs lose their epithelial-like features, including disruption of cell-cell junction, dissolution of microvilli and lose of apical-basal polarity; at the same time, MCs acquire mesenchymal characteristics such as front-back polarity, migration and invasion capacity. Adapted from Loper-Cabrera et al. (*3*)

2.1 MMT driving stimuli

2.1.1 Transforming growth factor *β*1 (TGF-*β*1)

TGFβ1 is the main member of the TGFβ superfamily of cytokines. TGFβ1 is secreted by different cell types and is involved in a myriad of functions. With respect to the processes analysed in this study, it is implicated in Collagen deposition, wound healing processes, neoangiogenesis and maintenance of fibrosis (*72*), TGF*β*1, as well as TGF*β* family members, activates signalling pathways, divided in Smad-dependent and Smad-independent. (**Fig 7**) Smadn comprise a familu of structurally similar proteins that are the main signal transducers for receptors of the TGF*β*. There are three distinct sub-types of Smads: receptor-regulated Smads (R-Smads), common partner Smads (Co-Smads), and inhibitory Smads (I-Smads). The R-Smads consist of Smad1, Smad2, Smad3, Smad5 and Smad8/9 and are involved in direct signaling from the TGF-B receptor (*73*).

TGFβ binds TGFβ receptor type II (TGFβRII) which promotes the recruitment of TGFβ receptor type I (TGFβRI). Dimerization of TGFβRI with TGFβRII results in TGFβRI transphosphorylation and activation. The activated TGFβRI, or activin receptor-like kinase 5 (ALK5), induces the phosphorylation and, consequently, the activation of the receptor-regulated Smads, R-Smads (Smad2 and Smad3). Smad2

and Smad3 trimerize with a co-mediator Smad, co-Smad (Smad4), and all together translocate to the nucleus to activate target gene transcription. In contrast, the type I receptor for BMP7 (ALK3), another cytokine of the TGFβ superfamily phosphorylates Smad1, Smad5 and Smad8; they also form heterodimers with Smad4 and the constituted heterocomplexes translocate to the nucleus where they bind DNA, activating genes involved in EMT reversal. There is also an important family of inhibitory Smads (I-Smad), comprising Smad6 and Smad7. They diverge structurally from other Smads. Inhibitory Smads limit the activation of the receptor-triggered Smads by targeting the receptors for degradation. In particular Smad6 blocks BMP7-regulated Smad signalling and Smad7 blocks TGFβ1-regulated Smad signalling. The inhibitory Smads interfere with the phosphorylation of the Smads, binding type I receptors, and prevent the formation and the traslocation of heteromeric Smad complexes (*3, 7, 74-77*). (**Fig 7**)

The balance between BMP7- and TGFβ1-mediated functions is critical in the control of MMT. BMP7 expression may counteract the MMT related changes in peritoneum. Loureiro et al. demonstrated the inhibition of mesenchymal conversion of MCs and the prevention of peritoneal damage by treatment with BMP7 (*78*). Besides BMP7, also treatment with Hepatocyte Growth Factor (HGF) may prevent MMT, activating the Smad transcriptional co-repressor SnoN, which interacts with Smad2 forming an inactive complex (*7, 79*). (**Fig 7**)

TGFβRII and/or TGFβRI also mediate the activation of other important pathways independently of Smads, Mitogen activated protein kinases (MAPKs), Rac and Rho GTPases and Phosphatidyl inositol 3 kinase (PI3Kinase)/Akt pathways. The non-Smad pathways integrate Smad signaling to regulate EMT response (*3, 7, 76*).

The family of serine/threonine **MAPKs** is composed by four subfamilies: Extracellular-regulated kinases (ERKs, i.e. ERK1 and ERK2), c-Jun N-terminal kinases (JNKs, i.e. JNK1, JNK2, and JNK3), p38 MAPK, and ERK5. Mitogenic stimuli activate ERK1/2, environmental and genotoxic stresses induce JNK and p38, whilst both types of signals activate ERK5 (*80, 81*). These subfamilies are involved in multiple actions, including cell differentiation, division, movement, and death (*81*).

The activation of **ERK1/ERK2** pathway, in response to TGFβ, starts with phosphorylation of Shc by TGFβRI and Shc association with Grb2/Sos. Shc/Grb2/Sos complex induces the activation of a sequential phosphorylation of a series kinase:, Raf, MEK1/2 and, finally, ERK1/2.

The activation of MEK1/2/ERK1/2 plays a crucial role in TGFβ-induced EMT, causing the down-regulation of E-cadherin and the up-regulation of a variety of mesenchymal genes (e.g. MMPs, Snail and N-cadherin), the induction of actin stress fibers and the acquisition of motile and invasive properties (*76, 81*). In mesenchymal-like MCs, the inhibition of MEK1/2/ERK1/2 pathway, using pharmacological inhibitors, blocks TGFβ-induced MMT, leading a rescue of epithelial features with an up-regulation of E-cadherin and Cytokeratins and a down-regulation of Snail expression (*82*).

MEK/ERK1/2 pathway is also involved in the regulation of TGFβ-induced Smad signaling. ERK1/2 can phosphorylate R-Smads in their linker region, inhibiting their nuclear translocation and reducing their activities. Recently, it has been

observed that phosphorylation of the linker region of nuclear localized Smads by ERK1/2 causes an increase duration of Smad2 and 3 phosphorylation at C-terminus and an increment of the duration of Smad target gene transcription (*83*). Strippoli and collaborators demonstrated that in MCs Smad3 activity in luciferase assay and C-terminus Smad3 phosphorylation are reduced by MEK1/2/ERK1/2 inhibition; at the same time, Smad1/5 activity and C-terminus Smad1/5 phosphorylation are increased (*84*).

TGFβ may also activate **p38 MAP kinase** and **JNK MAP kinase** (known as Stress Activated Protein, SAP) *via* TAK1 activation; they show activities during inflammation and in cell proliferation, survival, differentiation and migration (*80*). (**Fig 7**)

p38 MAPK may promote EMT during development and cancer, regulating cytoskeleton reorganization and α-SMA synthesis (*76, 81*). However, other studies have been suggested a role for p38α as a tumor suppressor, showing an anti-proliferative functions, a negative regulation of cell cycle progression and an induction of apoptosis (*80*). In quiescent MCs, p38 is constitutively active, and its activity increase when MCs are at confluence. p38 promotes E-cadherin expression in MCs by down-regulating TAK1–NF-kB pathway. JNK MAP kinase is important for TGFβ-induced MMT; thus, its inhibition leads to maintain E-cadherin expression and to hamper the MMT onset (*85*).

The serine-threonine kinase TAK1, also called Mitogen-activated protein kinase kinase kinase 7 (MAP3K7), is a cross point between MAPK and NF-kB pathways. TAK1 shows a critical role during EMT, it is not surprising that its inhibition blocks and reverse MMT in PD patients (*86*). Also, NF-kB inhibition leads to Snail repression and E-cadherin restoration in MCs (*82*).

Rho-like GTPases, comprised of the Rho, Rac and Cdc42 subfamilies of proteins, have a key role in the cytoskeleton organization, cell migration and gene regulation. TGFβ-activated Rho-A pathway induces stress fiber formation, EMT and mesenchymal features. RhoA inhibition blocks TGFβ-mediated EMT (*76, 87*).

Finally, TGFβ also activates **PI3 kinase**, leading to phosphorylation of serine 473 of Akt kinase (pAkt) and its activation. PI3 kinase pathway has a variety of functions including cell survival, cell size control, proliferation and cell migration. pAkt may complete its roles by activating mTOR complex 1 (mTORC1) and mTORC2 (*76, 86*). (**Fig 7**)

PI3 kinase/Akt are involved in EMT induction. In fact, treatment with rapamycin, an inhibitor of mTOR, decreases α-SMA expression and blocks the transition response associated with TGFβ in Smad3-deficient mice (*88*).

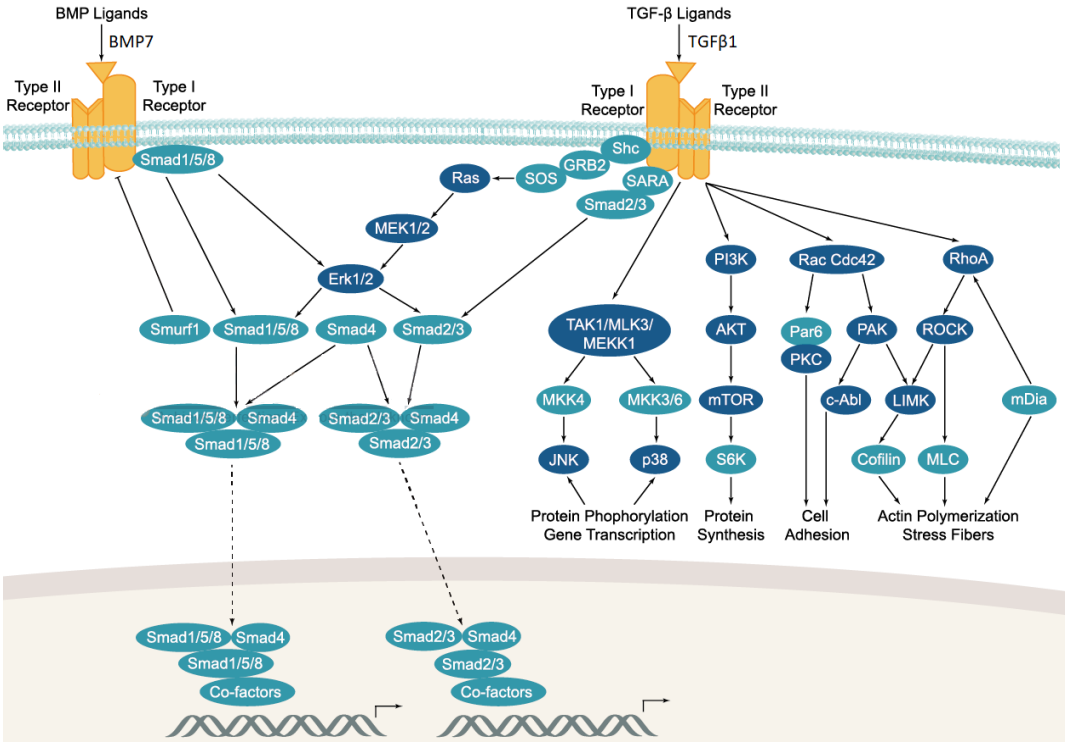

Figure 7 Type I and type II receptor activation involves SMAD-dependent and SMAD-independent signalling route, the balance between BMP7 and TGFβ1 is critical in the control of MMT. Adapted from (https://www.apexbt.com)

2.1.2 Mechanical stretch

Accumulating evidence demonstrated that biomechanical forces orchestrate complex cellular functions determining cell plasticity and cell fate, and are involved in many physio/pathological responses.

It has been demonstrated that changes in the stiffness of the extracellular matrix (ECM) surrounding a tissue and related mechanical forces in addition to soluble factors modify several cellular responses, including EMT and fibrosis (*89*). Tissue stiffness expresses the resistance to deformation in response to an applied force. Changes in matrix stiffness induce mechanosensing and mechanotransduction signalling pathways, converting external mechanical stimuli into biochemical signals (*89, 90*). In order to study *in vitro* the impact of different stiffness conditions in cell plasticity, techniques allowing cells to live in soft or stiff matrices have been developed (*91*). Alterations of ECM stiffness are also associated with tumor onset, progression and metastasis, stimulating angiogenesis, cell proliferation, migration and invasion (*92, 93*).

In addition to ECM stiffness, changes in cell plasticity may be generated by other biomechanical forces: fluid flow (including shear stress), hydrostatic/osmotic pressure, and mechanical stretch (*90*). These forces are physiologically active in tissues subjected to cyclic movements, such as respiratory and abdominal movements or cyclic blood circulation pulse wave (*94-96*). MCs upon exposure to mechanical stretch *in vitro* increase the expression of VEGF and of TGF-*β*1 (*97*).

Linear cyclic stretch *in vitro* leads to several cellular modifications corresponding to bona fide MMT induction in MCs (*98*).
During PD therapy, large PD solution volumes (2L) are injected in the abdominal cavity, increasing tension and mechanical stress by swelling the abdominal space. (**Fig 8**)
Besides PD-related events, mechanical forces have a relevance in post-surgery adherence (PAs) formation. Also, hypoxia and coagulation, peritoneal membrane traumas after abdominal laparotomies and surgery may induce PA formation.(*99, 100*).
The response to biomechanical forces, is mediated firstly by **Integrins**, the main adhesion receptors to the extracellular matrix proteins (ECM) acting with other molecules present at the level of plasma membrane, such as mechanosensitive ion channels (*96*) and mechanotransducers such as Caveolins and Cavins (*101*). These mechanoreceptor proteins mediate the conversion of external mechanical stimuli into biochemical signals, mechanical cues are transduced to the cytoplasm where they determine a general gene expression reprogramming associated to cytoskeletal remodeling (Actin stress fiber formation) and acquisition of an elongated mesenchymal-like morphology, (*96*). Interestingly, mechanical tension plays a role in the activation of TGFβ1 (*102*). Among pathways linking mechanical forces to gene expression, YAP/TAZ activation is dependent on both mechanical forces and soluble factors. The transcriptional coactivator YAP (Yes-associated protein) and its paralogs TAZ are effectors of the Hippo pathway. When Hippo pathway is inactive, YAP and TAZ translocate into the nucleus, where they regulate gene transcription. Since YAP/TAZ lack a sequence for direct interaction with DNA, their transcriptional activity is mediated by interactions of YAP/TAZ with TEAD transcription factors. Recently we demonstrated that exposure of peritoneal MCs to cyclic mechanical stretch in sufficient to promotes the activation of signaling pathways leading to increased TGF-β1 expression and induction of a MMT program. Exposure to mechanical stretch led to nuclear translocation of YAP/TAZ that cooperates with TGF-β1 signaling promoting the expression of genes involved in MMT. Interestingyl, YAP/TAZ also promote the expression of CAV1, which limits MMT, inducing a negative feedback loop (*98*). YAP/TAZ are involved in a multitude of activities: cell proliferation, growth of organs and their size control, differentiation, tissue-specific progenitor cells amplification, regeneration of tissues and organs; they identified cell shape, polarity and structure. YAP/TAZ play an important role during cancer progression and metastasis and during EMT (*103, 104*).

2.1.3 Inflammation

Peritonitis is a main cause of fibrosis induction in peritoneum and one of the most serious complications of PD (*105*). Peritoneal membrane and intestine contiguity may allow microorganisms to leak into the peritoneal cavity and to infect peritoneum. Medical typical practices of PD patients such as catheter positioning and dwelling, as well as abdominal surgery can facilitate the progression of infection state in peritoneum.
Peritonitis are often driven from skin gram-positive bacteria, and less frequently from enteric flora gram negative bacteria (*106*). Compared to bacteria, there are

limited reports on the role of viruses. In 20% of the cases the cultures from peritonitis result negative, and in these cases it is possible to hypothesize a viral peritonitis (*107*).
Innate pattern recognition receptors (PRRs) on peritoneum include Toll-like receptors (TLRs), RIG-I-like receptors, NOD-like receptors, and C-type lectin receptors. PRRs recognize pathogens through the interaction with pathogen-associated molecular patterns (**PAMPs**) molecules conserved among microbial species, and damage-associated molecular patterns **(DAMPs**) endogenous molecules released from damaged cells (*108*). PRRs activation triggers a signaling cascade that leads to elimination of pathogens and infected cells (*109*) TLRs have a main role in immune response. In particular, human MCs show a high expression of TLR1, 2, 3 ,4, 5 and 6, while TLR7-10 are less expressed(*110, 111*). Each of them recognizes different molecular patterns of microorganisms and self-components. (**Fig 8**) (See below).

2.1.4 Peritoneal Dialysis Solutions

There is a need in PD solutions to use molecules with osmotic activity that allow ultrafiltration of solutes. The main molecule used in this case is glucose. Commonly used glucose-based solutions have a non-physiological composition: they may contain high concentrations of Glucose, Glucose Degradation Products (GDPs), Advanced Glycation End-products (AGEs), Lactate. The may have high osmolality and low pH (*112, 113*). Each of these elements can influence the peritoneal integrity and dialysis efficacy and are associated with the release of inflammatory cytokines. (**Fig 8**)
High glucose solutions induce a proinflammatory and profibrotic reaction. High levels of glucose stimulate: a reduction in cell proliferation; a decrease in the intercellular junctional proteins levels, inducing a hyperpermeability; a mesothelial denudation; an increase of VEGF levels, with microvascular proliferation and neoangiogenesis; a rise of TGFβ production, with submesothelial fibrosis induction; an acceleration in tissue inhibitor of metalloproteinases (TIMP) release, causing a loss of balance in matrix metabolism and an accumulation of Collagen and FN-1 (*7, 112-116*).

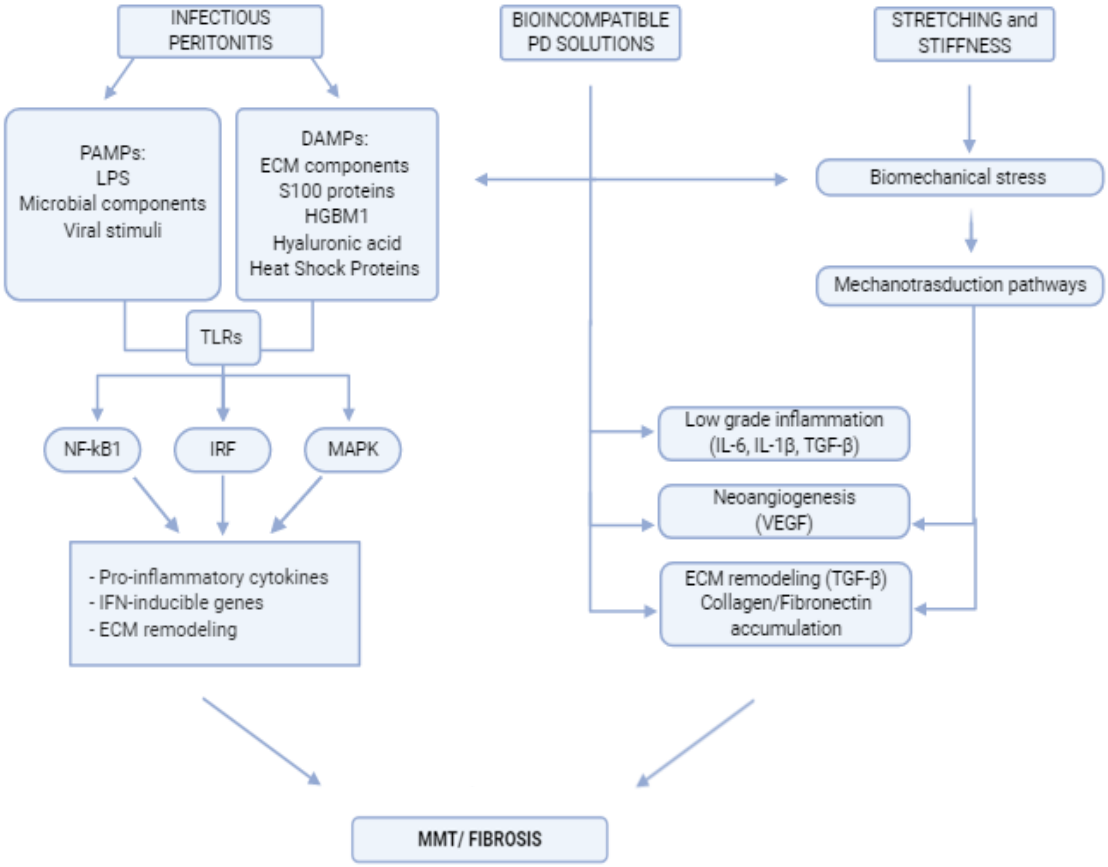

Figure 8 Main extracellular stimuli promoting peritoneal fibrosis and subsequent mesothelial cell response. Adapted from Terri et al (*1*)

Glucose degradation products (**GDPs**), such as Formaldehyde, Acetaldehyde, Glyoxal, Methylglyoxal (MGO), 2-furaldehyde, 5-hydroxymethylfurfurale, 3-deoxyglucosone and 3,4-dideoxyglucosone-3-ene, are released during the heat-sterilization under acidic pH and storage of PD fluid (*112, 113, 116-118*). GDPs play a cytotoxic effect on MCs (*118*) and all together stimulate a decrease in cell proliferation, in viability and in the synthesis of IL-6, mediated by IL-1β, and an increase in the production of TGFβ and Collagen (*113, 117, 119*). MGO, in particular, induces MCs and endothelial cells to synthetize VEGF, contributing to vascular proliferation (*116, 120*). Glucose and reactive carbonyl compounds can form **Advanced Glycation End-products** (**AGEs**), binding to free amino groups on proteins or lipids (*116, 118*). The accumulation of AGEs correlates with the duration of PD and with the events of peritonitis, decreases ultrafiltration capacity and gives at the peritoneum more permeability. This last effect is amplified in diabetic patients (*116, 121*). AGEs stimulate the release of ECM molecules and VEGF (*7, 24*). Moreover, the presence of high Glucose in dialysis fluid amplifies the Receptor for AGE (RAGE) expression in the submesothelial fibrotic tissue, in the mesothelium and in the blood vessel walls (*115, 116*).
Finally, **Lactate,** being a product of glucose metabolism, causes fibrotic changes, leading to an increment of the microvascular flow and the perfused capillary length per area of PM (*112, 116, 122*).

These negative effects have stimulated the research of new "biocompatible" dialysis solutions. In substitution of Glucose, different components are already in use or new components are presently tested. Current targets are the the reduction of GDP levels and the use of buffer with neutral pH.
To date, icodextrin and amino acids are the two main options to replace Glucose. Icodextrin is a poly-glucose molecule, slowly absorbed by peritoneal cavity, combined in a solution with Lactate, in conditions of low pH and low levels of GDPs. This solution improves ultrafiltration and maintain MCs structure. Amino acids solutions, combined with Lactate, eliminate GDPs and preserve MCs function (*113, 123*). In addition, another group of Glucose-based solutions with low GDPs, Lactate and/or Bicarbonate is presently in use. The osmotic agent and the buffers are enclosed in two separate bags to decrease degradation of Glucose and production of GDPs. This shrewdness allows to maintain neutral pH which reduces the levels of AGE and IL-6; in addition, a reduced damage of MCs and a slower decline of residual renal function are obtained (*123, 124*).
Overall, the new "biocompatible" solutions are less harmful and show some common improvements: maintenance of cell viability, preservation of residual renal function and peritoneal function, reduction of AGE and vasculopathy (*113, 123, 124*). However, the 'perfectly biocompatible' solution has still not been developed and research is active so far in this field.

2.2 MMT: effects and consequences

2.2.1 Fibrosis

MCs constitute a first defense against membrane damage operated by the various insults described in the previous section. The correct balance between denudation and regeneration of mesothelium is important for the maintenance of peritoneum homeostasis. This equilibrium can be disturbed by long-term PD or by repeated episodes of peritonitis (*24*). (**Fig 9**)
Peritoneum during PD is continuously and directly exposed to bioincompatible solutions causing membrane damage. In addition, peritoneal membrane suffers mechanical stress related to dwelling practice, episodes of catheter complication (i.e. peritonitis and hemoperitoneum), and chronic inflammation caused by bacterial and fungal infections. The consequences are deposition of collagen in the submesothelial compact zone, fibrosis, angiogenesis, vasculopathy, hyalinization of the blood vessels, and MMT of MCs. (*3, 7, 114, 125, 126*).

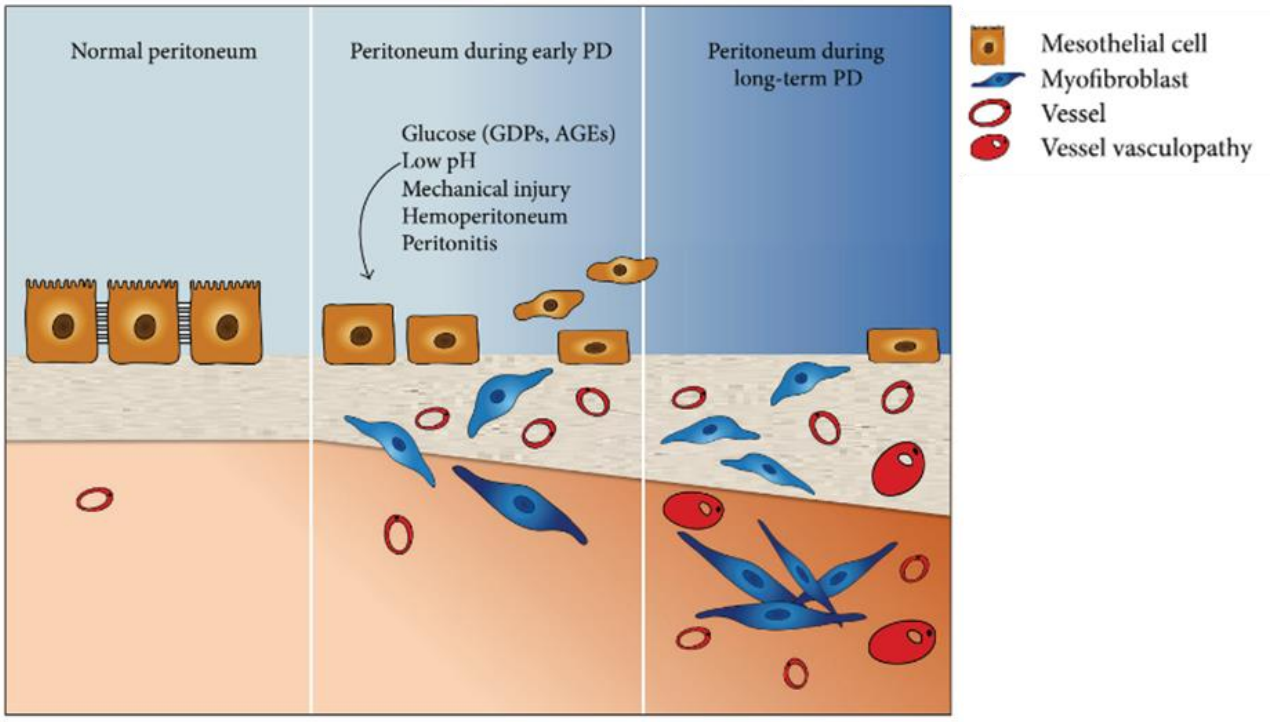

Figure 9 Schematic representation of changes in the peritoneal membrane during PD therapy. Adapted from M Lopez-Cabrera (*3*)

Peritoneal fibrosis is a progressive thickening of the submesothelial region induced by chronic inflammation and is a common consequence of PD. Its signs are found in 50% to 80% of patients within one or two years of PD practice (*7, 110, 127*).Peritoneal fibrosis represents an important cause of PD discontinuation, together with peritonitis and cardiac complication. PD is also a risk factor for the onset of **encapsulating peritoneal sclerosis** (**EPS**), the most serious complication of PD, with potentially fatal manifestation (*3, 7*). EPS is a syndrome characterized by loss of ultrafiltration function, anorexia, weight loss, diarrhea, intestinal obstruction, inflammation, peritoneal thickening, fibrin deposition, sclerosis, calcification and encapsulation (*3, 7, 128-130*). However, peritoneum during PD practice often presents only limited complications and many patients develop a **simple peritoneal sclerosis** (**SPS**), characterized by thickening of the peritoneum, calcification, presence of inflammatory elements, angiogenesis and dilatation of blood and lymphatic vessels in the absence of systemic disease (*131*).

2.2.2 Extracellular matrix deposition

Peritoneal fibrosis is the end result of chronic inflammatory reactions and it is characterized by an excessive deposition of ECM, predominantly type I Collagen and FN-1 but also Laminin, Elastin, Proteoglycans. The excessive deposition of ECM disrupts the normal architecture of the peritoneum and results in increased thickening and mesothelium dysfunction. TGF-β1, inflammatory cytokines and other fibrotic stimuli modulate the expression of Collagen and FN-1 (*132*). In response to fibrotic stimuli, resident peritoneal fibroblast become activated,

exhibiting a myofibroblast-like phenotype. Activated fibroblasts are primarily responsible for the excessive synthesis and deposition of ECM in submesothelial compact zone (*3*). Fibroblasts are also generated from mesothelial cells through MMT. In addition, endothelial-myofibroblast transition (EndoMT) has been implicated in fibrogenesis (*133, 134*).

Fibronectin (FN-1) is ubiquitously expressed in the ECM produced by a variety of cell types. FN-1 consists of two subunits with each one having an approximate size of 250 kDa that are covalently connected. FN-1 matrix is produced at the time of dynamic tissue remodeling (*135-137*) and its functional form *in vivo* is in fibrillar state. (*138, 139*). The fibril formation process is called fibrillogenesis. A variety of cellular processes are characterized by the production of FN-1 matrix fibers, including MMT and tumor progression. TGFβ treatment increases FN-1 matrix assembly (*140*). FN-1 binds to cells primarily to Integrin receptors, particularly α4β1 and α5β1 integrins (*141*). Integrins recognize two different binding-sites on FN-1: RGD domain and CS1 segment. FN-1/Integrin interaction is a key regulatory point for mechanosensing and cell adhesion (*142-144*). Many Integrins are involved in fibrillogenesis including α5β1 αvβ1, αvβ3, however, α5β1, is most efficient in mediating FN-1 matrix assembly (*145, 146*) Regarding to FN-1 turnover, at least two mechanisms exist for the degradation and removal of proteins from the ECM: extracellular proteolysis (*147-149*) and endocytosis followed by intracellular degradation (*150-152*). Several studies demonstrate that endocytosis in a major mechanism that regulates turnover of ECM FN-1 (*152, 153*). Shi and colleagues showed that extracellular cleavage of FN-1 by MT1-MMP is necessary for efficient endocytosis, this process is functionally dependent on β1 Integrin, and it is inhibited by treatment with blocking antibodies against β1 Integrin (*153, 154*). MT1-MMPs also activate MMP2 that provide FN-1 cleavage (*155*).

Collagens are the most abundant fibrous protein within the interstitial ECMs. Collagen is synthesized and secreted in the ECMs mainly by fibroblasts. By exerting tension on the matrix, fibroblasts organize Collagen fibrils into sheets and cables markedly influencing the alignment of collagen fibers (*156*). Collagen superfamily is comprised of twenty-eight different collagen types. Type I collagen is the archetypal collagen showing widespread and abundant expression among tissues. It forms heterotrimeric triple helices, which are self-assembled into fibrils. Collagen biosynthesis and structure are markedly modified during ECM remodeling by MCs having undergone MMT (*18, 21, 157*). TGFβ directly upregulates Collagen 1a1 expression levels via SMAD2/3 activation (*158*). Type I collagen in mesothelium has been related to interaction with α2β1 integrin in context of ovarian carcinoma, indicating a function on multiple levels to promote metastatic dissemination of ovarian carcinoma cells (*159*). ECM stiffening, induced by increased collagen deposition and cross-linking, disrupts tissue morphogenesis and contributes to fibrosis. Collagen scaffolds provide signals to cells affecting various cellular functions including cell migration, adhesion, angiogenesis, tissue development and repair (*156, 160*).

Laminins are large heterotrimeric cross-shaped glycoproteins, Laminin molecules interact with each other as well as with other ECM components and resident cells

participating in the organization of ECMs and cell adhesion. Laminin expression is up-regulated in wounded epithelium providing the substrate for the epithelial cells to adhere and move in order to cover the wounded area and therefore to re-establish the intact epithelium (*161*). Laminins are induced during fibrosis progression, and they are also implicated in angiogenesis.

Metalloproteinases (MMPs) are a family of multidomain zinc-dependent endopeptidases implicated in ECM degradation and remodelling (*162, 163*). Based on substrate specificity MMPs can be divided in: Collagenases, gelatinases, stromelysins, metrilysins, membrane-type MMPs, and other MMPs.

Collagenases (MMP-1, -8, -13) cleave some ECM proteins and other soluble proteins, but the most important role of this type of MMPs is the cleavage of fibrillar collagen. (*162, 164*).

Gelatinases (MMP-2 and -9) play an important role in many physiological processes, such as ECM degradation and remodeling, osteogenesis and wound healing (*165*). Gelatinases degrade gelatin (*166, 167*), collagen (*164*), elastin (*168*), proteoglycan core proteins (*166, 169*), FN-1 (*168*), Laminin (*166*), fibrillin-1, and TNFα and IL-1β precursor (*165*). The activity of gelatinases is crucial for metastatic cell output and metastasis site entry (*170*).

Stromelysins (MMP-3, -10 -11) have the same domain arrangement as collagenases, but do not cleave interstitial collagen (*162*).

Matrilysins (MMP-7 and -26) Besides ECM components, it processes cell surface molecules such as pro-a-defensin, Fas-ligand, protumor necrosis factor a, and E-cadherin. (*166*).

Membrane-type metalloproteinases (MT-MMP) can be subdivided into: type I transmembrane proteins (MMPs-14, -15, -16, and -24) and glycosylphosphatidylinositol anchored proteins (MMPs-17 and -25). MT-MMPs are activated intracellularly and the active enzymes are expressed on the cell surface, All MT-MMPs can activate proMMP-2 (*164, 166, 169*), MMMP-14 has collagenolytic activity on collagens.

Under normal conditions, the activity of MMPs is very low and is strongly regulated by natural tissue inhibitors (TIMPs). In the presence of specific stimuli, such as inflammatory/profibrotic cytokines (such as TGFβ), MMPs can be upregulated. Chronic activation of MMPs, due to an imbalance between the activity of MMPs and TIMPs, can result in excessive ECM degradation. MMPs and TMIPs are expressed in mesothelial cells and can be modulated by viral infection (*171*),(*172*)).

3. Toll-Like Receptors

The innate immune system acts trough germline-encoded patter-recognition receptors (PRRs) for the initial detection of microbial organisms. PRRs recognize microbe-specific molecular signatures also known as pathogen-associated molecular patterns (PAMPs) as well as self-derived molecules originated form damaged cells known as damage associated molecules patterns (DAMPs). PRRs activate downstream signalling pathways that lead to the induction of innate immune responses by producing inflammatory cytokines, type I interferon (IFN),

and other mediators. These processes not only trigger immediate host defensive responses such as inflammation, but also prime and orchestrate antigen-specific adaptive immune responses (*173*). These responses are essential for the clearance of infecting microbes as well as crucial for the consequent instruction of antigen-specific adaptive immune responses.

Mammals have several distinct classes of PRRs including Toll-like receptors (TLRs), RIG-I-like receptors (RLRs), Nodlike receptors (NLRs), AIM2-like receptors (ALRs), C-type lectin receptors (CLRs), and intracellular DNA sensors such as cGAS (*174*), (*175*). Among these, TLRs play a critical role in innate immune responses by specifically recognizing molecular patterns from a wide range of microorganisms, including bacteria, fungi and viruses. TLRs are responsible for sensing invading pathogens outside of the cell and in intracellular endosomes and lysosomes (*109*). The TLR family is composed by 10 members (TLR1–TLR10) in human and 12 (TLR1–TLR9, TLR11–TLR13) in mouse. TLRs are localized at the the cell surface or in intracellular compartments such as the ER, endosomes, lysosomes, or endolysosomes. They recognize distinct or overlapping PAMPs such as lipids, lipoproteins, proteins, and nucleic acids. Each TLR is composed of an ectodomain with leucine-rich repeats (LRRs) that mediate PAMPs recognition, a transmembrane domain, and a cytoplasmic Toll/IL-1 receptor (TIR) domain that initiates downstream signaling. The ectodomain displays a horseshoe-like structure. TLRs interact with their respective PAMPs or DAMPs as a homo- or heterodimer along with a co-receptor or accessory molecule (*176*). Upon PAMPs and DAMPs recognition, TLRs recruit TIR domain-containing adaptor proteins such as MyD88 and TRIF, which initiate signal transduction pathways that culminate in the activation of NF-κB, IRFs, or MAP kinases to regulate the expression of cytokines, chemokines, and type I IFNs that ultimately protect the host from microbial infection. Recent studies have revealed that proper cellular localization of TLRs is important in the regulation of the signalling pathways elicited, and that cell type-specific signaling downstream of TLRs determines specific innate immune responses.

3.1 PAMP recognition by TLRs

TLRs are expressed in innate immune cells such as dendritic cells (DCs) and macrophages as well as non-immune cells such as fibroblast cells and epithelial cells. TLRs are largely classified into two subfamilies based on their localization, cell surface TLRs and intracellular TLRs. Cell surface TLRs include TLR1, TLR2, TLR4, TLR5, TLR6, and TLR10, whereas intracellular TLRs are localized in the endosome and include TLR3, TLR7, TLR8, TLR9, TLR11, TLR12, and TLR13 (*177*), (*178*). Cell surface TLRs mainly recognize microbial membrane components such as lipids, lipoproteins, and proteins. TLR4 recognizes bacterial lipopolysaccharide (LPS). TLR2 along with TLR1 or TLR6 recognizes a wide variety of PAMPs including lipoproteins, peptidoglycans, lipotechoic acids, zymosan, mannan, and tGPI-mucin (*177*). TLR5 recognizes bacterial flagellin (*178*). TLR10 is pseudogene in mouse due to an insertion of a stop codon, but human TLR10 collaborates with TLR2 to recognize ligands from listeria (*179*). TLR10 can also sense influenza A virus infection (*180*). Intracellular TLRs recognize nucleic acids derived from bacteria and viruses, and also recognize self-nucleic acids in disease conditions such as

autoimmunity (*181*). TLR3 recognizes viral double-stranded RNA (dsRNA), small interfering RNAs, and selfRNAs derived from damaged cells (*182*), (*183*),(*184*). TLR7 is predominantly expressed in plasmacytoid DCs (pDCs) and recognizes single stranded (ss)RNA from viruses. It also recognizes RNA from streptococcus B bacteria in conventional DCs (cDCs) (*185*). Human TLR8 responds to viral and bacterial RNA (*186*). Structural analysis revealed that unstimulated human TLR8 exists as a preformed dimer, and although the Z-loop between LRR14 and LRR15 is cleaved, the N- and C-terminal halves remain associated with each other and participate in ligand recognition and dimerization. Ligand binding induces reorganization of the dimer to bring the two C termini into close proximity (*187*). TLR13 recognizes bacterial 23S rRNA (*188*),(*189*), (*190*) and unknown components of vesicular stomatitis virus (*191*). TLR9 recognizes bacterial and viral DNA that is rich in unmethylated CpG-DNA motifs; it also recognizes hemozoin, an insoluble crystalline byproduct generated by Plasmodium falciparum during the process of detoxification after host hemoglobin is digested (*192*). TLR11 is localized in the endolysosome and recognizes flagellin (*193*) or an unknown proteinaceous component of uropathogenic Escherichia coli (UPEC) as well as a profilin-like molecule derived from Toxoplasma gondii (*194*). TLR12 is predominantly expressed in myeloid cells and is highly similar to TLR11 and recognizes profilin from T. gondii (*195*). TLR12 functions either as a homodimer or a heterodimer with TLR11 (*196*),(*197*).

3.2 TLR signaling

After TLR engagement, MyD88 forms a complex with IRAK kinase family members, referred to as the Myddosome (*198*). During Myddosome formation, IRAK4 activates IRAK1, which is then autophosphorylated at several sites (*199*) and released from MyD88 (*200*). IRAK1 associates with the RING-domain E3 ubiquitin ligase TRAF6. TRAF6, along with ubiquitin-conjugating enzyme UBC13 and UEV1A, promotes K63-linked polyubiquitination of both TRAF6 itself and the TAK1 protein kinase complex. TAK1 is a member of the MAPKKK family and forms a complex with the regulatory subunits TAB1, TAB2, and TAB3, which interact with polyubiquitin chains generated by TRAF6 to drive TAK1 activation (*201*) Although the mechanisms of TAK1 activation within this complex remain unclear, K63-linked ubiquitination or close proximity-dependent transphosphorylation may be responsible for TAK1 activation. TAK1 then activates two different pathways that lead to activation of the IKK complex-NF-κB pathway and -MAPK pathway. The IKK complex is composed of the catalytic subunits IKKα and IKKβ and the regulatory subunit NEMO (also called IKKγ). TAK1 binds to the IKK complex through ubiquitin chains, which allows it to phosphorylate and activate IKKβ. The IKK complex phosphorylates the NF-κB inhibitory protein IκBα, which undergoes proteasome degradation, allowing NF-κB to translocate into the nucleus to induce proinflammatory gene expression. TAK1 activation also results in activation of MAPK family members such as ERK1/2, p38 and JNK, which mediates activation of AP-1 family transcription factors or stabilization of mRNA to regulate inflammatory responses (*202*). TAK1 deficiency in mouse embryonic fibroblast cells (MEFs) reduces phosphorylation of IKKs, p38, and JNK after LPS stimulation. However, TLR4-mediated IKK, p38, and JNK activation and cytokine induction are increased in neutrophils derived from TAK1-deficient mice, suggesting a cell type-

specific role for TAK1 in TLR signaling (*203*). Furthermore, the physiological roles of TAB proteins in TLR signaling also remain controversial: TAB1- or TAB2-deficient mice do not show any abnormality in TLR signaling pathways (*204*), and mice doubly deficient for TAB2 and TAB3 also exhibit normal cytokine production after TLR simulation in MEFs and macrophages (*205*). TAB family proteins may therefore compensate for each other in TLR signaling. TLR2 and TLR4 ligations in macrophages increase the production of mitochondrial ROS for bactericidal action and recruit mitochondria to phagosomes (*206*). TRAF6 is translocated to mitochondria following bacterial infection, where it interacts with ECSIT. TRAF6 promotes ECSIT ubiquitination, resulting in increased mitochondrial and cellular ROS generation.

TRIF interacts with TRAF6 and TRAF3. TRAF6 recruits the kinase RIP-1, which in turn interacts with and activates the TAK1 complex, leading to activation of NF-κB and MAPKs and induction of inflammatory cytokines (Fig 10). In contrast, TRAF3 recruits the IKK-related kinases TBK1 and IKKi along with NEMO for IRF3 phosphorylation. Subsequently, IRF3 forms a dimer and translocates into the nucleus from the cytoplasm, where it induces the expression of type I IFN genes. The Pellino family E3 ubiquitin ligases are implicated in TLR signaling (*207*). Pellino-1-deficient mice display impaired TRIF-dependent NF-κB activation and cytokine production (*208*). Pellino-1 is phosphorylated by TBK1/IKKi and thereby facilitates ubiquitination of RIP-1, suggesting that Pellino-1 mediates TRIF-dependent NF-κB activation by recruiting RIP-1. Furthermore, Pellino-1 regulates IRF3 activation by binding to DEAF-1, a transcription factor that facilitates binding of IRF3 to the IFNβ promoter (*207*). Recently, IRF3 activation was demonstrated to be regulated by an inositol lipid, PtdIns5P. PtdIns5P binds to both IRF3 and TBK1, and thus facilitates complex formation between TBK1 and IRF3. The accessibility of TBK1 to IRF3 mediated by PtdIns5P likely causes IRF3 phosphorylation in a closely proximal manner. Furthermore, PIKfyve was identified as a kinase responsible for production of PtdIns5P during virus infection (*209*).

In addition to IRF3 and IRF7, several other IRFs participate in TLR signaling. IRF1 interacts with MyD88 and contributes to TLR9- mediated cytokine production in the presence of IFNγ (*210*), while IRF5 is involved in the MyD88-dependent signaling pathway for inducing inflammatory cytokine production (*211*). IRF8 was proposed to be essential for TLR9-MyD88-dependent activation of NF-κB in pDCs (*212*). However, a subsequent analysis of IRF8- deficient mice demonstrated that IRF8 is involved in the second phase of type I IFN response after treatment of DCs with TLR agonists (*213*).

3.3 Mechanisms of inflammatory response

Recent studies have shown that the modulation of TLR2 and TLR4 activity through specific antibodies or soluble Toll-like receptor 2 (sTLR2), a TLR2 inhibitor, is able to cause a substantial reduction of inflammatory parameters to inhibit. A set of TLRs, comprising TLR3, TLR7, TLR8, and TLR9, act in the intracellular space in order to recognize nucleic acids derived from viruses and bacteria, as well as endogenous nucleic acids in pathogenic contexts (*109*). These TLRs respond by activating the production of type I IFNs and pro-inflammatory cytokines (**Fig10**). Viral stimuli are recognized by the intracellular TLR3, which is functionally expressed in MCs (*214*).

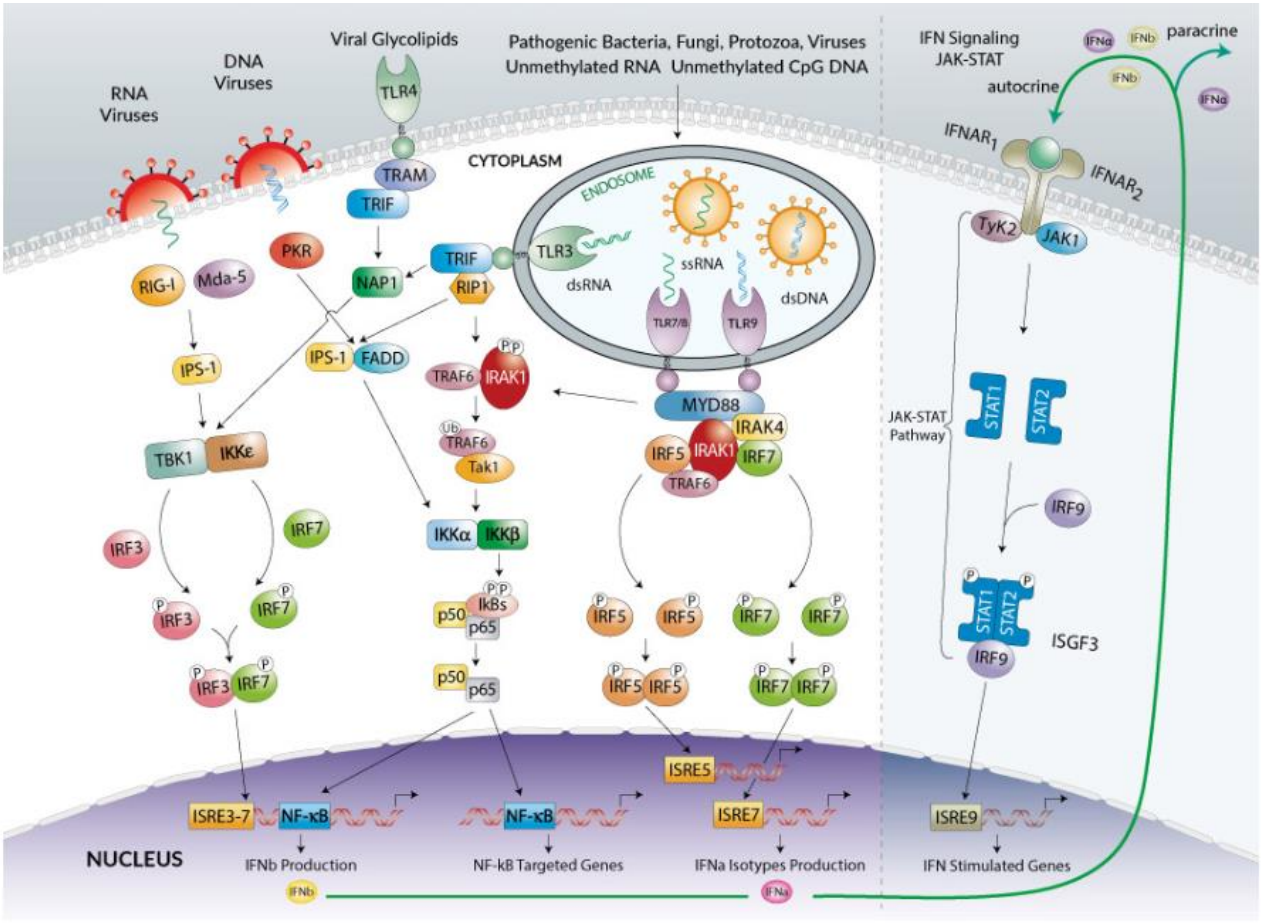

Figure 10 Schematic representation of TLRs activation of signalling cascade leading to type I interferon production and signalling. Adapted from (https://www.invivogen.com/review-type1-ifn-production).

While for several exogenous TLRs the signaling pathway depends on MyD88, known as the inductor of the early phase response in MØs, TLR3, specifically, acts thought TRIF that plays an essential role in inducing a NF-kB mediated fibrosis and a late phase immune response activation (*215*),(*216*). In human MCs, TLR3 is also involved in the regulation of the final common pathway of inflammation and fibrosis acting on matrix-remodeling proteins. In particular, TLR3 is correlated in time- and dose-dependent upregulation of MMP9 and TIMP1 (*171*). In addition to

PAMPs, TLR mediated response can be stimulated by endogenous TLR molecules, inducing sterile inflammatory processes (*217*),(*218*). Many endogenous TLRs derive from ECM components, such as fibronectin or fibrinogen or ECM interacting proteins such as tenascin-C (*219*),(*220*). Proteins with various functions may serve as endogenous TLRs such as cardiac myosin, S100 proteins, HGBM1(*221*),(*222*),(*223*),(*224*).

While the last protein may interact with several TLRs, the majority of these ligands are direct agonists of TLR2 and TLR4 (*225*). Interestingly, exposure to PD fluids promotes the expression of Hsp60, Hsp70 and hyaluronic acid (HA), all TLR2 and TLR4 ligands, by leukocytes and MCs, thus driving an inflammatory response in the absence of infectious stimuli (*126*).

Recent studies by Labéta et al focused on the ability of reducing inflammation and fibrosis induced by bacterial components through the use of a soluble form of TLR2 acting as a decoy, sTLR2. When administered together with the repeated peritoneal injection of S. epidermidis in mice, sTLR2, was found to prevent fibrosis development (*110*). This effect was accompanied by a substantial reduction of inflammatory parameters, including the peritoneal levels of a number of pro-inflammatory cytokines and chemokines, polymorphonuclear neutrophils (PMN) and monocytes at the peak time of their influx to the peritoneum as well as the prototypical pro-fibrotic cytokine TGF-β. Thus, peritoneal fibrosis resulting from repeated peritoneal bacterial infections like those associated with PD can be inhibited by sTLR2 by acting on a variety of pro-inflammatory and fibrotic mediators, but notably, without affecting infection clearance (*111*). Of note, the development of peritoneal fibrosis by long exposure to peritoneal dialysis solution can also be prevented by administering sTLR2, which inhibits pro-inflammatory and fibrotic mediator production and controls the expansion of inflammatory cells (*111*).

4. The role of epigenetics

The definition of **epigenetics** has undergone numerous changes during the past 50 years (*226*). The term 'epigenetics' was coined by Conrad Waddington in the 1940s to explain "the branch of biology which studies the causal interactions between genes and their products which bring the phenotype into being" (*227, 228*). Considering the following discoveries, especially in genetics, over the years the definition of epigenetics has evolved (*229*). The currently accepted definition for epigenetic trait was formulated in 2008: "stably heritable phenotype resulting from changes in a chromosome without alterations in the DNA sequence". This definition also considers "the heritability of a phenotype, passed on through either mitosis or meiosis" (*230*). Through the use of molecular biology techniques, it was demonstrated that, despite the fact that all the somatic cells in each organism share the same genetic information, differences in patterns of gene expression among diverse cell types may be inherited, either in the progeny of cells or of organisms.

The understanding of DNA organization is crucial to analyse the different epigenetic modifications. DNA is wrapped around **histone octamers** (composed of one H3–H4 tetramer and two separate H2A–H2B dimers) to form **nucleosomes** that are the

basic repeating units of **chromatin**. The nucleosomes are connected through the linker DNA, associated with linker histone H1 (*229, 231*). The DNA presents in living cells can be distinguished in: i) **heterochromatin**, a closely packed form of DNA, corresponded to low gene density and a transcriptionally inactive region; ii) **euchromatin**, a poorly packed form of DNA, enriched in transcriptionally active regions (*231*). The organization of DNA in both euchromatin and heterochromatin is regulated by specific epigenetic mechanisms of chromatin remodeling such as, DNA methylation and histone modifications (**Fig 11**). Epigenetic regulators are grouped together into three sets: epigenetic writers lay on DNA and histones the epigenetic marks, epigenetic erasers remove the epigenetic marks and epigenetic readers recognize the epigenetic marks (*232*). Besides covalent modifications of DNA or DNA-related proteins, epigenetic changes are mediated also by a wide array of non-coding RNAs. Among non-coding RNAs, small RNAs, including microRNAs (miRNAs), and long noncoding RNAs (lncRNAs) have been identified some years ago. Their discovery unveiled a new layer of regulation of gene expression. Due to the fact that the analysis of the impact of non-coding RNAs were not object of this doctoral thesis, this topic is not dealt in the introduction section.

Epigenetic changes are main determinants of EMT induction and may explain many features of cellular plasticity such as the persistence of the EMT phenotype and the reversibility of the EMT process (*231, 233*). As explained in previous paragraphs, during EMT onset, different transcription factors (i.e. TWIST, SNAIL, ZEB) are induced to repress epithelial gene expression (*233*). In addition, several epigenetic modifiers modulate the activity of these transcriptional factors (*231, 234, 235*). While the majority of discoveries about the relationships between EMT and epigenetic mechanisms were obtained in tumour experimental systems, a relatively limited number of studies focused on non-transformed cells. To this regard, information obtained in tumours is extremely useful but cannot directly translated to other EMT systems.

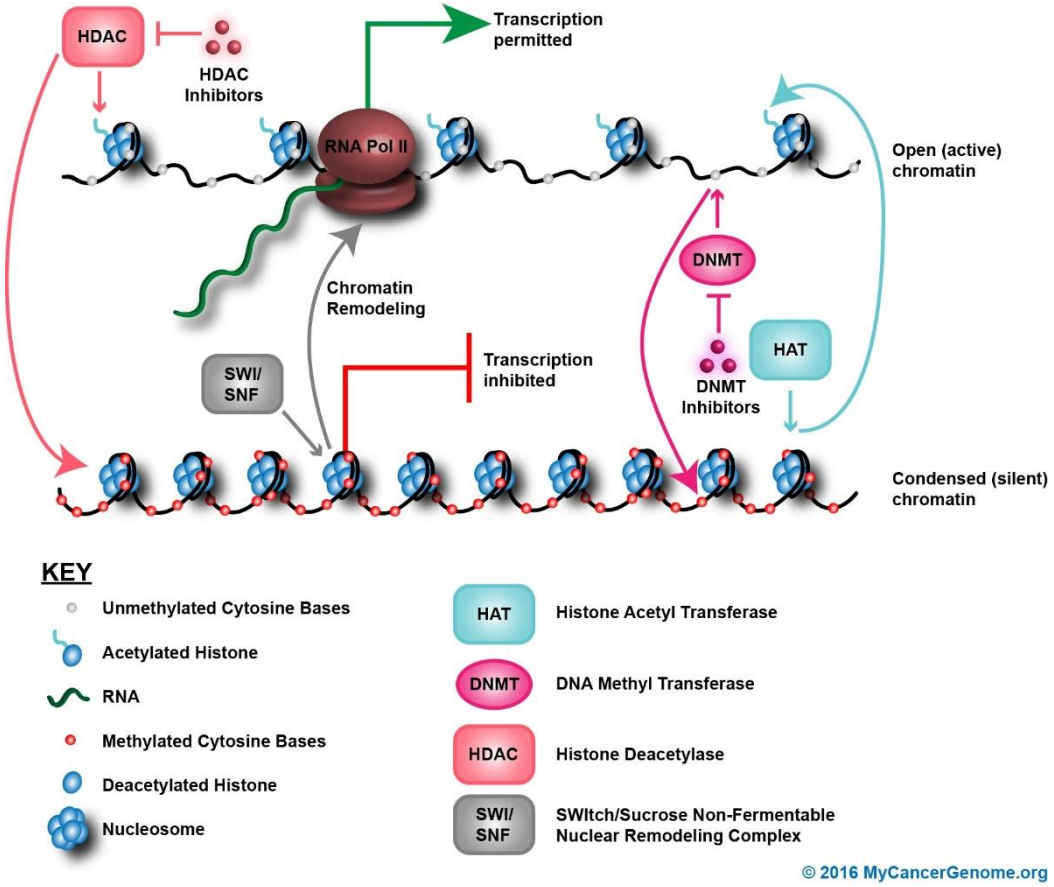

F**igure 11** Schematic illustration of the principal epigenetic mechanisms. The short arrows represent targets of the enzymes, while the long arrows indicate the results of the enzyme activities. DNA methyltransferase (DNMT) induces the methylation of cytosine resid residues and induces gene silencing. Histone acetylase (HAT) activates the transcription, adding acetyl groups to histones, while Histone Deacetylase (HDAC) remove these acetyl groups. ATP-dependent chromatin remodeling enzymes, such as SWI/SNF, can mobilize nucleosomes along DNA, and change DNA accessibility. Adapted from (https://www.mycancergenome.org).

4.1 Chromatin remodelling

ATP-dependent chromatin remodeling enzymes are tightly conserved among different organisms. These enzymes use the energy of ATP hydrolysis to perform several activities: to mobilize nucleosomes along DNA, to remove histones or replace them with histone variants, changing the DNA accessibility and thus regulating gene expression and DNA replication. ATP-dependent chromatin remodeling complexes include: the SWI/SNF (switching defective/sucrose non-fermenting) family, the ISWI (imitation SWI) family, the NuRD (nucleosome remodeling and deacetylation)/Mi-2/CHD (chromodomain, helicase, DNA binding) family and the INO80 (inositol requiring 80) family (**Fig 11**) (*231, 236*).

They play an important role during EMT; for example, the interaction between ZEB1 and SWI/SNF chromatin-remodeling protein BRG1 was demonstrated to be causal to repress E-cadherin promoter during tumor progression (*237*).

4.2 DNA methylation

DNA methylation is a common covalent epigenetic modification in mammals, generally associated with gene silencing (*231, 233*). DNA methylation occurs commonly at the 5-position of cytosine (5mC) and typically in CpG (--C--phosphate--G--) dinucleotides; in fact, about the 70–80% of CpGs are methylated (*229, 231*).
DNA methylation is mediated by a group of specific enzymes, known as **DNA methyltransferases** (**DNMTs**), composed by different members: i) DNMT1, implicated in the maintenance of DNA methylation patterns during cell replication; ii) DNMT3, in particular 3A and 3B, responsible for *de novo* DNA methylation mostly during embryogenesis. Another member belongs to the DNMT3 family, DNMT3-like non-enzymatic regulatory factor DNMT3L, binds unmethylated lysine 4 (Lys 4) of histone H3 (*229, 231, 235, 238*). (**Fig 11**)
RASAL1 encodes an inhibitor of Ras oncoprotein, and its hypermethylation mediated by DNMT1 and consequent genetic silencing, is associated with fibroblast activation and renal fibrosis (*239*). During EMT, changes of DNA methylation can be regulated by TGFβ in both breast and ovarian cancer. In epithelial ovarian cancer (EOC), TGFβ can modulate the expression and activity of DNMTs, inducing global changes in DNA methyloma and specific changes of DNA methylation of target genes (e.g. E-cadherin and COL1α1 promoter) (Cardenas et al., 2014).
Studies on the role of DNA methylation in non-tumoral EMT and fibrosis in peritoneum and other organs are scarce. Kim and colleagues studied the effects of the demethylating agent 5-azacytidine in non-uremic model of rat in which it was induced EPS. 5-azacytidine stimulated a reduction of the pathological effects of EPS on peritoneum and a decrease of TGFβ, α-SMA, Col1 and fsp-1. A reduction of DNMT1 expression and RASAL1 hypermethylation was linked with all these improvements (*240*). EMT reversal may be achieved through the regulation of DNA methylation by pharmacological inhibitors. To date, common DNA methylation inhibitors are 5-aza-2'-deoxycytidine or decitabine (5-Aza-dC) and azacitidine (known as 5-azacytidine) (*231, 232, 235*).

4.3 Histone modifications

Histone are characterized by the presence of two different domains: i) a globular domain, which interacts directly with DNA; ii) a N-terminal domain, which forms the histone tails protruding from the nucleosome. The histone tail undergoes a series of posttranslational modifications on specific serine (S), lysine (K), and arginine (R) residues. The pattern of modifications constitutes an information code that controls processes that mediate gene transcription; this pattern is called "**histone code**" (*241*). A variety of modifications has been identified: methylation, acetylation, sumoylation, ubiquitination and phosphorylation. The most common are the acetylation and methylation of lysine residues on histones 3 and 4 (H3 and H4). The acetylation of lysine residues is always associated with a transcriptional

activation, while the methylations may adopt a function of transcriptional repression or activation, in relation with the kind of methylated amino acid and the extension of methylation (monomethylation -me, dimethylation -me2, or tri-methylation -me3).
During EMT, all these modifications are present and they regulate the contemporaneous repression of epithelial genes and activation of mesenchymal genes (*229, 231*).

4.4 Histone methylation

The methylation of lysine residues is mediated by histone methyltransferases (HMTases), divided in SET domain-containing and non-SET domain-containing.
Lysine methylation may be associated with transcriptional activation in a variety of cases (H3K4, H3K36, and H3K79). The methylation of arginine residues by protein arginine methyltransferases (PRMTs) may be associated with transcriptional activation only in the case of H4R3.
DOT1L, a H3K79 HMTase, can mediate the expression of Snail and ZEB1/2 to promote EMT and metastasis. An increment of H3K4me3 and H3K36me3 was found in a TGFβ-induced EMT model (*231*).
In addition, histone de-methylation is regulated by LSD and Jumonji-domain-containing families of histone demethylases (HDMs). LSD1 is over-expressed in several tumors. Snail can interact with LSD1 and recruits it on E-cadherin promoter, where LSD1 demethylates H3K4m2 and suppresses E-cadherin expression (*231, 235*) LSD1 can also induce demethylation of the inactive H3K9me3 mark, causing gene derepression (*233*).
The methylations induced by histone H3K9, H4K20, H3K27, and H4R3 are often associated with transcriptional repression in numerous tumors. H3K27 methylation is mediated by the PRC2/EZH2 complex, which is often upregulated in cancer cells. PRC2 is recruited by Snail on E-cadherin promoter, and reduces its expression. Histone demethylase KDM6B induces demethylation of H3K27m2/3 during TGFβ-induced EMT. Suv39H1 is responsible of trimethylation on H3K9. G9a causes the mono and dimethylation of H3K9(*231, 235*).
Although the vast majority of studies on histone methylation regulators have been performed in tumor models, some reports have analysed the effect of this pathway in MC EMT and fibrosis.
EZH2 is highly expressed in peritoneum of mice during peritoneal fibrosis. Treatment with the EZH2 inhibitor 3-DZNeP attenuated peritoneal fibrosis and inhibited activation of several profibrotic signaling pathways (*242*).
Maeda and collaborators demonstrated that the pharmacological inhibition of G9a, reducing monomethylation of H3K9, attenuates the effects of peritoneal fibrosis, collagen deposition, and TGFβ1 levels in a mouse model and in human MCs (*243*).
Tamura and colleagues used Sinefungin, an inhibitor of SET7/9, promoted the suppression of TGFβ1-induced expression of fibrotic markers and accumulation of collagen through decreased H3K4 monomethylation (*244*). The authors observed an upregulation of both G9a and SET7/9 in nonadherent cells isolated from the effluent of PD patients (*243, 244*). The above-mentioned pharmacological inhibitors were demonstrated to be effective also in models of renal fibrosis (*245, 246*).

4.5 Histone acetylation

Histone acetylation occurs on H3 and H4 histones in many euchromatic regions and it is generally associated with transcriptional activation. Histone acetylation consists in the addition of an acetyl group on lysine residues (e.g. K9 and K14 residues of histone H3). This modification induces the neutralization of lysine positive charges, increasing accessibility of DNA and promoting gene transcription. Histone acetylation is performed by **Histone Acetyl Transferases** (**HATs**) such as PCAF, p300/CBP, TIP60, and hMOF. Instead, transcriptional repression is catalysed by **Histone Deacetylases** (**HDACs**), which remove acetyl residues. Both HATs and HDACs work in multi-protein complexes containing specific co-activators or co-repressors (*231, 233, 234, 242, 247*).

Since the analysis of HAT is not object of this doctoral thesis, only HDACs will be treated extensively. In humans, 18 HDACs have been discovered so far. They are involved in a myriad of activities: gene silencing, DNA replication and DNA damage repair, cell cycle progression, development and differentiation. HDACs may be classified in four classes (Class I-IV) based on their homology to yeast proteins (*241, 248, 249*).

Class I HDACs (homology to yeast RPD3) is composed of four members: HDAC1, HDAC2, HDAC3 and HDAC8. They are ubiquitously expressed and have a constitutive nuclear localization except HDAC8, which is present also in the cytoplasm. All members have a deacetylase catalytic domain (*241, 249*) and are detected in multi-protein complex. HDAC1 and HDAC2 in general are present in repressive complexes such as the Sin3, NuRD, CoResT and PRC2 complexes. HDAC3 also forms complexes such as the N-CoR–smRT complex, while HDAC8 does not appear to be bound to other proteins (*250*).

Class I HDACs, in particular HDAC1 and HDAC2, play an important role during the induction of EMT (*235*). In fact, class I HDACs activity is essential to repress epithelial genes, markedly E-cadherin and ZO-1, and to maintain an EMT status in many tumor cell lines (*231, 251*). Recent studies have revealed that Class I and Class II HDACs are also associated with organ fibrosis (*252, 253*).

Class II HDACs (homology to yeast HDA1) has a tissue specific-expression and a nuclear/cytoplasmic localization. This class is constituted by two subgroups: class IIa HDAC, composed by HDAC4, HDAC5, HDAC7, HDAC9 and class IIb HDAC, composed by HDAC6 and HDAC10 (*241, 254*).

Class III HDACs (homology to yeast Sir2) is composed of Sirtuins (SIRT1/7). Their activity profit from nicotinamide adenine dinucleotide (NAD+) (*235, 241, 250, 254*).

Class IV HDACs (no homology to yeast) contains only one member, HDAC11. It has the same structure of class I HDACs, but its expression is restricted to brain, heart, skeletal muscle, kidney and testis. It has a nuclear localization and has a deacetylase domain (*241, 250*).

4.6 HDAC pharmacological inhibitors (HDACis)

HDACis are a group of natural or newly synthesized compounds able to block HDAC activity, restoring or increasing the levels of histone acetylation. HDACis are a promising class of anticancer drugs. HDACis may be separated in different classes are (*232, 241, 255*):

1. hydroxamic acid, e.g trichostatin A (TSA), vorinostat (SAHA), belinostat (PXD101), and panobinostat (LBH589);
2. cyclic tetrapeptides, e.g. trapoxin B, Apicidin;
3. benzamides, e.g. entinostat (MS-275) and mocetinostat (MGCD0103).

Among all these HDACis, only MS-275 will be described in detail since it has been used in the results section. **Entinostat** (**MS-275**) is a synthetic benzamide specific for class I HDAC and it is a selective inhibitor expecially for HDAC1/2, being HDAC3 inhibited at higher concentration (*256, 257*). Treatment with MS-275 can provoke a variety of effects: changes in cell cycle distribution, cell apoptosis, arrest of cell growth, EMT reversion, block of tumour progression, angiogenesis and metastasis (*248, 258-262*).. In addition, MS-275 promote MMT reversal followed by reduction of invasive and migratory of MCs (*263*). It inhibits deposition of collagen fibrils and expression of collagen I, TGFβRI, FN-1, α-SMA (*263, 264*).

4.7 HDACis in non-tumoral fibrosis

The antifibrotic role HDACis has been validated in a number of in vitro and experimental models of non-tumoral fibrosis.

Choi and colleagues studied the effect of class I HDACs in the human kidney proximal tubule epithelial cell line HK2 and in a model of renal fibrosis. They demonstrated that class I HDACis have more crucial role in renal fibrosis than class II HDACis. Moreover, they demonstrated the role of HDAC8 in the control of E-cadherin re-expression in renal fibrosis (*265*). Lei and collaborators demonstrated that class I HDACis TSA and MS-275 suppress TGFβ1-induced EMT in AML-12 hepatocytes and primary hepatocytes (*266*).

In a rat liver fibrosis model induced by bile duct ligation HDACis treatment is able to reduce hepatic stellate cells activation, to ameliorate hepatic dysfunction and improve survival rate (*267*).

In cardiac fibrosis, HDACis can successfully control both atrial fibrosis and ventricular fibrosis. Liu et al. demonstrated that treatment with TSA ameliorated atrial fibrosis and subsequent atrial fibrillation (AF) (*268*).

Other studies have reported the therapeutic potential of HDACis in idiopathic pulmonary fibrosis. TSA abrogated normal human lung fibroblast (NHLF) differentiation into myofibroblasts whereas small interfering RNA against HDAC4 blocked α-smooth muscle actin accumulation (*269*), Coward et al. demonstrated that epigenetic alterations of cyclooxygenase-2 expression were restored by HDAC inhibition, which induced resistance to pulmonary fibrogenesis (*270*). Thus, while to date several HDACis are approved by US FDA (see below) only for the treatment of hematological malignancies, their validation and the search for new drugs for the treatment of non-tumoral fibrotic diseases is a field of intense study (*253*).

Only a few reports focused so far on the effect of HDACs on MC plasticity and peritoneal fibrosis. Tubastatin A targets HDAC6 of Class II (*271*) and suberoylanilide hydroxamic acid (SAHA) targets all classes of HDACs (*272*). A recent study conducted in our laboratory demonstrated that MS-275 promoted the downregulation of mesenchymal markers (MMP2, COL1α1, PAI-1, TGFβ1, TGFβRI) and upregulation of epithelial markers (E-cadherin, Occludin) in primary peritoneal MCs from PD patients. Gene expression changes were followed by reacquisition of an epithelial-like morphology and marked reduction of cellular invasiveness (*263*).

4.8 HDACis in inflammatory cytokine production and in the interferon response

Although the importance of the inhibition of pro-inflammatory cytokines by HDACis was already demonstrated (*273*), their effects on inflammatory gene expression may vary according to the cell type and the stimulus (*273*). VA has been shown to significantly inhibit LPS-induced production of TNFα and IL-6 by human monocytic leukaemia cells (*274*). SAHA and others HDACIs, including VA, were shown to reduce the production of pro-inflammatory cytokines in vivo and in vitro (*275*). Similarly, the HDACi ITF2357 reduced pro-inflammatory cytokine production in primary cells in vitro, and exhibited anti-inflammatory effects in vivo (*276*), while KBH-A42, another HDACi, inhibited production of proinflammatory cytokines in macrophages (*277*). All these studies point out to the importance of the inhibition of pro-inflammatory cytokines as TNFα in the anti-inflammatory effects of HDACIs. A most recent study (*278*) demonstrated the anti-nociceptive and mainly anti-inflammatory properties of VA at lower doses, making it a very promising drug to be used for new therapeutic indications.

The use of histone deacetylase (HDAC) inhibitors has revealed an essential role for deacetylation in transcription of IFN-responsive genes. HDAC1 associates with both signal transducer and activator of transcription (STAT)-1 and -2, and IFN-α stimulation induces deacetylation of histone H4. Inhibition of HDAC1 by small interfering RNA (siRNA) decreases IFN-α responsiveness whereas expression of HDAC1 augments the IFN-α response, demonstrating that HDAC1 modulates IFN-α-induced transcription (*279*). Specifically, the study demonstrates that the deacetylase protein HDAC1 can interact with both the STAT1 and STAT2 subunits of ISGF3. Importantly, the innate antiviral response is inhibited in the absence of deacetylase activity (*279*).

5. SARS-CoV-2

5.1 Coronaviruses

Coronaviruses are a group of diverse viruses infecting many different animals. They are characterized as zoonotic agents as they can jump from non-human species (usually a vertebrate) to human causing mild to severe respiratory infections. There are four common human coronaviruses that are considered 'seasonal': HcoV-HUK1, HCoV-NL63, HCoV-OC43 and HCoV-229E (*280*). Each year they account for about 15% of the cases of common colds.

In 2002 and 2012 respectively, two highly pathogenic coronaviruses with zoonotic origin, severe acute respiratory syndrome coronavirus (SARS-CoV) and Middle East respiratory syndrome coronavirus (MERS-CoV), emerged in humans and caused fatal respiratory illness, making emerging coronaviruses a new public health concern in the twenty-first century (*281*). At the end of 2019, a novel coronavirus designated as SARS-CoV-2 appeared in the city of Wuhan, China, and caused an outbreak of unusual viral pneumonia. Being highly transmissible, this novel coronavirus disease, also known as coronavirus disease 2019 (COVID-19), has

spread fast all over the world (*282*),(*283*). It has overwhelmingly surpassed SARS and MERS in terms of both the number of infected people and the spatial range of epidemic areas.

5.2 COVID-19 clinical manifestations and epidemiology

Severe acute respiratory syndrome (SARS)-CoV-2 pathogenesis, characterized by clinical phenotypes spanning from asymptomatic infection to mild disease with symptoms related to airways tract implication, severe pneumonia, acute respiratory distress syndrome (ARDS) and multiple organ failure, has been largely studied during the last three years (*284*). The pathophysiological mechanisms underlying these conditions are complex. The early infection phase includes an asymptomatic incubation of 1-14 days followed by disease manifestation (**Fig12**). Seven to 14 days after onset of symptoms, some patients can develop a severe clinical condition. As explained before, this fraction of patients includes mostly elderly patients and/or patients with pre-existing comorbidities. Among COVID-19 patients it was determined that about 30% experienced flu-like symptoms: 25% of them required hospitalization and 1/3 of hospitalized patients was treated in Intensive Care Unit (ICU) (*285*). Overall hospital mortality account 20% of COVID-19 patients, being 81% among those who needed mechanical ventilation, most of them were older with pre-existing morbidities (*286*). Individuals older than 65 are much more at risk of requiring hospitalization or death, than those affected by obesity, hypertension, congestive heart failure, diabetes, asthma, chronic kidney disease or immune-depressed, including cancer patients (*287*). These pre-existing diseases significantly increase the risk of hospitalization, ICU requirement and death upon SARS-COV-2 infection, especially among males (*288*).

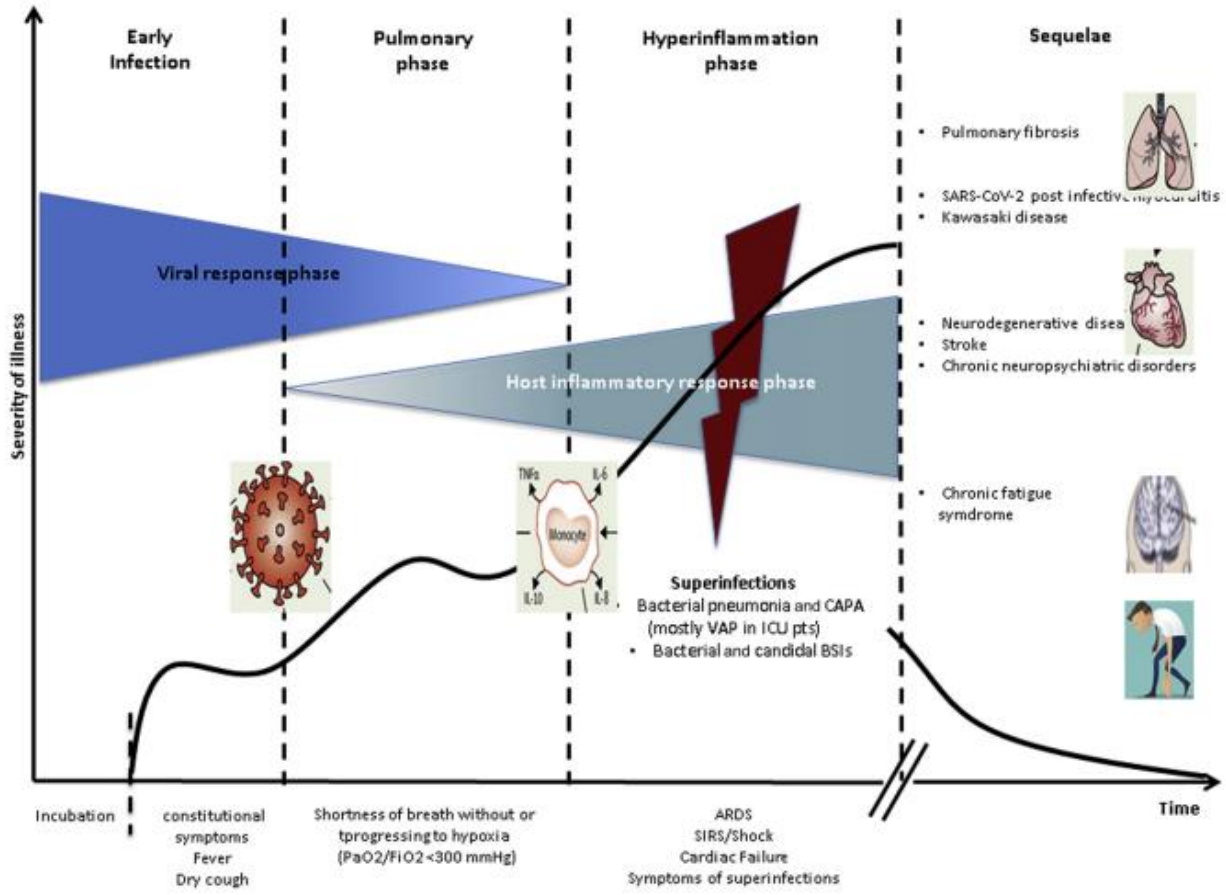

Figure 12 Schematic illustration of SARS-CoV-2 stages over the time.

Epidemiological studies reported the variance of 'predicted COVID-19' phenotype due to genetic factors, reflecting inter-individual variation in the host immune response (*289*). Lucas et al. reported that the immune-profile of patients that easily recovered from COVID-19 were different from those who did not (*290*). There were also pointed out the loss of function mutation in 13 human loci regulating TRL3- and IRF-7 dependent type-1 immunity, transmitted either in autosomal dominant or recessive way, underling susceptibility to life threatening COVID-19 pneumonia. Zhang et al. study estimated that 3,55% of patient with life-threatening COVID-19 disease had genetic defeat ad 8 of these 13 loci (*291*). In a parallel study, it was also estimated that 12,5% of men and 2,6% of women who develop life-threatening COVID-19 disease have autoantibodies against interferon; thus their immune response against viral infection is impaired (*292*). The presence of autoantibodies in the population was estimated at 0,33% and patient with autoantibodies were mostly older than 65. Therefore, these studies identified as subset of individuals with genetic predisposition or acquired predisposition (autoantibodies) to develop severe COVID-19 disease.

The risk of death for young and healthy people is instead very small, and deaths outside the high-risk group are quite rare (*287*). Considering age group and comorbidities, men have a higher risk than women to require ICU treatment or die. This due to genetic predisposition, presence of autoantibodies and testosterone production. Testosterone was related to transmembrane serine protease 2

(TMPRSS2) production, as it is necessary to bind testosterone to its specific receptor (*293*). As it was demonstrated that testosterone levels influence susceptibility to SARS.CoV2 infection, an ongoing phase 2 clinical trial at the University of California in Los Angeles (UCLA) is testing whether temporary suppression of androgens reduces hospital stay, the rate of admission in ICU and death among COVID-19 patients. Several other clinical trials aimed at interfering with androgens are actually ongoing.

Children also can be infected by SARS-CoV-2, but rarely show clinical symptoms and only in exceptional cases require hospitalization. However, a small fraction of them may develop Kavasaky's disease which has been defined as 'multisystem inflammatory syndrome in children'. Besides coronaviruses, Kavasaki's disease can be caused by various pathogens. Overall, the risk that children develop Kavasaki's disease in response to COVID-19 pathogenesis remains very small.

5.3 SARS-CoV-2 pathogenesis

Asymptomatic, mild, and severe diseases have been correlated to different cytokine signatures and to differences in innate and adaptive responses to SARS-CoV-2 infection (*294*),(*295*). It is now well assessed that SARS-CoV-2 first infects epithelial cells of the upper respiratory tract (nasal passages and throat) and especially lungs (bronchi and alveoli), where alveolar type I and type II cells (AT1 and AT2, respectively) are believed to mediate the first encounter with the virus (**Fig13**). Infection of alveolar macrophages is determinant in mediating the amplification of the inflammatory and immune responses (*296*). As the severity of COVID-19 symptoms increase, some patients develop dyspnea with hypoxia. Chest imaging shows the appearance of ground glass opacities in the lung that subsequently acquire a 'crazy paving pattern'. Up to this, laboratory markers of inflammation and organ involvement, as C reactive protein, lactate dehidrogenas, IL-6, ferritin or prothrombin, increase rapidly, while the peripheral blood T- and B-lymphocytes may significantly decrease ((*297*),(*298*),(*299*),(*300*),(*301*)).

Several studies pointed out a role of viral secondary targets implied in the worsening of the pathology. The virus can penetrate in the blood circulation resulting in secondary organ infection. A molecular investigation on COVID-19 autopsies evaluate SARS-CoV-2 secondary infection organs, detecting high viral positivity in nasopharynx (90.4%) followed by bilateral lungs (87.30%), peritoneal fluid (80%), pancreas (72.72%), bilateral kidneys (68.42%), liver (65%) and even in brain (47.2%)(*302*). Literature reports kidney as one of the most probable secondary organs for SARS-CoV-2 infection ((*303*),(*304*),(*305*),(*306*)).

Mechanistically, cell entry is mediated by the engagement of the receptor angiotensin-converting enzyme (ACE2) (*296*) (**Fig13**). ACE2 is also expressed by cells in the kidney, blood vessels, heart, whose infection by SARS-CoV-2 may mediate the characteristic multi-organ pathology (*296*). Viral uptake is also promoted by transmembrane protease serine (TMPRSS)2, which cleaves the spike protein allowing the viral membrane to fuse with the cell and entering. Disintegrin and metallopeptidase domain (ADAM)17 was related to the cleavage of ACE2, in addition to activating the S protein of the virus for membrane fusion (*298,* (*307*). Neuropilin-1 (NRP1) also potentiates SARS-CoV-2 cell entry and infectivity (*308*).

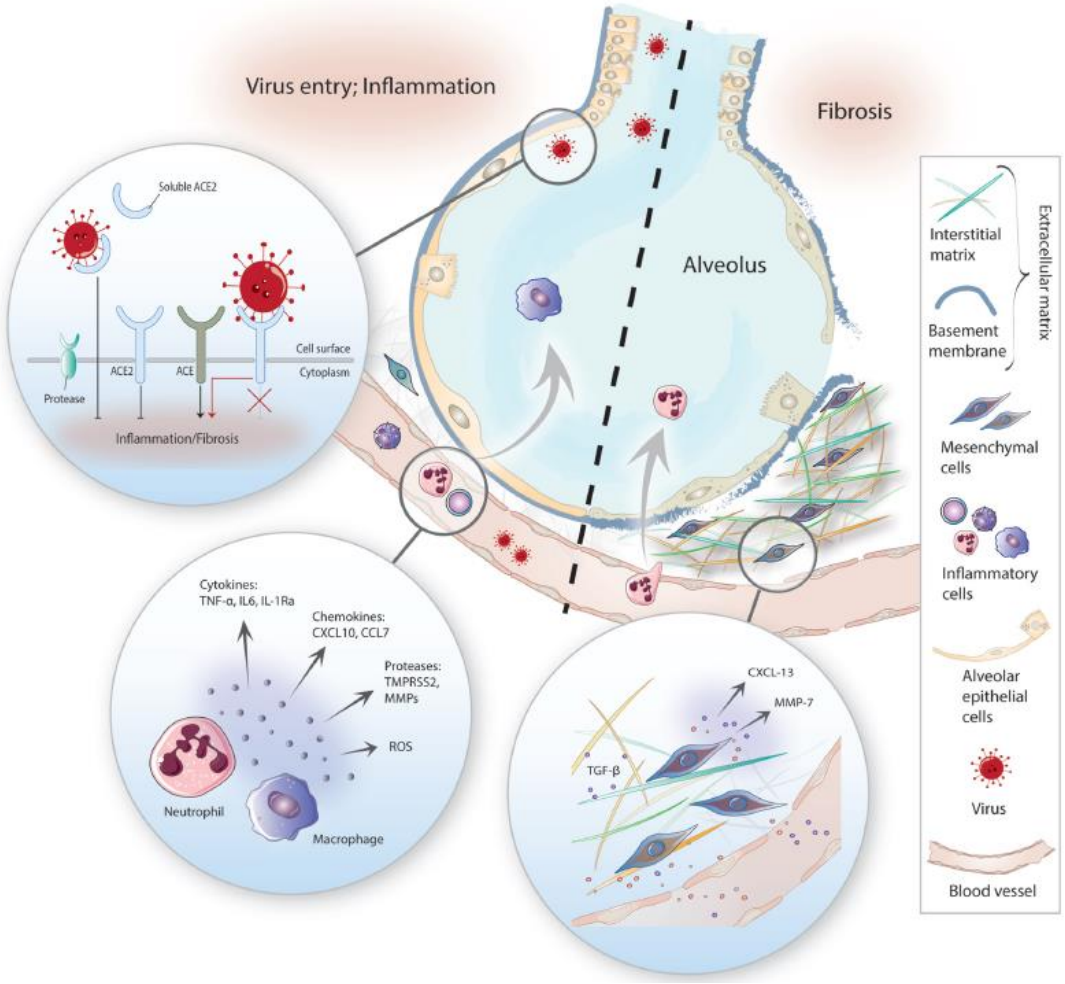

F**igure 13** Schematic illustration of SARS-CoV-2 infection, inflammation and fibrosis pathways.

Epithelial and endothelial infected cells appear strongly damaged after SARS-CpV2 infection and lead to vascular leakage, trigger blood clotting and cause inflammation, which in the worst cases produce a lethal cytokine storm (*309*) (**Fig13**). Histologic analysis of the lung samples from COVID-19 patients show diffuse alveolar damage and pneumocyte hyperplasia, extravasation of fibrin, focal patchy inflammatory infiltration and massive congestion resulting in the thickening of alveolar walls preventing oxygen exchange (*310*). Moreover, the

endothelial damage leads to alveolar capillary micro-thrombi and neoangiogenesis (*311*).

5.4 Approaches to counteract SARS-CoV-2 infection

To date, there are no generally proven effective therapies for COVID-19 or antivirals against SARS-CoV-2, although some treatments have shown some benefits in specific context and patients courts. Researchers and manufacturers are conducting large-scale clinical trials to evaluate various therapies for COVID-19. Here we summarized the ongoing approach to contrast SARS-CoV-2 entry, replication or induced strong immune response. Vaccination is the most effective method for a long-term strategy for prevention and control of COVID-19 in the future. Many different vaccine platforms against SARS-CoV-2 have been developed. The strategies include recombinant vectors, DNA, mRNA in lipid nanoparticles, inactivated viruses, live attenuated viruses and protein subunits (*312*),(*313*),(*314*). The whole-virus COVID-19 vaccine had a low rate of adverse reactions and effectively induced neutralizing antibody production (*315*).

SARS-CoV-2 uses ACE2 as the receptor and human proteases as entry activators; subsequently it fuses the viral membrane with the cell membrane and achieves invasion. Thus, drugs that interfere with entry may be a potential treatment for COVID-19. A potential therapeutic strategy is to block binding of the S protein to ACE2 through soluble recombinant hACE2, specific monoclonal antibodies or fusion inhibitors that target the SARS-CoV-2 S protein (*316*),(*317*),(*318*). The safety and efficacy of these strategies need to be assessed in future clinical trials.

Other approach could be to inhibit viral replication. Among replication inhibitors have been evalued remdesivir (GS-5734), favilavir (T-705), ribavirin, lopinavir and ritonavir and many other in the clinical practice to counteract COVID-19 pathology. Except for lopinavir and ritonavir, which inhibit 3CLpro, the other three all target RdRp128,135. Remdesivir has shown activity against SARS-CoV-2 in vitro and in vivo (*319*),(*320*) and it has been approved for treatment in clinical practice (https://www.aifa.gov.it/documents/20142/1123276/remdesivir_update01_24.11.2020.pdf).

SARS-CoV-2 triggers a strong immune response which may cause cytokine storm syndrome (*321*),(*322*). Thus, immunomodulatory agents that inhibit the excessive inflammatory response may be a potential adjunctive therapy for COVID-19The interferon response is one of the major innate immunity defences against virus invasion. Interferons induce the expression of diverse interferon-stimulated genes, which can interfere with every step of virus replication. Previous studies identified type I interferons as a promising therapeutic candidate for SARS (*323*). In vitro data showed SARS-CoV-2 is even more sensitive to type I interferons than SARS-CoV, suggesting the potential effectiveness of type I interferons in the early treatment of COVID-19 (*324*). A recent study demonstrated the role of M2 in SARS-CoV-2 infection: treatment with extracellular vesicles generated from activated M2 against SARS-CoV-2 effectively reduce excessive cytokine, as TNFα and IL-6, released in vitro and in vivo, attenuating oxidative stress and multiple organ (lung, liver, spleen and kidney) damage in endotoxin-induced cytokine storms (*325*).

Convalescent plasma treatment is another potential adjunctive therapy for COVID-19. Preliminary findings have suggested improved clinical status after the treatment (*326*),(*327*). However, this treatment may have adverse effects by causing antibody-mediated enhancement of infection, transfusion-associated acute lung injury and allergic transfusion reactions. Monoclonal antibody therapy is an effective immunotherapy for the treatment of some viral infections in select patients. Recent studies reported specific monoclonal antibodies neutralizing SARS-CoV-2 infection in vitro and in vivo (*328*),(*329*),(*330*),(*331*). Compared with convalescent plasma, which has limited availability and cannot be amplified, monoclonal antibodies can be developed in larger quantities to meet clinical requirements. Hence, they provide the possibility for the treatment and prevention of COVID-19. The neutralizing epitopes of these monoclonal antibodies also offer important information for vaccine design. However, the high cost and limited capacity of manufacturing, as well as the problem of bioavailability, may restrict the wide application of monoclonal antibody therapy.

Epigenetic anticancer drugs have been evaluated as potential therapeutic in SARS-CoV-2 infected patients (*332*). In particular, HDAC6 selective inhibition has proposed as therapeutic strategy to restore the downregulated immune response in severe COVID-19 patients (*333*). Recent studies have identified valproic acid (VPA), an HDAC3 inhibitor, able to reduce ACE2 expression in different epithelial and endothelial cell lines (*334*),(*335*),(*336*), and TMPRSS2 expression in prostate cancer cells (*337*).

AIM OF THE PhD THESIS

To characterize MC response to viral infections mimicked by TLR3 stimulation with Poly(I:C) or upon exposure to SARS-CoV-2 on MCs in terms of inflammatory/profibrotic response.

To analyse the role of HDAC1/2 inhibition on the regulation of MC response to TLR3 stimulation with Poly(I:C) or SARS-CoV-2 infection.

MATERIALS and METHODS

1. Patients and Cell culture

Effluent-derived MCs were isolated from 11 PD patients as described previously by Lopez-Cabrera et al. (*157*), with some changes. Demographic and clinical features of the patients are described in **Table 1**. The bags with peritoneal dialysates from patients were left untouched for about 12 hours to allow the deposition of floating cells at the bottom of the bags. The supernatant was removed, with a sterile pipette leaving approximately 200 ml of sediment at the bottom of the bags. The cells in 50-ml tubes were centrifuged at 2000 rpm for 5 minutes. The cell pellets were suspended in 4 ml of culture medium and were seeded in 60-cm tissue culture dish. The culture medium was replaced every 2 days and the cell were washed to remove all detached peritoneal leukocytes. Baseline clinical data from these patients are reported in **Table 1**. MCs from PD effluents express the mesothelial markers intercellular adhesion molecule (ICAM)-1 and cytokeratins 8–18, although at lower levels than healthy HPMCs. MC cultures were negative for the endothelial marker CD31 and the pan-leukocyte marker CD45 ((*21*),(*82*),(*86*)). Effluent-derived MCs were cultured in Earle's M199 supplemented with 10% FBS (Gibco-Life Technologies) 2 mM L-glutamine (EuroClone), 100 U/ml penicillin, 100 µg/ml streptomycin (Gibco-Life Technologies) and amphotericin B (2,5 µg/ml).
The human mesothelial cell line MeT-5A (ATCC, Rockville, MD) was cultured in Earle's M199 as above (except for amphotericin B). This cell line was isolated from pleural fluids obtained from a non-cancerous individual.
Cell lines were grown at 37°C, in a humidified atmosphere with 5% CO2. MCs from patients were treated with DMSO or MS-275 (0,25 µM), Poly(I:C) 2ng/ml and TGFβ 2ng/ml. MeT5A cells were treated with DMSO or MS-275 in a dose dependent experimental model at the following doses: 1 µM; 0.5 µM; 0.25 µM; 0.125 µM; 0.06 µM and 0.03 µM. Treatment with DMSO or MS-275 was repeated every 48 hours during the experimental procedure.

Experiments on effluent-derived MCs were performed according to guidelines from the ethics committee of Sant'Andrea Hospital, Sapienza University (Rome, Italy). Written informed consent was obtained from all PD patients. The protocol and informed consent were reviewed and approved by the Ethics Committee of Clinic Investigation of Sapienza University ref: 4697_2017 (Roma, Italy).

Table 1 Demographic and Clinical features of PD patients.

Patient	sex	age	cause of kidney failure	Diabetes	Hypertension	months on PD	PD technique	exchanges	glucose (mg/dl)	peritonitis	hemoperitoneum	escapes
1	M	56	malignant hypertension	no	yes	40	CAPD	1	2270	no	no	no
2	M	69	unknown	no	yes	44	CAPD	4	1580	no	no	no
3	F	85	p-ANCA vasculitis	no	yes	58	CAPD	3	1815	no	no	no
4	M	75	Ig A GNF	no	yes	92	APD	15 liters/night	1360	no	no	no
5	M	61	diabetes/hypertension	yes	yes	12	CAPD	1	2270	no	no	yes
6	F	66	p-ANCA vasculitis	no	yes	31	CAPD/ CCPD	4/20 liters/24 h	2270	no	no	no
7	M	66	Chronic pielonephritis	no	yes	72	CAPD	2	2270	2	no	no
8	M	53	ADPKD	no	yes	6	CAPD	3	2270	2	no	yes
9	M	54	unknown	no	yes	13	CAPD	1	1360	no	no	no
10	M	64	Ig A GNF	no	yes	55	CCPD	25 liters/24 h	1580	2	no	yes
11	M	57	type 1 diabetes mellitus	yes	yes	56	CCPD	20 liters/24 h	1815	no	no	no

2. Viral infection

Subconfluent MeT5A (200.000 cells/well) at different experimental conditions (NT, DMSO or MS-275) were incubated with SARS-CoV-2 (SARS-CoV-2 isolate SARS-CoV-2/Human/ITA/ PAVIA1073 4/2020, clade G, D614G (S) obtained from Dr. Fausto Baldanti, Policlinico San Matteo, Pavia, Italy) in serum free Eagle's Minimum Essential Medium at a multiplicity of infection (MOI) of 1 for 1.5 h at 37° C, 5% CO2. Then, cells were washed three times with PBS to remove viral inoculum, and complete culture medium was added. Culture supernatants and cell lysates were collected at 24, 48 and 72 h post infection (p.i.).

3. Viral titration

To estimate the production of infectious SARS-CoV-2, serial dilutions of MeT5A cell culture supernatants of various conditions (NT, DMSO or MS-275) were put in contact with sub-confluent Vero E6 cells seeded in 96-well plates. To evaluate the viral production in Vero E6 cells, the supernatants harvested from the cells infected for the Cytopathic effect (CPE) assay were back-titrated by serial dilutions in three replicates using MEM supplemented with heat-inactivated 2% FBS and 2 mM L-glutamine and added in 96-well plates containing 2.5x104 Vero E6 cells/well. At day 5 after infection, cells were observed for CPE and tissue culture infective dose (TCID) 50/ml was measured and analysed by Reed-Muench method.

4. Antibodies and chemicals

The primary antibodies for western blotting experiments mAb anti-E-cadherin (BD610181) was form BD Transduction Laboratories (Franklin Lakes, NJ). mAbs anti- Mx1(sc-34128) -TUBULIN (sc-32293), -HSP90 (sc-13119), -GAPDH (sc-32233) and –Histone H4 were from Santa Cruz Biotechnology (Dallas, TX). Abs anti-

activated caspase 3, -IFIT1 (23247-1-AP), -SNAIL (L70G2), -STAT1 (9172), -phospho STAT3 (Y701) and -STAT3 (9132) were from Cell Signaling technology (Danvers, MA). pAb anti-IFITM1 (600-74-1) was from Proteintech (Rosemont, IL). pAbs anti –ACE2 (AB_2792286), -ADAM-17 (AB_10980438) were from Invitrogen (Waltham, MA). pAbs anti- TMPRSS2 (ab109131), -MMP14 (ab53712) were from Abcam (Cambridge, UK). Ab anti-acetyl-H3 (06599) was from Millipore (Merk, Kenilworth, NJ). pAbs anti -phospho STAT1(s727), -acetyl H4 (06598) wew from Upstate (SIGMA ALDRICH, Saint Louis, MO).

HRP– conjugated secondary antibodies used were purchased from Jackson immune research: anti-rabbit (JI 711–036-152), anti-mouse (JI 715–036-150).

Antibodies for Immunofluorescence: anti-SAR-CoV Nucleocapsid (#200-401-A50 Rockland Immunochemicals, Inc), anti-dsRNA (Nordic-MUbio, 10010200), anti-FN-1 (ABCAM, ab2413), anti-ACE2 (Invitrogen, AB_2792286), anti-CALNEXIN (Santa Cruz Biotechnology, sc-23954). Cy3-conjugated anti-rat secondary antibodies (Jackson ImmunoResearch, 112-165-003), anti-rabbit Alexa Fluor 488-conjugated (Thermo Fischer, A21206), anti-mouse Alexa Fluor 488-conjugated (Thermo Fischer, A32723). DRAQ5 staining solution (#130-117-343) was from Miltenyi Biotec.

Antibodies for Immunohistochemistry: anti-WT1 (#12609-2-AP) was from Proteintech; anti-cytokeratin AE1/AE3/PCK26 (760-2595) was from Ventana; anti-ACE2 (AB_2792286) was from Invitrogen.

Antibodies for ELISA: anti- TNFα, -IL-1β, -IL-6, -CXCL8 and -CXCL10 were from R&D Systems (MN, USA).

Poly(I:C) (HMW) was from Invivogen (San Diego, USA). MS-275 was from Mai lab. Sodium arsenite was from Sigma-Aldrich.

5. Western blotting

Monolayers of effluent-derived MCs or MeT-5A cells were lysed in CelLytic™ MT Cell Lysis Reagent (Sigma-Aldrich), proteins were quantified by Bradford protein assay reagent (Bio -Rad).

Laemli SDS sample buffer was added, and samples were boiled for 5' at 95°C and were loaded on acrylamide gels. Gels were electrophoresed at 100V in Running Buffer (25mM Tris, 190 mM glycine; 0.1% SDS) and then transferred to a Nitrocellulose or PVDF membranes in Transfer Buffer (50 mM Tris, 40 mM glycine; 0.1% SDS; 20% Methanol). Blots were blocked in 5% non-fat milk prepared in TBS-Tween (10mM Tris-HCl pH 7.5; 150 mM NaCl; 0.05% Tween 20) and incubated overnight with the primary antibody. The day after the blots were incubated with HRP-conjugated species-specific secondary antibodies. Nitrocellulose-bound antibodies were detected by chemiluminescence with ECL (Immobilon Western HRP substrate, Millipore) Acquisition of blots was performed with Chemidoc Touch imaging system and analysed with Image Lab Software release 6.0 (Bio-Rad Laboratories). Molecular size marker ladder (#PM2610, ThermoFisher Scientific).

6. Gelatine Zymography

The protein concentration of cell culture supernatant was measured by BCA assay (P0010, Beyotime) and then mixed with non-reducing sample buffer 5x (4% SDS, 20% glycerol, 0,01% bromophenol blue, 125mM Tris HCL pH 6.8). Equal amounts of proteins were loaded onto 7,5% SDS polyacrylamide gel containing Gelatin (4 mg/ml) (Thermo-Fisher Scientific) and electrophoresed for 2 h. The gels were washed two times with renaturing buffer (2.5% Triton X-100, 50mM Tris HCL pH 7.5, 5mM CaCl2, 1µM ZnCl2). Then, the gels were incubated in incubation buffer (1% Triton X100, 50mM Tris HCL pH 7.5, 5 mM CaCl2, 1µM ZnCl2) while gently shaking at 37◦ C for 16~18 h. Next, the gels were then stained with staining buffer buffer (0.5 g Coomassie blue, 40% methanol, 10% acetic acid, 50% H2O) for 30 min while gently shaking. Finally, the gels were destained with destain buffer (40% methanol, 10% acetic acid, 50% H2O). The area of enzymatic activity is characterized by no Coomassie blue staining (white bands).

7. Reverse-transcriptase polymerase chain reaction

Cellular RNA was extracted from cell cultures using TRIzol reagent (Life Technologies, Carlsbad, CA) or RNeasy Mini Kit (Qiagen), according to the manufacturer's instructions. cDNA synthesis was generated using a reverse transcription kit (A3500) from Promega (Madison, WI), according to the manufacturer's recommendations. cDNAs were amplified by qPCR reaction using Maxima SYBR Green/ROX qPCR Master Mix (K0253) from Thermo Fisher Scientific (Waltham, MA). qPCR reactions were performed with the Rotor-Gene 6000 thermocycler (Corbett Research, Cambridge, United Kingdom). The primer sequences used in this study are shown in **Table 2**. Relative amounts, obtained with 2 (−ΔCt) method, were normalized with respect to the housekeeping gene L34. Statistical significance was determined with a t test with Prism version 8.0. Differences were considered significant at $p < 0.05$. Values are reported in the graphs.

Target gene	Forward Sequence	Reverse Sequence
hACE2	GGGATCAGAGATCGGAAGAAGAAA	AGGAGGTCTGAACATCATCAGTG
hADAM17	GGGCAGAGGGGAAGAGAGTA	GACTTGAGAATGCGAATCTGCT
hCALB2	ATCCTGCCAACCGAAGAGAA	GCCAAGCCTCCATAAACTCG
hCXCL-8	AGCCTTCCTGATTTCTGCAGCTCT	AATTTCTGTGTTGGCGCAGTGTG
hECAD	TACGCCTGGGACTCCACCTA	CCAGAAACGGAGGCCTGAT
hFN-1	GGCTGACAGAGAGAGFTTCCCG	AGCTGGGTCTGCTAACATCAC
hHDAC1	CATCGCTGTGAATTGGGCTG	CCCTCTGGTGATACTTTAGCAGT
hHDAC2	GAATCCGCATGACCCATAAC	TTCTTCGGCAGTGGCTTTAT
hIFIT1	CTTCAGGATGAAGGACAGGAAG	ACTTGGCTGCATATCGAAAGA
hIFITM1	GAAGTCTAGGGACAGGAAGA	CAGAGCCGAATACCAGTAAC
hIFNα	CTCGCCCTTTGCTTTACT	CATCAAGGTCCTCCTGTTATC
hIFNβ	TGGGAGGCTTGAATACTGCCTCAA	TCTCATAGATGGTCAATGCGGCGT
hIL-1β	AGCCATGGCAGAAGTACCTG	CCTGGAAGGAGCACTTCATCT
hIL-6	AGTCCTGATCCAGTTCCTGC	CATTTGTGGTTGGGTCAGGG
hISG15	CAAATGCGACGAACCTCT	GCTCACTTGCTGCTTCA
hL34	GTCCCGAACCCCTGGTAATAGA	GGCCCTGCTGACATGTTTCTT
hMMP14	TCTGGCGGGTGAGGAATA	CTCTCGTAGGCAGTGTTGATG
hMMP9	GCGCTGGGCTTAGATCATT	GCCATTCACGTCGTCCTTAT
hMx1	AAGCCTGATCTGGTGGACAAAGGA	AACCCTTCTTCAGGTGGAACACGA
hNRP1	AAGGTTTCTCAGCAAACTACAGTG	GGGAAGAAGCTGTGATCTGGTC
hproACE	GTCCCCTGTGAGCCAAGAT	AACCCAAGTTCAAAGGCTGA
hproTMPRSS2	GCATCTCAGCGAGTTTCCAG	GTGCGCCTTTTCTCTTTGGG
hSNAIL	CACTATGCCGCGCTCTTTC	GCTGGAAGGTAAACTCTGGATTAGA
hTLR1	CAATGCTGCTGTTCAGCTCTTC	GCCCAATATGCCTTTGTTATCC
hTLR2	AATCCTCCAATCAGGCTTCTCT	TGTAGGTCACTGTTGCTAATGTAGGT
hTLR3	GAAAGGCTAGCAGTCATCCAAC	GTCAGCAACTTCATGGCTAACA
hTLR5	ACAAGATTCATACTCCTGATGCTACTG	CCAGGAAAGCTGGGCAACTA
hTMPRSS2	AATCGGTGTGTTCGCCTCTAC	CGTAGTTCTCGTTCCAGTCGT
hTNFα	GCTGCACTTTGGAGTGATCG	TCACTCGGGGTTCGAGAAGA

Table 2 List of primers used in the study.

8. siRNA-mediated knockdown

siGENOME SMARTpool siRNAs HDAC1(3065), siHDAC2 and SiRNA control were purchased from Dharmacon. 200×103 MeT5A were seeded on 12-well plates 24h prior transfection. Cells were transfected with 25pmol of siRNAs and 3,5 µl Lipofectamine® RNAiMAX Reagent (Thermo Fisher Scientific) were diluted in two different tubes with 200 µl Opti-MEM (Gibco-Life Technologies). The two solutions were mixed gently and were incubated for 10-20 minutes at room temperature. Transfection solutions were added to cells with 0.6 ml of supplemented medium. Efficiency transfection was evaluated using RT-PCR.

9. Immunofluorescence and Confocal Microscopy

After specific treatment cells were fixed for 20 minutes in 4% formaldehyde in PBS, were permeabilized in 0.2% Triton X-100/PBS for 5 minutes and were blocked with 2% BSA for 20 minutes. Coverslips were mounted in Prolong Gold antifade (Life Technologies) and examined under a confocal microscope (Leica TCS SP2, Wetzlar, Germany). Digital images were acquired with the Leica software and the image adjustments and merging were performed by using the appropriated tools of ImageJ software. A minimum of 4 fields per sample (at least 150 total cells per total) from two independent experiments was analysed. ImageJ was used to quantify relative florescence.

10. Cytokine detection

Supernatants from SARS-CoV-2 infected MeT5A cell cultures were collected at 24 and 72 h after infection. We performed multianalyte profiling of 37 cytokines, chemokines, and soluble mediators in the supernatants of all samples, using the Luminex based multiplex bead technology (Bio-Plex Pro Human Cytokine Panel group I: APRIL / TNFSF13, BAFF / TNFSF13B, sCD30 / TNFRSF8, sCD163, Chitinase-3-like 1, gp130 / sIL-6Rβ, IFN-α2, IFN-β, IFN-γ, IL-2, sIL-6Rα, CXCL8, IL-10, IL178 11, IL-12 (p40), IL-12 (p70), IL-19, IL-20, IL-22, IL-26, IL-27 (p28), IL-28A / IFN-λ2, IL-29 / IFN λ1, IL-32, IL-34, IL-35, LIGHT/TNFSF14, MMP-1, MMP-2, MMP-3, Osteocalcin, Osteopontin, Pentraxin-3 sTNF-R1 sTNF-R2, TSLP, TWEAK / TNFSF12, (Biorad, Laboratories, CA, USA). The assay was conducted accordingly to manufacturer's recommendations. Plates were measured using the Bio-Plex MagPix System and analysed with the Bio-Plex Manager version 6.0 (BioRad Laboratories, CA, USA).

Supernatants of NT, Poly(I:C) and/or MS-275 treated MCs were collected after treatment. TNFα, IL1-β, IL-6, CXCL8 and CXCL10 were measured in supernatants samples by using an ELISA assay (R&D Systems, Inc, MN, USA).

11. Autoptic lung and pleura

Lung tissue samples, including pleura, were obtained from post-mortem examination of four SARS-CoV-2-infected patients, performed at the National Institute for Infectious Diseases Lazzaro Spallanzani-IRCCS Hospital (Rome, Italy). All patients were diagnosed as COVID-19 by SARSCoV-2 RT-PCR performed on nasopharyngeal and oropharyngeal swabs. Demographics and clinical characteristics of patients are shown in **Table 3**. Autopsies were performed according to guidance for post-mortem collection and submission of specimens and biosafety practices to reduce the risk of transmission of infectious pathogens during and after the post-mortem examination (*338*). The study was approved by the local Clinical Research Ethics Committee (approval number: no 9/2020). Written informed consent was waived by the Ethics Commission due to public health outbreak investigation. Lungs samples, including pleura, of four non-COVID-19 patients were used as comparative controls (**Table 4**). Specimens from lung tissues were fixed in 10% neutral buffered formalin, and routinely processed to paraffin blocks.

Table 3 Demographic and clinical features of COVID-19 patients.

Patient	Gender	Age	Comobidities	Cause of Death
1	M	81	Hypertension cardiomyopathy, Aortic aneurysm	Myocardial infraction, Diffuse alveolar damage (ARSD), Interstitial pneumonia
2	M	54	None	Interstitial neumonia, Myocarditis
3	M	82	Not known	Interstitial neumonia, Cardiorespiratory failure
4	M	74	Hypertension, Knee arthroplasty	Interstitial neumonia, Cardiorespiratory failure

Table 4 Demographic and clinical features of non-COVID-19 patients.

Patient	Gender	Age	Comobidities	Cause of Death
1	M	58	Hemicolectomy	H1N1 Pneumonia
2	M	43	Alcoholic cirrhosis	Interstitial pneumonia and pulmonary fibrosis
3	M	47	None	Cardiorespiratory failure
4	F	47	Surgery for frontotemporal meningioma and kidney cancer	Myocarditis and Interstitial pneumonia

12. Immunohistochemistry of pleura

Deparaffinized and rehydrated sections were used for immunohistochemistry. Organ sections were immersed in 10 mM sodium citrate, pH 6.0 and microwaved for antigen retrieval and immunostained on BenchMark ULTRA system fully automated instrument (Roche, Basel, Switzerland). All cases were independently analysed by two pathologists.

13. Proteomics: Protein digestion, peptide purification and nanoLC analysis

Primary human MCs with or without MS-275 samples (n = 2) were lysed in RIPA Buffer and quantified by Bradford assay. 15 ug of protein extract per sample were treated with DL-Dithiothreitol (10 mM at 56 C) and Iodoacetamide (55 mM at RT) for disulfide bond reduction and alkylation, respectively. After 100% ethanol precipitation, samples were resuspended in 50 mM NH4HCO3 and 2 M urea before being digested by trypsin (0.6 lg/ sample) overnight at 37 C. The peptide mixture was acidified with 0.5% trifluoroacetic acid and fractionated using the High pH Reversed-Phase Peptide Fractionation Kit (Thermo Fisher Scientific) following the manufacturer's protocol. Peptides in each fraction (8/sample) were dried, resuspended in 2.5% acetonitrile 0.1% TFA and 0.1% formic acid and then analysed by an UltiMate 3000 RSLCnano-LC system, (Thermo Fisher Scientific) connected on-line via a nano-ESI source to an Q Exactive plusTM Hybrid Quadrupole-OrbitrapTM Mass Spectrometer (Thermo Fisher Scientific). Each peptide mixture was separated on the analytical C18 column (PepMapTM RSLC C18, 150 mm × 75 lm, Thermo Fisher Scientific) using a 100 min multistep elution gradient from 4% to 90% of mobile phase B (0.1% formic acid in 80% ACN) at a constant flow rate of 300 nl/min. Eluted peptides were electrosprayed directly into the mass spectrometer with an ESI voltage of 2.0 kV. Mass spectrometry data were acquired in a positive mode using a data-dependent mode selecting the 15 most intense ions with the following parameters: full scan spectra range from m/z 350.0 to m/z 1,700.0, resolution of 70,000, injection time 100 ms, AGC target 3×106, isolation window ± 2.0 m/z and the dynamic exclusion 20 s. For HCD fragmentation, resolution was set to 17,500, AGC target to 10,000 and injection time to 80 ms. Proteins were automatically identified by MaxQuant (v. 1.6.17.0) software. Tandem mass spectra were searched against the Homo sapiens dataset of UniprotKB database (Release: Feb 2016; 550,552 sequences). Quantitative comparison among MMT-induced MeT5A with or without MS-275 samples was performed using the label-free quantification algorithm calculated by MaxQuant.

14. Magna ChIP

Chromatin crosslinking and sonication were performed like conventional ChIP (*339*). After determining the DNA concentrations, for each sample were used 50 µg of chromatin. It was diluted 10 folds with dilution buffer (TE 1x, sodium dodecyl sulfate (SDS) 0.5% and protease and phosphatase inhibitors) and was incubated overnight with 5 µg of acethyl-H3 antibody or rabbit IgG and 20 µl magnetic beads. Immuno-precipitated samples were put on a magnetic rack and Input sample was recovered by the supernatant of the IgG control. The samples were washed with four successive buffers: I) Low salt Buffer, II) High salt Buffer, III) LiCl Buffer, IV) TE Buffer. During the washes, the samples were in rotation, and, at the end of each wash, magnetic beads were recovered. Then, the samples were dissolved in 300 µl of elution buffer (1% SDS, 0.1M NaHCO3) and 10 mg of RNase A; 0.5% SDS and RNase were added to the Input sample for 10 min at RT. 30 µl of Proteinase K (10 mg/ml) were added to all the samples (included input). Elution, proteinase K and

reversal cross-link steps were performed at 62°C for 5 hours while vortexing. DNA extraction was performed like conventional ChIP, see above. Finally, DNA was resuspended in 50 µl of nuclease free water.

15. Statistical analysis

Statistical significance was determined with a t-test using GraphPad Prism version 8.0 (La Jolla, CA, USA). Differences were considered significant at $P < 0.05$. Statistical significance for viral infection was determined with a nonparametric Wilcoxon signed rank test with GraphPad Prism version 8.0 (La Jolla, CA, United States). Differences were considered significant at $p < 0.05$.

Perseus software (version 1.6.7.0) after log2 transformation of the intensity data was applied to proteomic study. Statistical analysis was carried out on proteins identified in 100% of the samples. Results were considered statistically significant at $P < 0.05$. To improve visualization, a z-score plot and a cluster heat map were generated and Gene ontology enrichment analysis of biological processes, molecular functions and cellular components were performed.

RESULTS

1. Stimulation with Poly(I:C), a TLR3 agonist, induces the expression of TLR3 and other TLRs relevant in the response to pathogens in primary MCs from PD patients

In order to analyse MCs sensing of microorganisms-related molecules, we analysed the expression of TLRs implicated in the response to pathogens. In these experiments primary MCs from PDs patients were used. Untreated MCs were found to express TRL1, TRL2, TRL3 and TLR5 (**Fig 14A**).
Once treated with Poly(I:C), a synthetic analog of dsRNA used to mimic double-stranded RNA (dsRNA) released during viral infections and inducing TLR3 mediated responses, TLR3 expression was further induced. Interestingly, Poly(I:C) treatment promoted an increase of also TLR1, TLR2 and TLR5 gene expression (**Fig 14B**). This result suggests that viral sensing by TLR3 may modulate the response towards other microorganisms, such as bacteria, in peritoneum MCs.

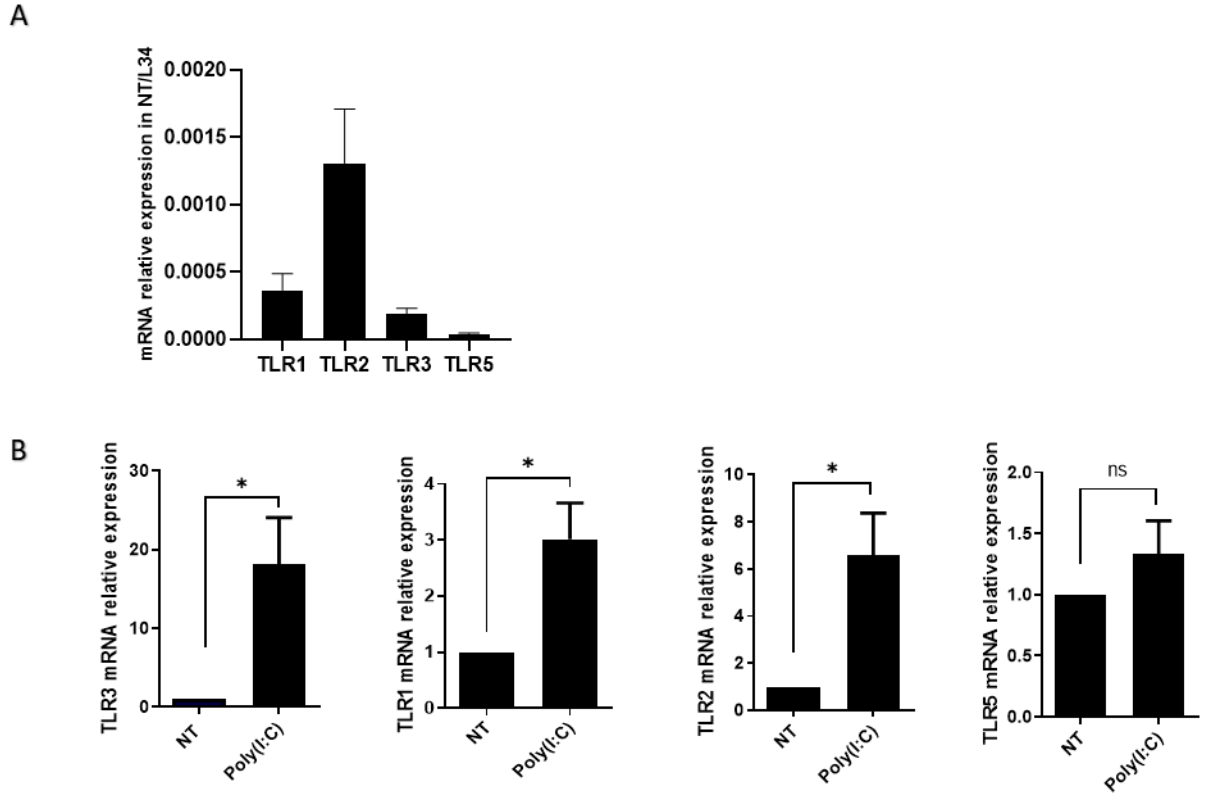

Figure 14 MCs express a specific subset of TLRs, which result modulated upon Poly(I:C) stimulation. (A) Quantitative RT-PCR expression analysis of *TLR1, TLR2, TLR3* and *TLR5* in untreated MCs. L34 mRNA levels were used for normalization. Bars represent the mean ± SEM of triplicate determinations in at least seven independent analysis. **(B)** Cells were treated for with 2 ng/ml Poly(I:C) for 48 hours. Quantitative RT-PCR expression analysis of *TLR1, TLR2, TLR3* and *TLR5* in Poly(I:C) treated MCs compared to NT. L34 mRNA levels were used for normalization. Bars represent the mean ± SEM of triplicate determinations in at least six independent experiments. *P* was calculated with respect to NT samples. Differences were considered significant at $p < 0.05$.

2. Poly(I:C) stimulation induces MMT

To analyse the role of TLR3 stimulation in the modulation of MC plasticity, we stimulated primary MCs derived from PD patients with Poly(I:C) for 48 hours. Alternatively, MCs were stimulated with TGFβ1 as a positive control of MMT induction.

Treatment with Poly(I:C) promoted the acquisition of a spindle-like shape in MCs (**Fig 15A**). Gene expression analysis revealed the upregulation of the mesenchymal marker Snail, the EMT master gene, and the downregulation of the epithelial markers E-cadherin and Calretinin (**Fig 15B, 15D**).

Moreover, fibrosis related genes such as Fibronectin and Metalloproteinase (MMP)-9 and -14 were also induced **(Fig 15C-D**). Immunofluorescence experiments revealed Fibronectin fibre formation upon Poly(I:C) treatment (**Fig 15E**).

These results indicated that stimulation of TLR3 with Poly(I:C) is sufficient to induce a bona fide MMT in MCs from PD patients.

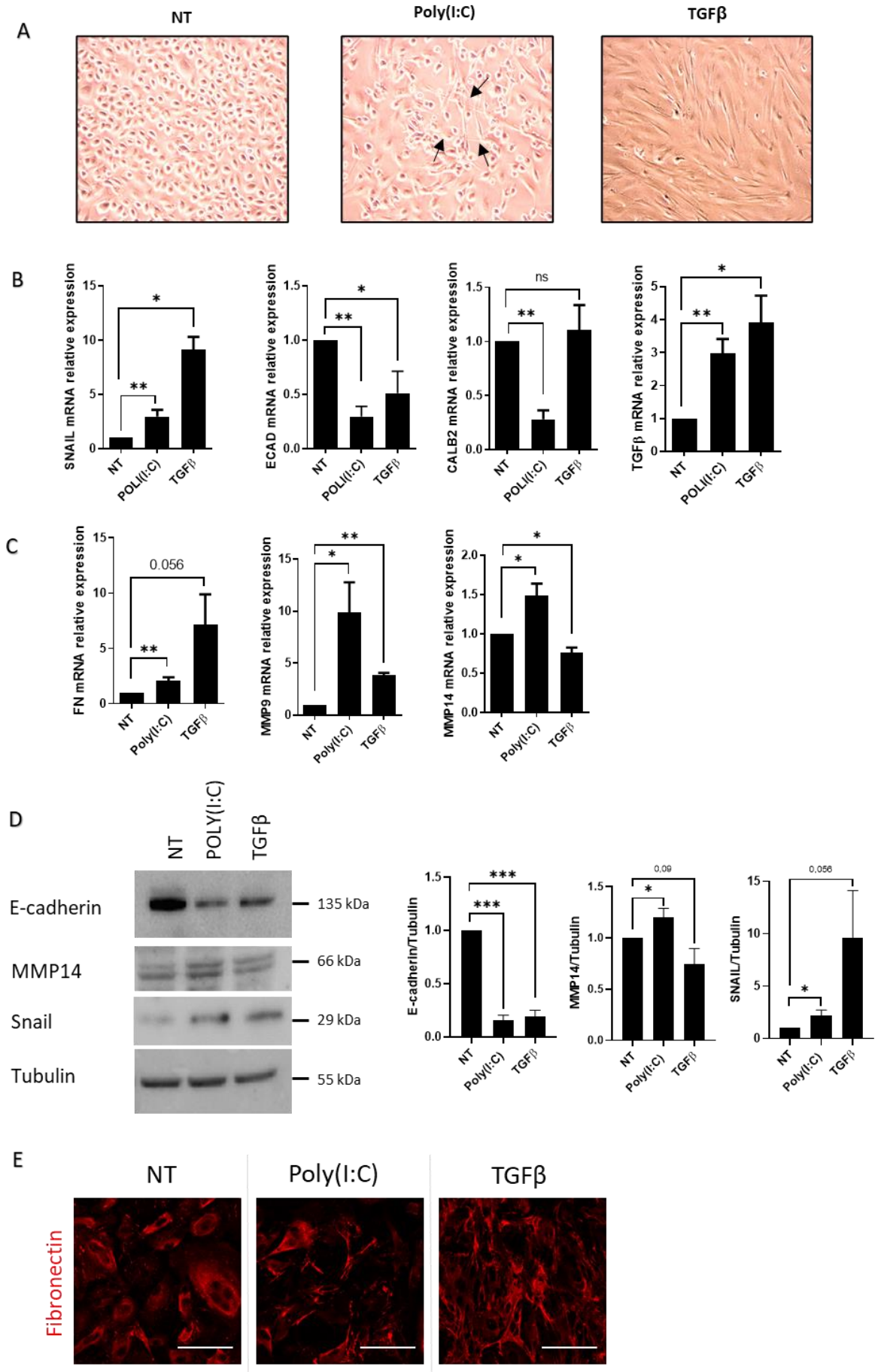

Figure 15 Poly(I:C) induces MMT in MCs. *(continues on the following page)*

(*following*) Cells were treated for with 2 ng/ml Poly(I:C) or 2 ng/ml TGFβ for 48 hours **(A)** MCs after Poly(I:C) or TGFβ stimulation compared to NT. Poly(I:C) stimulated MCs present a typical spindle shape (arrow) indicating changes in cellular plasticity. **(B-C)** Quantitative RT-PCR expression analysis of *SNAIL, E-CAD, CALB2, TGFβ, FN, MMP9* and *MMP14* in Poly(I:C) or TGFβ treated MCs compared to NT. L34 mRNA levels were used for normalization. Bars represent the mean ± SEM of triplicate determinations in at least six independent experiments. *P* was calculated with respect to NT samples. Differences were considered significant at $p < 0.05$. **(D)** Left: Western blot showing the expression of E-Cadherin, MMP14 and SNAIL from total lysates of MCs. Tubulin was detected as a loading control. Right: WB quantification in Poly(I:C) or TGFβ treated MCs compared to NT. Bars represent the mean ± SEM of triplicate determinations in at least four independent experiments. P was calculated with respect to NT samples. Differences were considered significant at $p < 0.05$. **(E)** Immunofluorescence of MCs treated with Poly(I:C) or TGFβ compared with NT cells. Fixed cells were stained with antibody against Fibronectin. A minimum of 150 cells per sample from three independent experiments were analysed. Scale bar: 50 μm

3. Poly(I:C) stimulation promotes the expression of inflammatory cytokines and chemokines

MMT induction is generally linked to the release of extracellular mediators contributing to the shaping of the microenvironment and of the modulation of the local immune response. Thus, we analysed whether TLR3 stimulation could induce the expression of inflammatory cytokines in MCs.
Poly(I:C) treatment induced upregulation of TNFα, IL-6 and CXCL8 gene expression (**Fig 16A**). Significant increases of TNFα, IL-1β, IL-6, CXCL8 and CXCL10 were confirmed by ELISA assay (**Fig 16B-C**). Of since these cells have been isolated by PD patients, different basal values may reflect specificities of each patient.
These data indicated that, upon TLR activation, MCs from PD patients may activate a pro-inflammatory response.

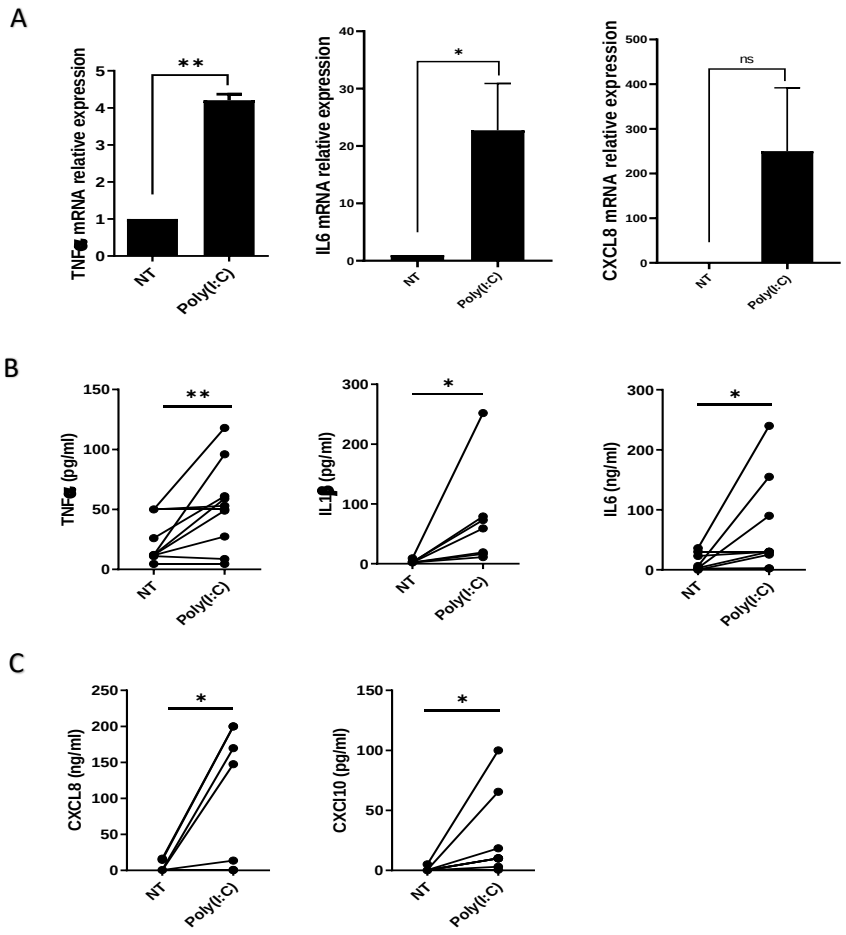

Figure 16 Poly(I:C) induces inflammatory cytokine and chemokine expression in MCs. Cells were treated for with 2 ng/ml Poly(I:C) for 48 hours **(A)** Quantitative RT-PCR expression analysis of *TNFa, IL-6* and *CXCL8* in Poly(I:C) treated MCs compared to NT. L34 mRNA levels were used for normalization. Bars represent the mean ± SEM of triplicate determinations in at least six independent experiments. *P* was calculated with respect to NT samples. Differences were considered significant at $p < 0.05$. **(B-C)** Analysis of cytokine and chemokine secretion from supernatants of MCs treated with Poly(I:C) compared with NT. Poly(I:C) stimulation promoted the release of TNFα, IL-6, IL-1β, CXCL8 and CXCL10. Cytokine were measured by ELISA assay. *P* was calculated with respect to NT samples. Differences were considered significant at $p < 0.05$.

4. Proteomic analysis of MS-275 treated primary MCs reveals a complex reprogramming of MC proteome

Class I HDACs are main determinants of MCs plasticity. It was previously demonstrated that inhibition of HDAC1/2 by MS-275 was sufficient to promote MMT reversal in mesenchymal-like MCs form PD patients ((*263*),(*340*)). Here, we aimed at analyzing the role of HDAC in the profibrotic and proinflammatory response observed upon treatment with Poly(I:C).

To check the ability of MS-275 to limit HDAC activity at the non-cytotoxic concentration (0,25 µM) used in this study, histone (H)3 and H4 acetylation status was analysed. As shown in **Fig 17A**, H3 and H4 were strongly acetylated upon treatment of MCs with MS-275.

In order to clarify molecular mechanisms underlying the effect of HDAC inhibition in this inflammatory context, the proteome from MCs cells left untreated or treated with MS-275 was analysed by quantitative mass spectrometry analysis. Following proteolytic digestion, peptides were separated in 8 fractions based on their hydrophobicity before being analysed by label-free liquid chromatography-mass spectrometry.

Principal component analysis (PCA) indicated that untreated MCs are distributed in a distinct group from MCs treated with MS-275. (**Fig 17B**) Hierarchical clustering classified the samples into two groups based on differentially expressed proteins, as represented by Heat map visualization. (**Fig 17C**). In differential expression analysis (DEA) comparing samples represented by Volcano plot, 859 proteins identified were differentially expressed with FDR<0.05 (**Fig 17D**)

Analysis of specific proteins revealed modulation of proteins implicated in cell plasticity, actine cytoskeleton polymerization, ECM remodeling, inflammatory cytokine production and interferon type-I response (**Table 5**). These data represent the starting point for the further identification of molecular mechanisms controlling MS-275 mediated effects in Poly(I:C) stimulated MCs.

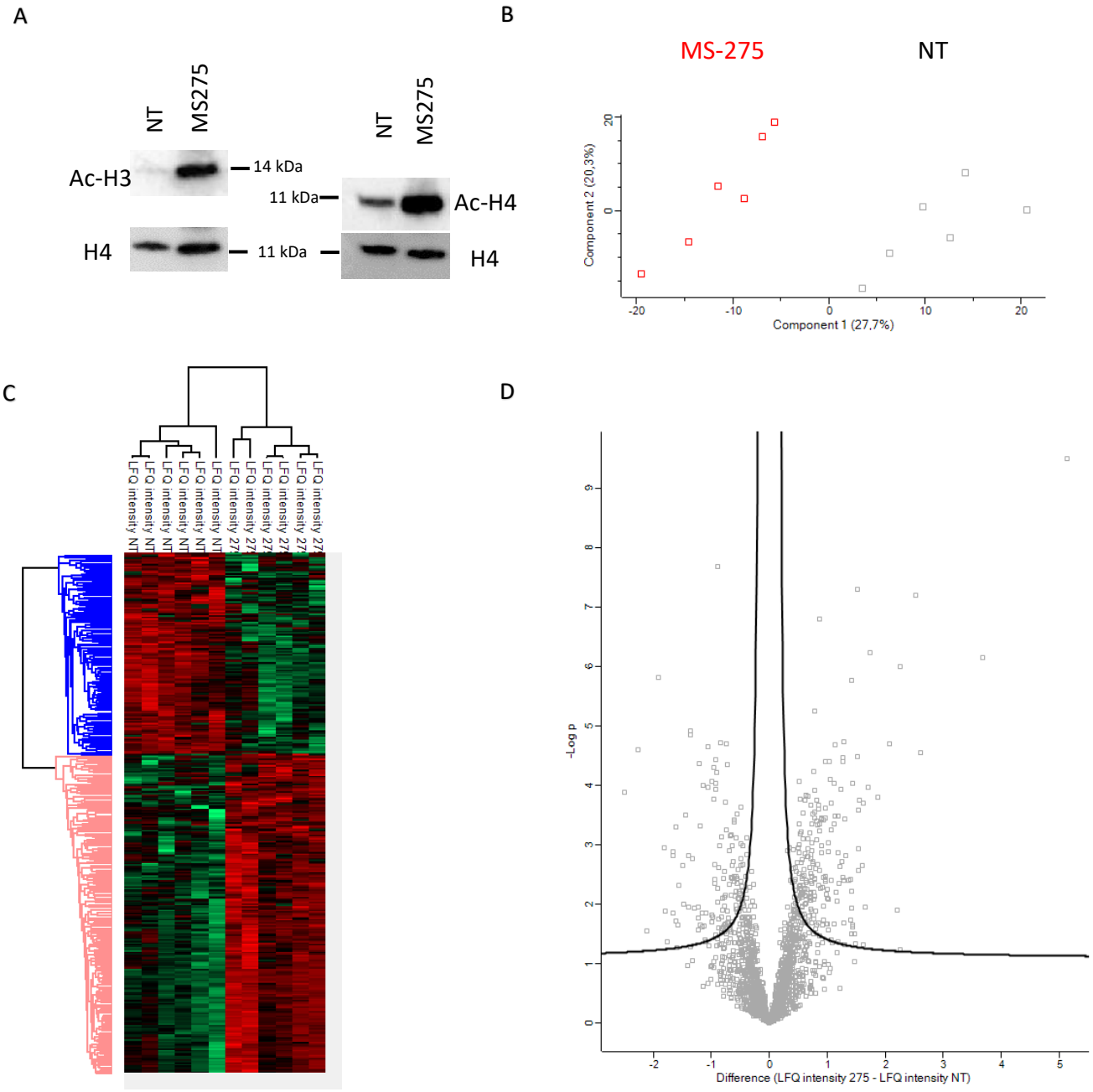

Figure 17 Treatment with MS-275 modifies the proteome of mesenchymal-like MCs. Cells were treated with MS-275 0,25 µM for 48 hours **(A)** Western blot showing the expression of Acetylated H3 and H4 from histone extraction of MCs with MS-275. Total H4 was detected as a loading control. **(B)**Principal component analysis (PCA) of the LFQ intensities obtained in NT and MS-275 treated sample datasets. **(C)** Heat map of differentially expressed proteins in NT and MS-275 samples. LFQ intensities were expressed in z-score values (range of intensity z-score: ±2.4). Up-regulated and down-regulated proteins are expressed in red and green scale respectively. Hierarchical clustering was performed using Euclidean distance and average linkage using the Perseus software. **(D)** Volcano plots comparing NT and MS-275 upregulated proteins. Black curves represent the significance threshold at false discovery rate (FDR) of 0.05 and S0 of 0.1.

Table 5 List of selected protein from proteomic analysis of MS-275 treated MCs vs NT.

Gene names	-log (p value)	Difference (MS275-NT)	Protein names	Peptides	Unique peptides
MX1	3,311663409	-3,088023186	Interferon-induced GTP-binding protein Mx1;Interferon-induced GTP-binding protein Mx1, N-terminally processed	23	23
PXN	2,581957539	-0,915050507	Paxillin	7	7
FILIP1L	2,377091294	-1,675042152	Filamin A-interacting protein 1-like	9	9
STAT1	2,258739737	-1,0362463	Signal transducer and activator of transcription 1-alpha/beta;Signal transducer and activator of transcription	22	22
COL12A1	2,196680386	-0,848173141	Collagen alpha-1(XII) chain	92	92
ZYX	2,181357302	-0,8536129	Zyxin	15	15
IFIT1	2,145186197	-2,775994301	Interferon-induced protein with tetratricopeptide repeats 1	10	10
COL3A1	1,876690489	-0,86049366	Collagen alpha-1(III) chain	15	15
IFI16	1,786550094	-0,579545975	Gamma-interferon-inducible protein 16	12	12
GBP2	1,549655131	0,364129066	Interferon-induced guanylate-binding protein 2	8	5
YAP1	1,45304907	-0,62368679	Transcriptional coactivator YAP1	4	4
ACTA1	1,3798574	-0,547822952	Actin, alpha cardiac muscle 1;Actin, alpha skeletal muscle	25	1
FBLIM1	1,241479819	-1,344466209	Filamin-binding LIM protein 1	8	8
CEMIP	1,235650426	-1,240023613	Cell migration-inducing and hyaluronan-binding protein	29	29
EGFR	1,008111612	-0,917181015	Receptor protein-tyrosine kinase;Epidermal growth factor receptor	12	12
CTNNB1	0,848004368	-0,319928169	Catenin beta-1	12	10
MMP14	0,781902223	-1,061106682	Matrix metalloproteinase-14	3	3
EIF2AK2	0,665573352	-0,218777657	Interferon-induced, double-stranded RNA-activated protein kinase	4	4
IL18	0,660118938	0,775450706	Interleukin-18	8	8
ANXA3	0,639015718	-0,439673424	Annexin A3;Annexin	24	24
VCAM1	0,53865967	-0,57334137	Vascular cell adhesion protein 1	3	3
PRKRA	0,179874635	0,244564056	Interferon-inducible double-stranded RNA-dependent protein kinase activator A	4	4
SERPINE1	0,134158116	-0,119371414	Plasminogen activator inhibitor 1	6	6

5.Treatment with MS-275 rescues Poly(I:C) induced MMT

Since gene ontology analysis revealed also modulation in proteins involved in cytoskeleton and matrix remodelling, we hypothesized that HDAC1/2 inhibition limits Poly(I:C) induced MMT. Pre-treatment with MS-275 rescued the expression of epithelial markers E-Cadherin and Calretinin in Poly(I:C)-treated MCs (**Fig 18A-B**). Confocal microscopy analysis confirms gene expression data of Calretinin downregulation with MS-275 (**Fig 18C**), here we can also observe Calretinin predominant cytoplasmic localization in the cells. Interestingly, Snail, FN and MMP9 mRNA expression resulted to be upregulated upon MS-275 treatment (**Fig18D**). With respect to MMP9 upregulation, MS-275 treatment was shown to impair its activity (**Fig18E**). This apparently paradoxical observation (induction of SNAIL in a frame of MMT reversal) may be interpreted with the help of a previous study from our laboratory showing upregulated Snail expression coupled with its functional inactivation upon MS-275 treatment in MCs (*252*). Also, Fibronectin is increased by MS-275 although not fully functional (Terri et al., Submitted). Overall, these results demonstrated that MS-275 treatment rescues Poly(I:C) induced MMT.

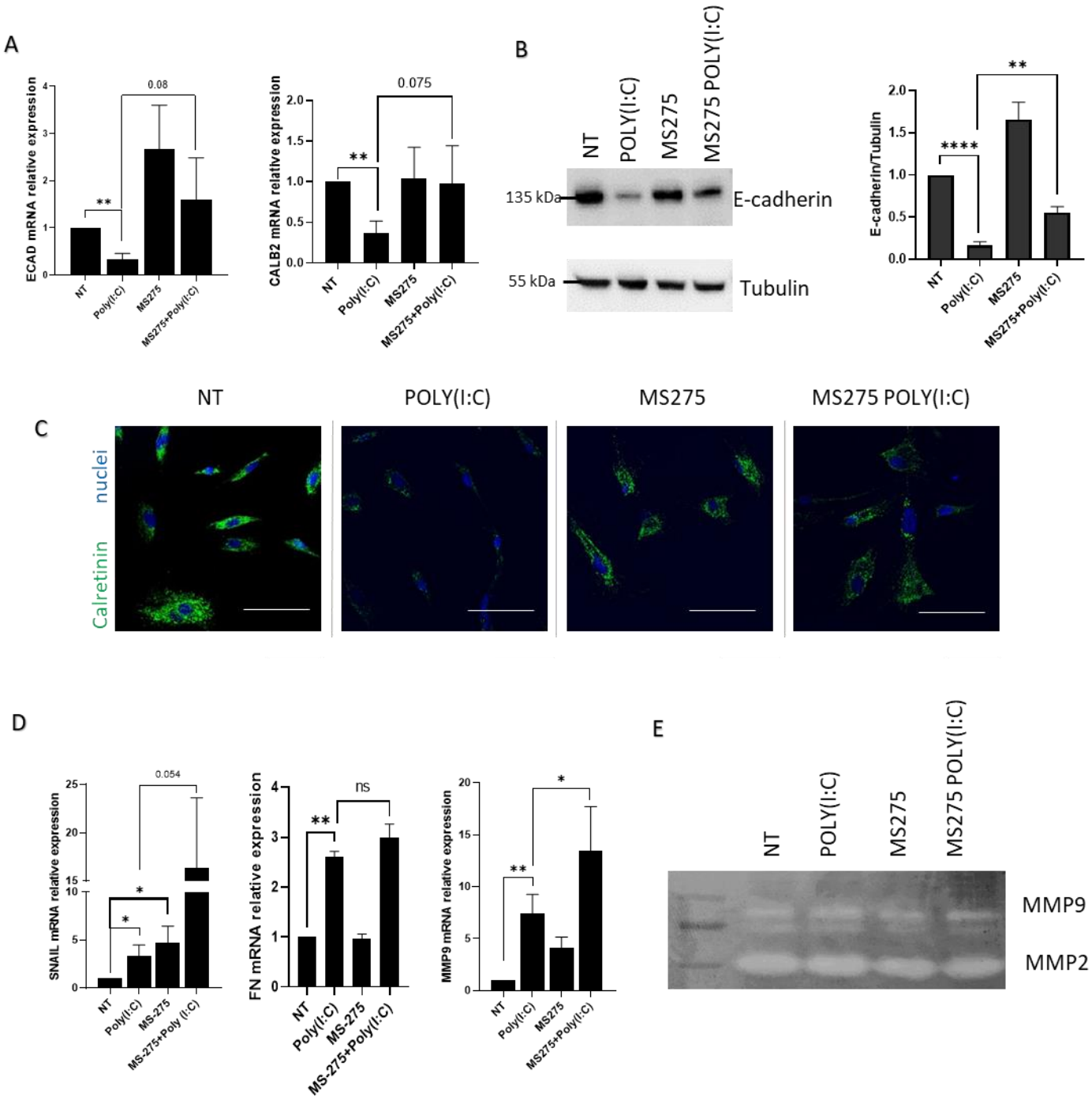

Figure 18 Treatment with MS-275 rescues Poly(I:C) induced MMT in MCs. Cells were treated with 2 ng/ml Poly(I:C) for 48 hours and/or 0,25 µM MS-275 for 72 hours with a second pulse after 48h from the first stimulation; experimental conditions are valid for combinatory or single treatment. **(A)** Quantitative RT-PCR expression analysis of *ECAD* and *CALB2* in Poly(I:C) with/or MS-275 treated MCs compared to NT. L34 mRNA levels were used for normalization. Bars represent the mean ± SEM of triplicate determinations in at least five independent experiments. *P* was calculated with respect to NT or Poly(I:C) samples. Differences were considered significant at $p < 0.05$. **(B)** Left: Western blot showing the expression of E-Cadherin in total cellular extract of MCs. Tubulin was detected as a loading control. Right: WB quantification of E-cadherin expression in Poly(I:C) with/or MS-275 treated MCs compared to NT. Bars represent the mean ± SEM of triplicate determinations in at least four independent experiments. *P* was calculated with respect to NT or Poly(I:C) samples. *(continues on the following page)*

(following) **(C)** Immunofluorescence of MCs treated with Poly(I:C) with/or MS-275 compared with NT cells. Fixed cells were stained with antibody against Calretinin. Nuclei were stained with DRAQ5. A minimum of 150 cells per sample from two independent experiments were analysed. Scale bar: 50 μm **(D)** Quantitative RT-PCR of *Snail, FN* and *MMP9* expression in Poly(I:C) with/or MS-275 treated MCs. L34 mRNA levels were used for normalization. Bars represent the mean ± SEM of triplicate determinations in at least five independent experiments. *P* was calculated with respect to NT or Poly(I:C) samples. Differences were considered significant at $p < 0.05$. **(E)** Gelatin zymography showing the activity of MMP9 and MMP2 in native protein extracted from MCs treated with Poly(I:C) with/or MS-275 compared to NT.

6. Inhibition of Poly(I:C)-induced type-I Interferon response by MS-275 is associated to reduced STAT1 tyrosine phosphorylation

Proteomic analysis on MCs treated with MS-275 revealed the effect of this compound in inhibiting interferon induced anti-viral response (**Fig 17**) (**Table 5**). The role of MS-275 in downregulating type I interferon response induced by Poly(I:C) was confirmed at mRNA and protein expression level. Anti-viral target genes associated with IFNβ response, Mx1, IFIT1 and IFITM1, were downregulated by MS-275 pretreatment (**Fig 19A**). WB analysis confirmed gene expression results on the target genes Mx1, IFIT1 and IFITM1 (**Fig 19B**). We linked the impaired type-I interferon response to reduced tyrosine phosphorylation of STAT1, a main inducer of this pathway, upon MS-275- Poly(I:C) treatment (**Fig 19C**).

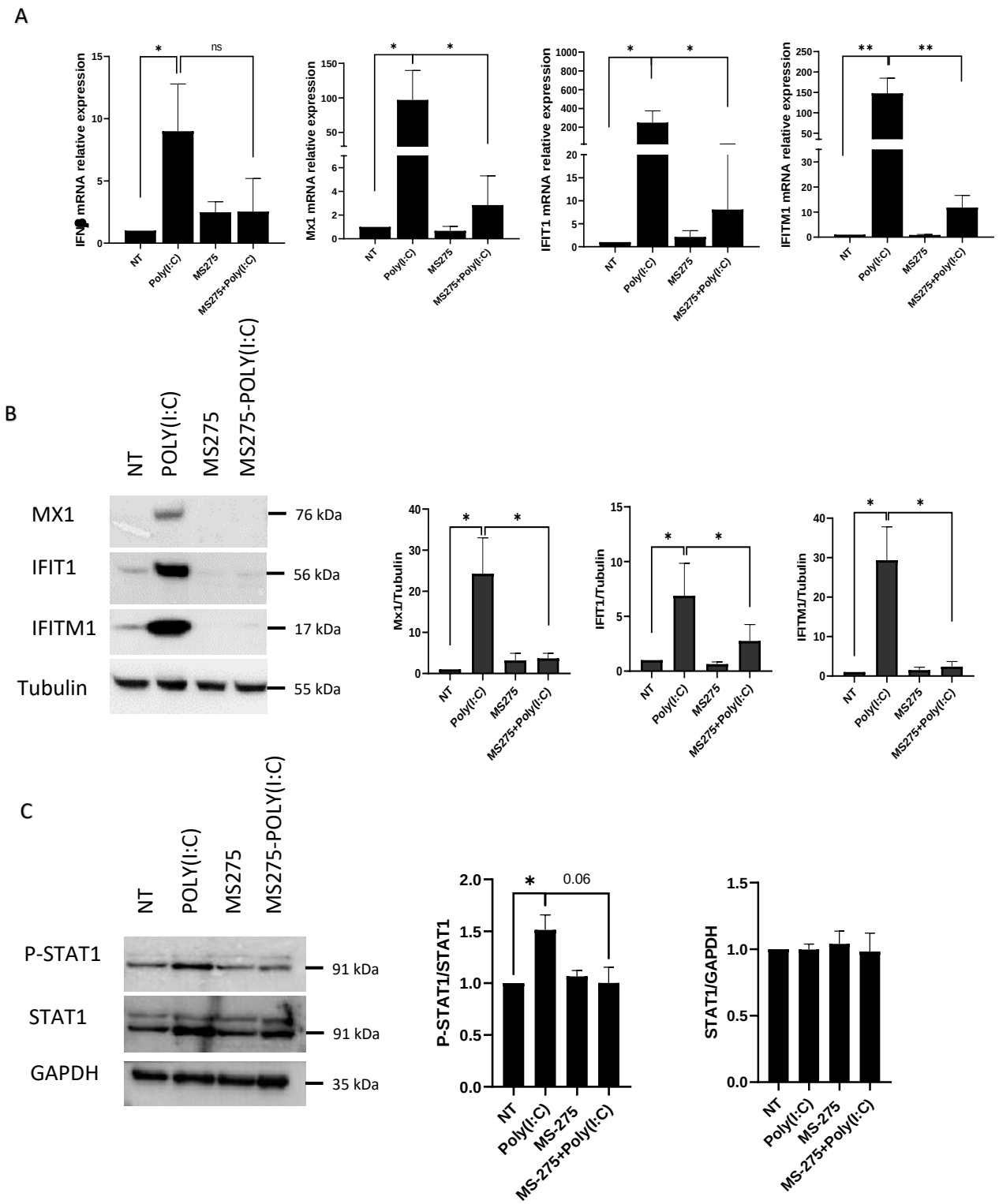

Figure 19 MS-275 promotes inhibition of type-I IFN response in Poly(I:C) stimulated MCs and inhibits STAT1 phosphorylation status promoted by Poly(I:C). Cells were treated with 2 ng/ml Poly(I:C) for 48 hours and/or 0,25 μM MS-275 for 72 hours with a second pulse after 48h from the first stimulation; experimental conditions are valid for combinatory or single treatment. (*continues on the following page*)

(*following*) **(A)** Quantitative RT-PCR of *IFNβ, Mx1, IFIT1* and *IFTM1* expression in Poly(I:C) with/or MS-275 treated MCs. L34 mRNA levels were used for normalization. Bars represent the mean ± SEM of triplicate determinations in at least five independent experiments. *P* was calculated with respect to NT or Poly(I:C) samples. Differences were considered significant at $p < 0.05$. **(B**) Left: Western blot showing the expression of Mx1, IFIT1 and IFITM1 in total cellular extract of MCs. Tubulin was detected as a loading control. Right: WB quantification of Mx1, IFIT1 and IFITM1expression in Poly(I:C) with/or MS-275 treated MCs compared to NT. Bars represent the mean ± SEM of triplicate determinations in at least four independent experiments. *P* was calculated with respect to NT or Poly(I:C) samples. **(C)** Cells were treated with 2 ng/ml Poly(I:C) for 3 hours and/or 0,25 μM MS-275 for 72 hours. Left: WB showing the phosphorylation status of P-STAT1 compared to STAT1 expression level in total cellular extract of MCs. GAPDH was detected as a loading control. Right: WB quantification of P-STAT1 and total STAT1 protein levels in Poly(I:C) with/or MS-275 treated MCs compared to NT. Bars represent the mean ± SEM of triplicate determinations in at least four independent experiments. *P* was calculated with respect to NT or Poly(I:C) samples.

7.Treatment with MS-275 differently modulates Poly(I:C)-induced pro-inflammatory cytokine/chemokine production

The role of MS-275 in the production of inflammatory cytokines was then analysed. MS-275 enhanced Poly(I:C) induced mRNA expression of IL-6 and CXCL8, but not of TNFα, which was downregulated (**Fig 20A**). Significant increases of IL-6 and CXCL8 upon MS-275 treatment were confirmed by ELISA assay (**Fig 20B**). Overall, the effect of MS-275 in the induction of inflammatory cytokines should be further analysed, also considering the fact that the increased expression of IL-6 did not obviously correlate with the observed differences in Tyrosine Phosphorylation of its downstream effector STAT3 (**Fig 20C**).

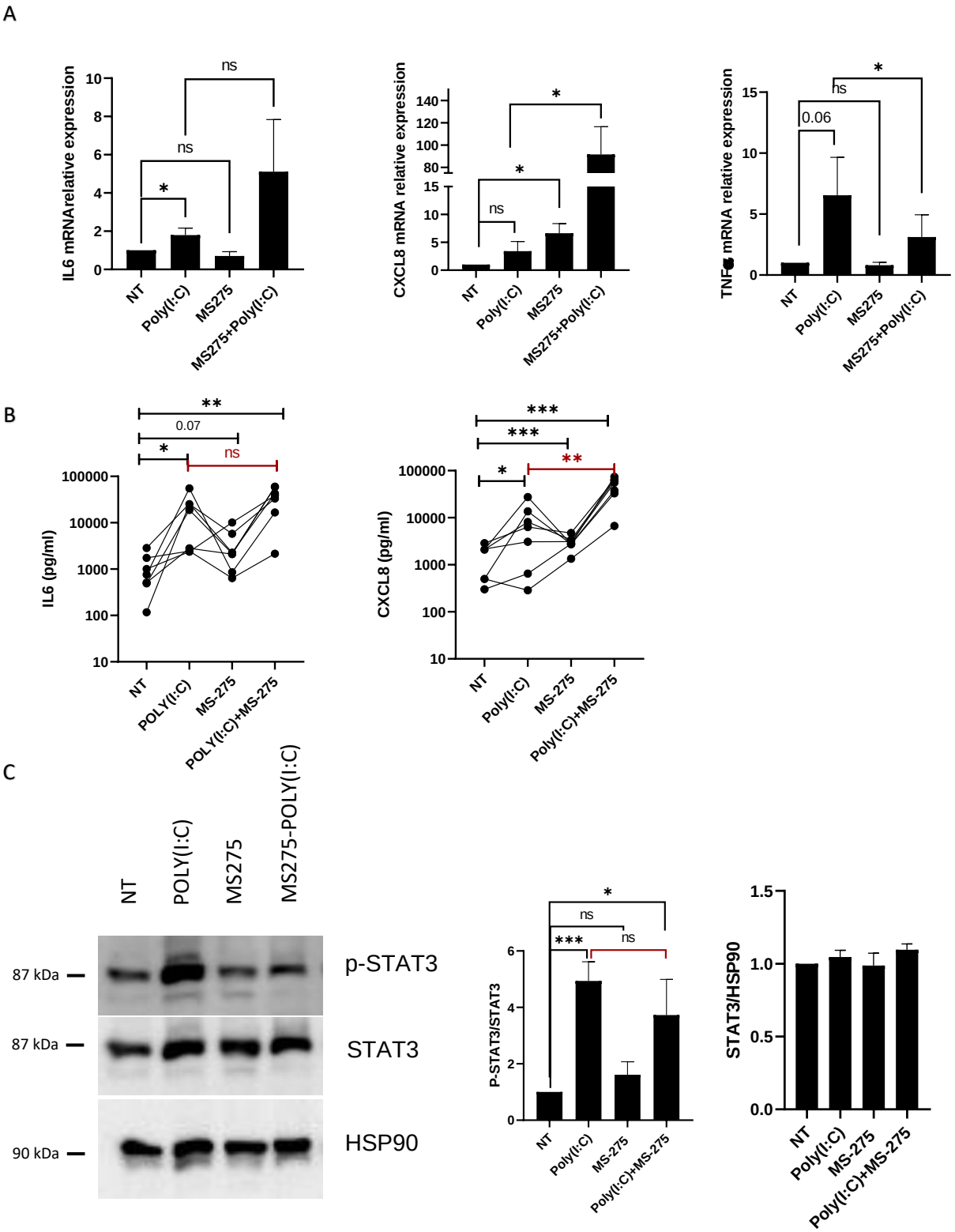

Figure 20 MS-275 differently modulates Poly(I:C) induced pro-inflammatory cytokine/chemokine production. (*continues on the following page*)

(*following*) **(A)** Cells were treated with 2 ng/ml Poly(I:C) for 48 hours and/or 0,25 μM MS-275 for 72 hours with a second pulse after 48h from the first stimulation; experimental conditions are valid for combinatory or single treatment. Quantitative RT-PCR of *IL-6, CXCL8* and *TNFα* expression in Poly(I:C) with/or MS-275 treated MCs. L34 mRNA levels were used for normalization. Bars represent the mean ± SEM of triplicate determinations in at least five independent experiments. *P* was calculated with respect to NT or Poly(I:C) samples. Differences were considered significant at $p < 0.05$. **(B)** Analysis of IL-6 and CXCL8 secretion from supernatants of MCs treated with Poly(I:C) with/or MS-275 compared to NT. Cytokine were measured by ELISA assay. *P* was calculated with respect to NT or Poly(I:C) samples. Differences were considered significant at $p < 0.05$. **(C)** Cells were treated with 2 ng/ml Poly(I:C) for 3 hours and/or 0,25 μM MS-275 for 72 hours with a second pulse after 48 hours from the first stimulation. Left: WB showing the phosphorylation status of P-STAT3 compared to STAT3 expression level in total cellular extract of MCs. HSP90 was detected as a loading control. Right: WB quantification of P-STAT3 and total STAT3 protein levels in Poly(I:C) with/or MS-275 treated MCs compared to NT. Bars represent the mean ± SEM of triplicate determinations in at least four independent experiments. P was calculated with respect to NT samples.

8. MeT5A cells support SARS-CoV-2 infection/replication

Having demonstrated that MCs sense mediators released during viral infection, we analysed where these cells respond to viral infection. To this purpose, MeT5A, a pleura non-transformed MC line were chosen to evaluate the effect SARS-CoV-2 infection as an *in vitro* model of viral infection.
MeT5A, are widely used in the study of pleura pathophysiological functions, such as mesothelial plasticity and fibrosis ((*82*),(*263*),(*341*),(*342*)). SARS-CoV-2 infection (MOI=1) of MeT5A resulted in a progressive accumulation of viral RNA in the supernatants at 24 (fold increase mean 8.2) and 72 (fold increase mean 16.4) hours post infection (p.i.) (**Fig 21A**). Moreover, intracellular SARS-CoV-2 RNA peaked at 24 and slightly declined at 72 h p.i (**Fig 21A**). The presence of infectious SARS-CoV-2 viral particles in MeT5A supernatants was demonstrated by productive infection of Vero E6 cells (**Fig 21A**). To further confirm viral infection of MeT5A, double-strand (ds) RNA and viral nucleoprotein (N) were detected by confocal microscopy at 72 h p.i. (**Fig 21B**). Exposure of MeT5A cells to SARS-CoV-2 viral particles did not cause an evident cytopathic effect and cell death, as demonstrated by cleaved caspase 3 detection (**Fig 21C**). To provide mechanistic evidence on SARS-CoV-2/MC interactions, we analysed the expression of the plasma membrane receptors implicated in viral entry, namely ACE2, the protease TMPRSS2, and the co-factors NRP1 and ADAM17. As shown in **Fig 22**, MeT5A cells express ACE2, TMPRSS2, NRP1, and ADAM17. As demonstrated by kinetic infection studies, ACE2 expression has a trend to increase after SARSCoV-2 infection, whereas no significative changes in expression of the other receptors were observed (**Fig 22A**). Expression of ACE2, TMPRSS2 and ADAM17 in non-infected MeT5A was confirmed at protein level by western blot analysis (**Fig 22B**). With respect to cellular specific response, SARS-CoV-2 infection promoted a rapid induction of Type I interferons (IFN-I), as demonstrated by IFN-α and IFN-β mRNA expression already induced at 1.5 h and still significantly expressed at 72 h upon infection (**Fig 22C**).

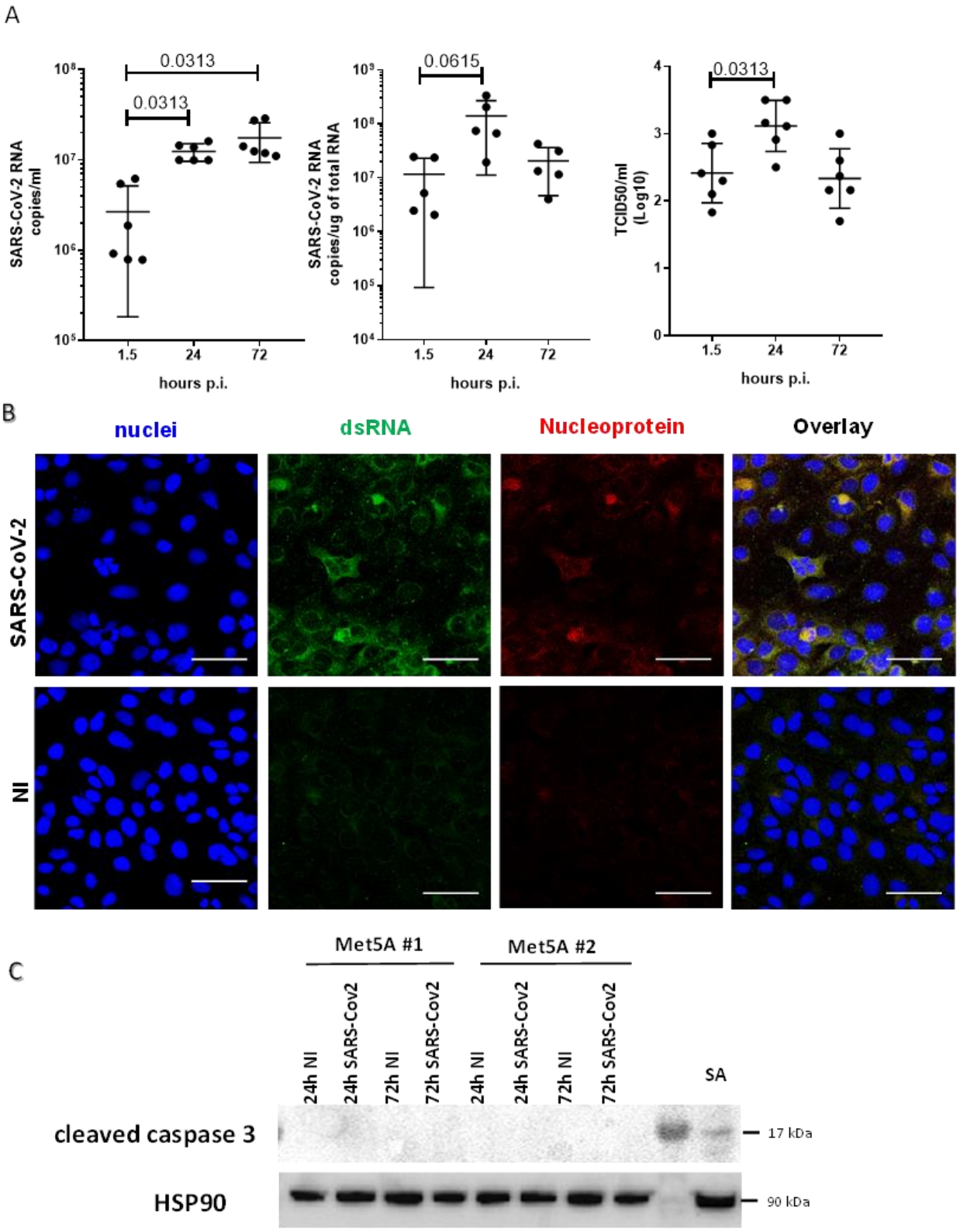

Figure 21 MeT5A are permissive to SARS-CoV-2 infection (**A**) Left: Quantification of SARS-CoV-2 viral RNA expression in culture supernatants of MeT5A cells at 1.5, 24 and 72 hours post viral inoculum (MOI=1). Six independent experiments were performed. Middle: Quantification of SARS-CoV-2 viral RNA expression in total RNA of MeT5A cultured as above. Five independent experiments were performed. Right: A TCID50 (Median Tissue Culture Infectious Dose) assay was performed adding serial dilutions of MeT5A cell culture supernatants to sub-confluent VeroE6 cells seeded in 96-well plates. Six independent experiments were performed. *P* was calculated with respect to time 0 of infection. Differences were considered significant at $p < 0.05$. (*continues on the following page*)

(*following*) (**B**) Immunofluorescence of MeT5A cells exposed for 120 hours to SARS-CoV-2 (MOI=1) compared with non-infected (NI) cells. Fixed cells were stained with antibodies against SARS-CoV Nucleocapsid and dsRNA. Nuclei were stained with DRAQ5. A minimum of 150 cells per sample from two independent experiments were analysed. Scale bar: 50 µm
(C) Western Blot showing the expression of cleaved caspase 3 in MeT5A left untreated or infected at 24 or 72 hours. Sodium Arsenite MeT5A treatment for 1 hour was used as positive control. HSP90 was detected as loading control.

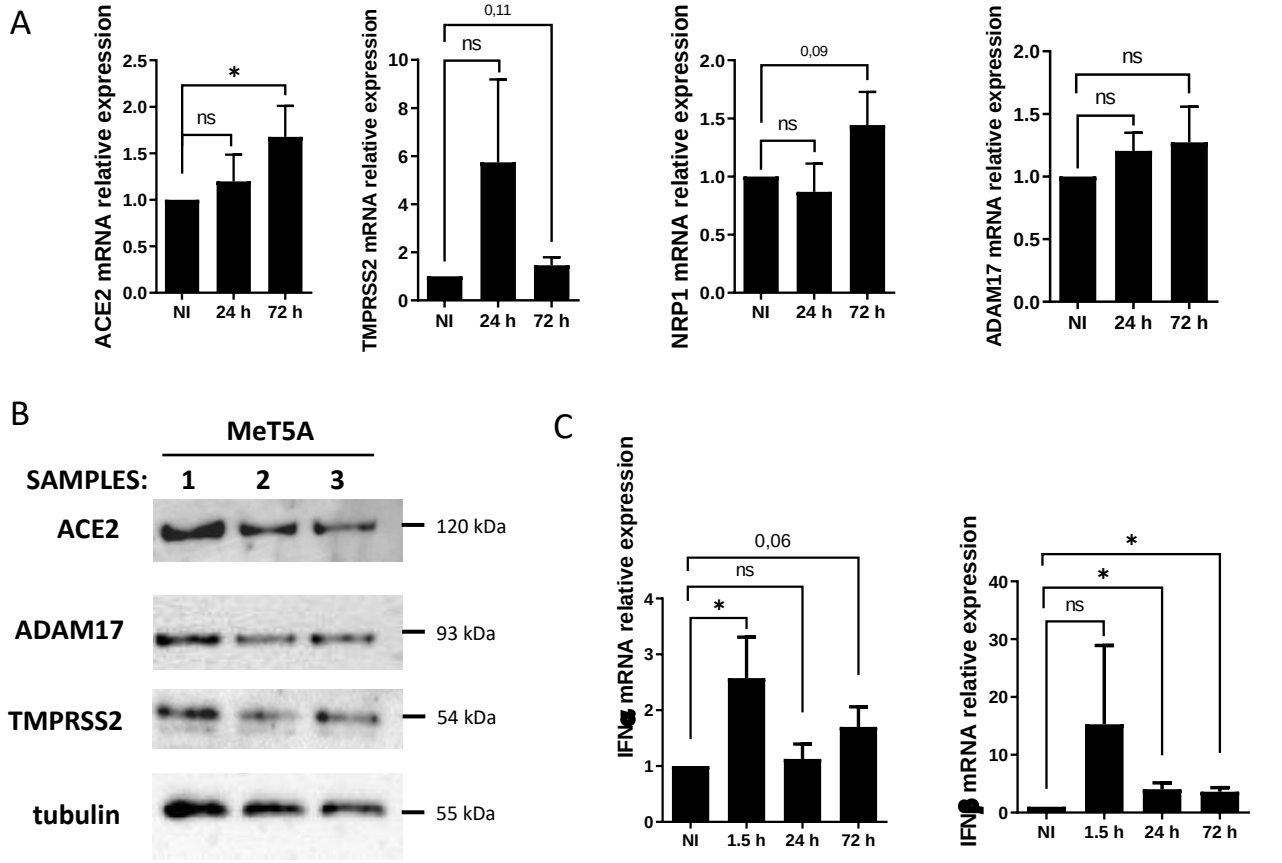

Figure 22 Met5A express SARS-CoV-2 associated receptors and activate an early Type-I IFN response. MeT5A cells exposed to SARS-CoV-2 infection (MOI=1) for 24 or 72 hours compared with non-infected (NI) cells. (**A**) Quantitative RT-PCR expression analysis of *ACE2*, *TMPRSS2*, *NRP1* and *ADAM17* from total RNA. L34 mRNA levels were used for normalization. Bars represent the mean ± SEM of triplicate determinations in at least four independent experiments. *P* was calculated with respect to NI samples. Differences were considered significant at $p < 0.05$.
(**B**) Western blot showing the expression of ACE2, TMPRSS2 and ADAM17, SARS-CoV-2 plasma membrane receptors, from total lysates of non-infected MeT5A cells. Tubulin was detected as a loading control. (**C**) Quantitative RT-PCR expression analysis of *IFN-α* and *IFN-β* in MeT5A cells exposed to SARS-CoV-2 for 1.5, 24 or 72 hours (MOI=1) compared with NI cells. Quantitative RT-PCR was performed on total RNA. L34 mRNA levels were used for normalization. Bars represent the mean ± SEM of triplicate determinations in at least four independent experiments. *P* was calculated with respect to NI samples. Differences were considered significant at $p < 0.05$.

9. The infection of MeT5A cells by SARS-CoV-2 promotes cytokine production

The specific contribution of the infected MCs in the modulation of the inflammatory response and extracellular matrix (ECM) remodelling was therefore explored. Supernatants from SARS-CoV-2-infected MeT5A cells were analysed at 72 h after infection. 37 extracellular inflammatory mediators were evaluated by Luminex technology. Furthermore, the analysis was extended to another panel of inflammatory cytokines (IL-1β, TNFα, IL-6, CXCL8) measured by automatic ELLA assay. The significant induction of cytokines (observed at 72 h after infection) is shown in **Fig 23**. The induction of an IFN response previously observed at mRNA level was confirmed by the presence of increased levels of IFNα, IFNβ, IFNγ and IFNλ (IL-28, IL-29) (**Fig 23A**). Secretion of cytokines with inhibitory activity belonging to TNF superfamily, (sTNF-R1, sTNF-R2 and sCD30/TNFRSF8) was increased (**Fig 23B**). On the other hand, production of TNFα and IL-1β, that are known to be secreted by MCs, was negligible upon SARS-CoV-2 infection ((*53*),(*111*)) (**Fig 23D**). Interestingly, the increase in the production of IL-10 and the structurally related IL-20 was highly significant (**Fig 23C**), whereas the abundant production of IL-6, characteristic of these cells, was not significantly increased by SARS-CoV-2 infection (**Fig 23D**) (*343*). Of note, CXCL8 production was significantly increased upon SARS-CoV-2 infection (**Fig 23D**). Moreover, MCs produced increased amounts of IL-2, IL-12p40 and IL-27, known modulators of innate and adaptive immunity (**Fig 23E**). Last, MCs secreted increased levels of MMP1-3, and of osteocalcin (**Fig 23F**). These data suggest that infected MCs may impact both the immune response to SARS-CoV-2 via the predominant production of anti-inflammatory mediators and the modification of the pleural stroma via the production of ECM remodelers.

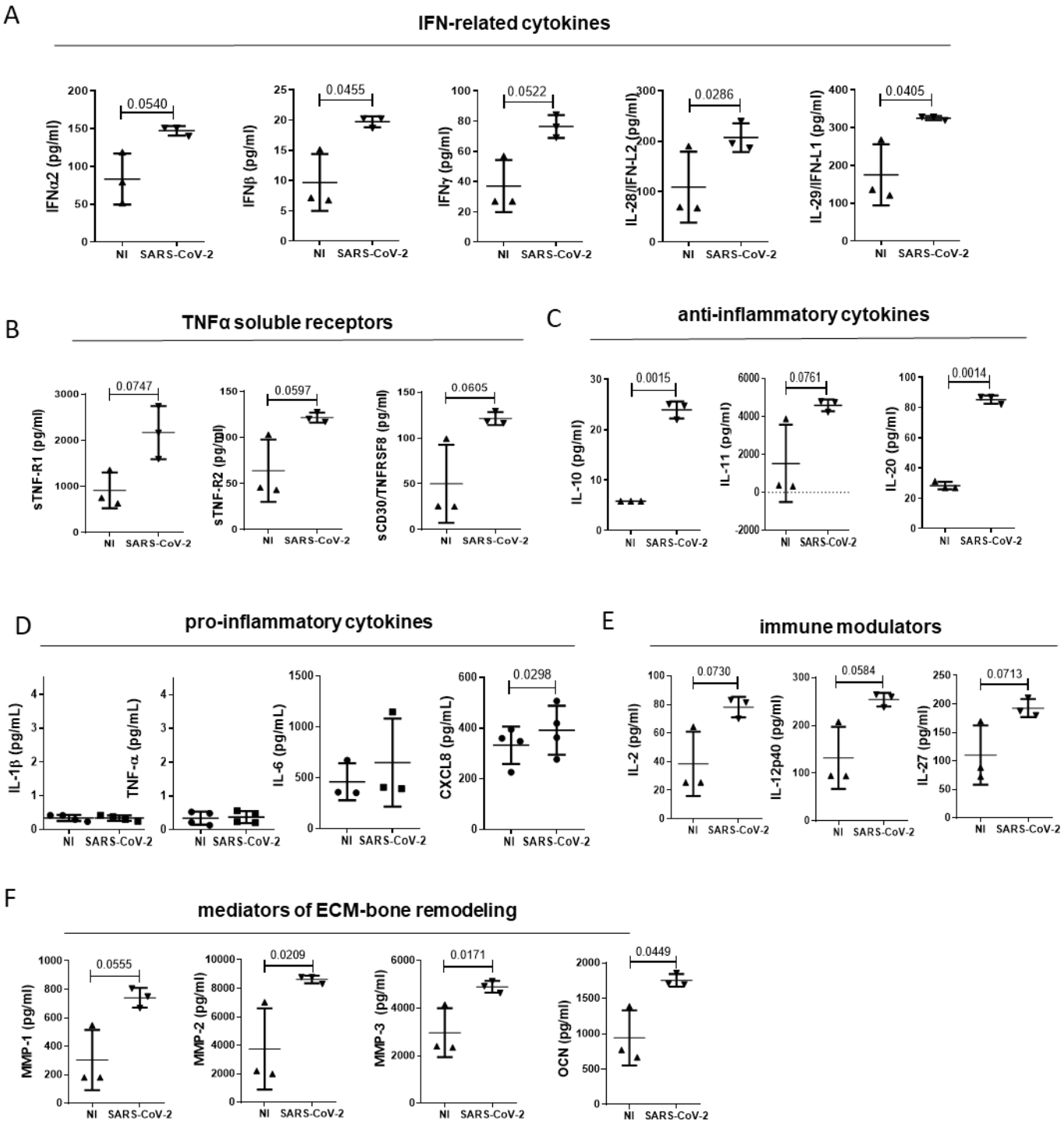

Figure 23 Analysis of cytokine secretion from supernatants of Met5A. Cells were infected with SARS-CoV-2 or left uninfected for 72 hours (MOI=1). SARS-CoV-2 infection promoted the production of IFN-related cytokines (**A**); TNFα-soluble receptors (**B**); anti-inflammatory cytokines (**C**); pro-inflammatory cytokines (**D**); immune modulators (**E**) and mediators of ECM-bone remodelling **(F**). Cytokines shown in A, B, C, E, and F were measured by Luminex assay; cytokines shown in D were measured by ELLA assay. P was calculated with respect to NI samples. Differences were considered significant at $p < 0.05$.

10. Treatment with MS-275 potentiates SARS-CoV-2 infection in MeT5A cells

To analyse the role of HDAC1/2 inhibition in this process, MeT5A were treated with MS-275, or DMSO as control for 24 hours before infection with SARS-CoV-2 (MOI=1). The presence of infectious SARS-CoV-2 viral particles in MeT5A supernatants was demonstrated by productive infection of Vero E6 cells.
Dose response experiments demonstrated that MS-275 treatment potentiates SARS-CoV-2 viral infection in MeT5A cells (**Fig 24**). These results demonstrated that HDAC1/2 pharmacological inhibition favours SARS-CoV-2 infection in MeT5A cells.

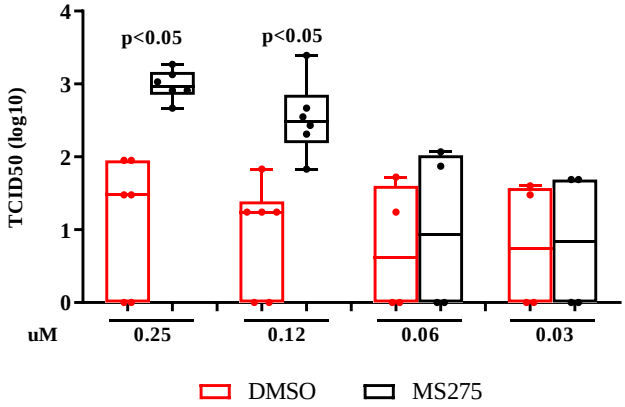

Figure 24 MS-275 potentiates SARS-CoV-2 infection in MeT5A. Cells were pre-treated with DMSO or MS-275 for 24 hours at the following doses: 0.25, 0.125, 0.06 and 0.03 µM. Then, cells were infected with SARS-CoV-2 or left uninfected for 72 hours (MOI=1). A TCID50 (Median Tissue Culture Infectious Dose) assay was performed adding serial dilutions of MeT5A (MS-275 or DMSO treated) cell culture supernatants to sub-confluent VeroE6 cells seeded in 96-well plates. Six independent experiments were performed. *P* was calculated for MS-275 treated with respect to DMSO treated MeT5A. Differences were considered significant at $p < 0.05$.

11. Treatment with MS-275 modulates interferon response to SARS-CoV-2 in MeT5A cells

As we observed the effects of HDAC1/2 in modulating with type-I IFN response, we wonder about this correlation in SARS-CoV-2 response. Thus, we evaluate the effect of MS-275 on IFN-β response genes at the non-cytotoxic concentration of 0,25 µM. This HDAC1/2 pharmacological inhibition characterizes a down-modulation of STAT1 driven genes in MS-275 pre-treated SARS-CoV-2 infected MeT5A (**Fig 25**).

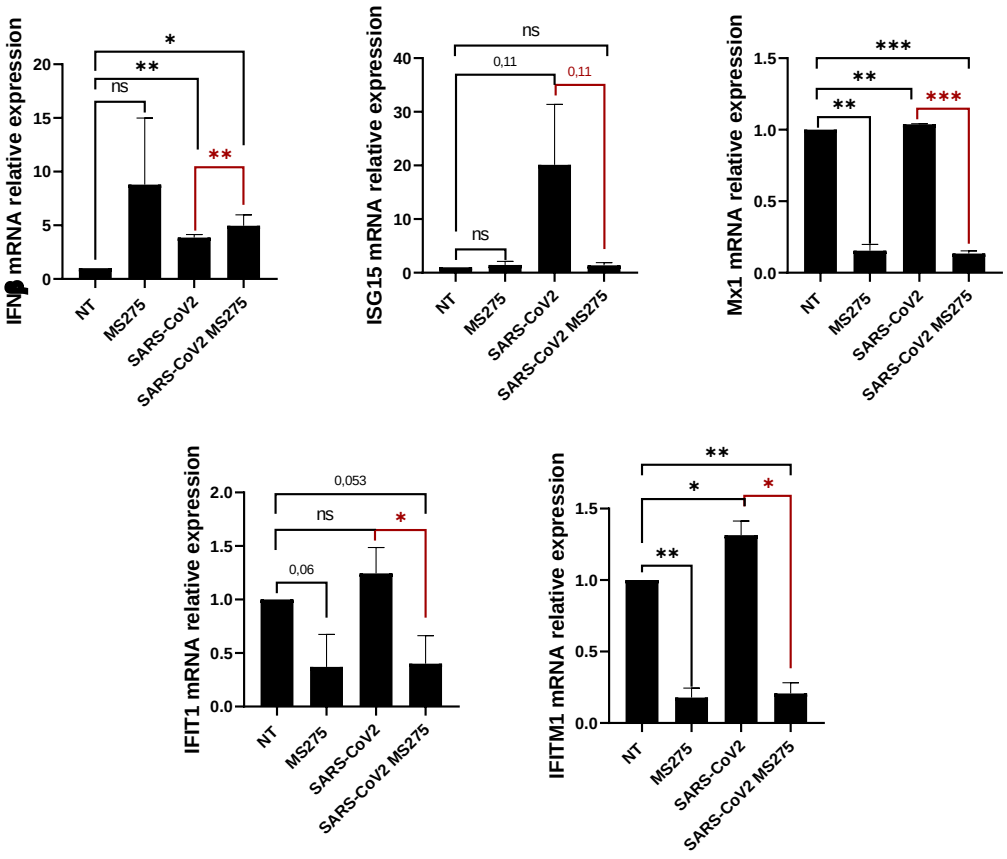

Figure 25 MS-275 modulates type-I IFN response after SARS-CoV-2 infection. Cells were pre-treated with 0,25 µM DMSO or MS-275 for 24 hours pre-infection. Then, cells were infected with SARS-CoV-2 or left uninfected for 72 hours (MOI=1). Quantitative RT-PCR expression analysis of *IFNβ, ISG15, Mx1, IFIT1* and *IFITM1* from total RNA of MS-275 treated MeT5A cells exposed to SARS-CoV-2 infection (MOI=1) for 72 hours compared with SARS-CoV-2 infected MeT5A left untreated. L34 mRNA levels were used for normalization. Bars represent the mean ± SEM of triplicate determinations in at least four independent experiments. *P* was calculated with respect to NT or SARS-CoV-2 infected samples. Differences were considered significant at $p < 0.05$.

12. Treatment with MS-275 increases the expression of ACE2 and TMPRSS2 in MeT5A cells

In respect to SARS-CoV-2 infection, the expression ACE2 and TMPRSS2, plasma membrane receptors associated with SARS-CoV-2 entrance, was analysed upon treatment with MS-275 in a dose response experiment (**Fig 26A**). 0,25 µM MS-275 was chosen to better characterize the molecular mechanisms underlying as it resulted the condition in which SARS-CoV-2 can reach the maximal levels of amplification without causing mesothelial cells toxicity. This HDAC1/2 pharmacological inhibition was characterized to strong upregulate ACE2 and TMPRSS2 expression (**Fig 26B-D**) as evaluated by quantitative PCR, Western Blot and Confocal analysis. The specific role of HDAC1 and 2 depletion was confirmed also by target specific genetic silencing (**Fig 26E**).

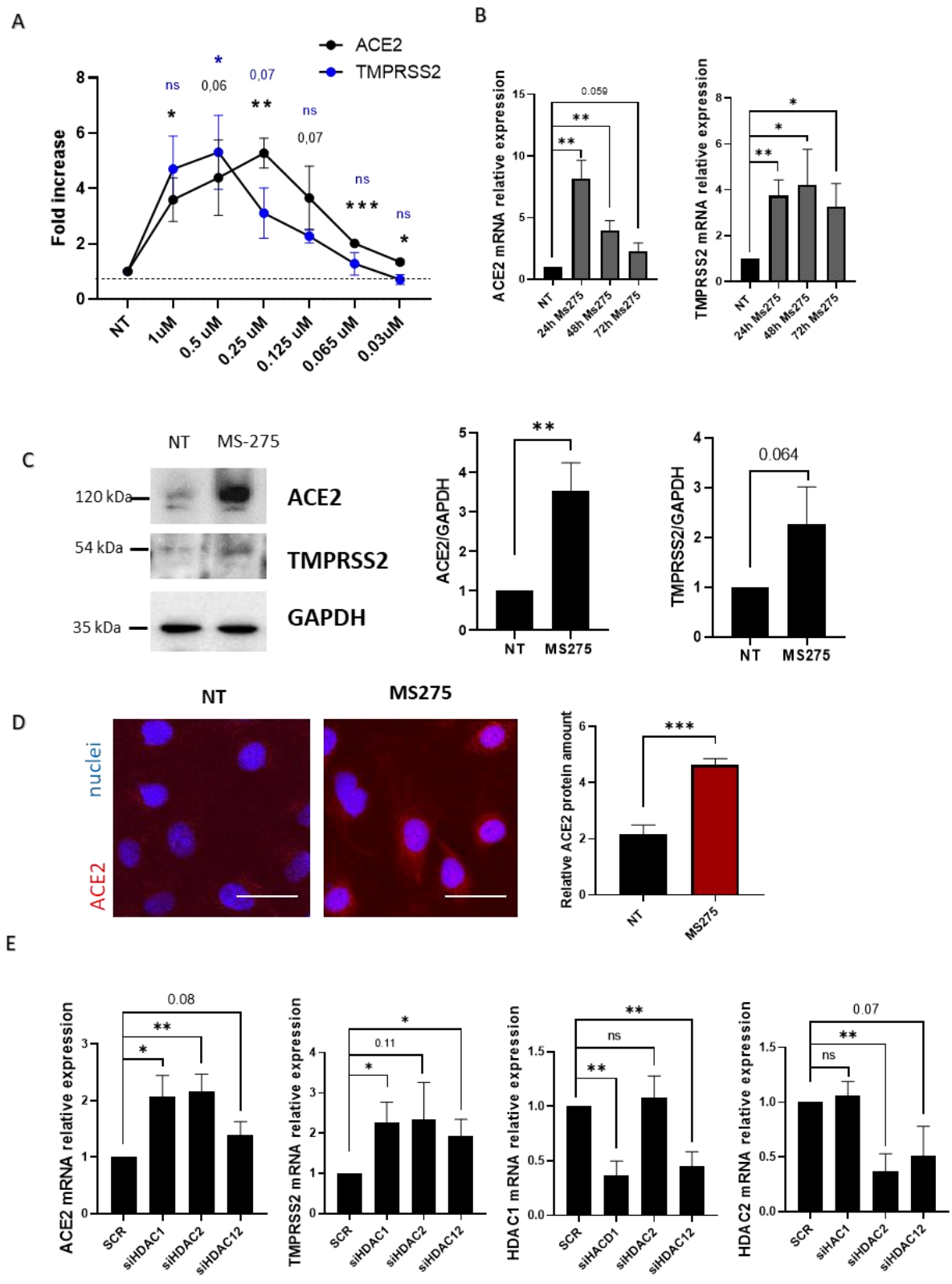

Figure 26 : HDAC1/2 inhibition promotes gene expression of ACE2 and TMPRSS2. (*continues on the following page*)

(Following) **(A)** Cells were treated with DMSO or MS-275 for 24 hours at the following doses: 1, 0.5, 0,25, 0.125, 0.06 and 0.03 μM. Quantitative RT-PCR expression analysis of ACE2 and TMPRSS2 from total RNA of MS-275 treated MeT5A compared to NT. L34 mRNA levels were used for normalization. Bars represent the mean ± SEM of triplicate determinations in at least four independent experiments. P was calculated with respect to NT infected samples. Differences were considered significant at $p < 0.05$ **(B)** Cells were treated with 0,25 μM MS-275 for 24, 48 and 72 hours. Quantitative RT-PCR expression analysis of *ACE2* and *TMPRSS2* from total RNA of MS-275 treated MeT5A compared to NT. L34 mRNA levels were used for normalization. Bars represent the mean ± SEM of triplicate determinations in at least four independent experiments. *P* was calculated with respect to NT samples. Differences were considered significant at $p < 0.05$ **(C)** Left: Western blot showing the expression of ACE2 and TMPRSS2 in total cellular extract of MCs. GAPDH was detected as a loading control. Right: WB quantification of ACE2 and TMPRSS2 expression in 48h 0,25 μM MS-275 treated MeT5A compared to NT. Bars represent the mean ± SEM of triplicate determinations in at least four independent experiments. *P* was calculated with respect to NT samples. **(D)** Immunofluorescence of MeT5A cells treated with 0,25 μM Ms-275 for 48 hours compared to NT. Left: Fixed cells were stained with antibodies against ACE2. Nuclei were stained with DRAQ5. A minimum of 150 cells per sample from two independent experiments were analysed. Scale bar: 25 μm. Right: ACE2 fluorescence signal quantification in MS-275 treated cells compared to NT. Bars represent the mean ± SEM of triplicate determinations in at least three independent experiments. *P* was calculated with respect to NT infected samples. Differences were considered significant at $p < 0.05$ **(E)** Cells were treated with gene silencing smart pool to silence HDAC1 and/or HDAC2 gene expression for 48 hours. Quantitative RT-PCR expression analysis of *ACE2*, *TMPRSS2, HDAC1* and *HDAC2* from total RNA of treated MeT5A compared to scramble (SCR) treatment. L34 mRNA levels were used for normalization. Bars represent the mean ± SEM of triplicate determinations in at least four independent experiments. *P* was calculated with respect to SCR samples. Differences were considered significant at $p < 0.05$.

13. Treatment with MS-275 increases H3 histone acetylation on ACE2 and TMPRSS2 promoters in MeT5A cells

To mechanistically demonstrate an effect of HDAC1/2 inhibition in the expression of SARS-CoV-2 receptors, the acetylation status of ACE2 and TMPRSS2 promoters was investigated. Ac-H3 Magna ChIP assay demonstrated that treatment with MS-275 enhances H3 acetylation on ACE2 and TMPRSS2 promoters. These results suggest that MS-275 directly promotes ACE2 and TMPRSS2 mRNA expression by favouring an opened chromatin conformation in the ACE2 and TMPRSS2 promoters (**Fig 27**).

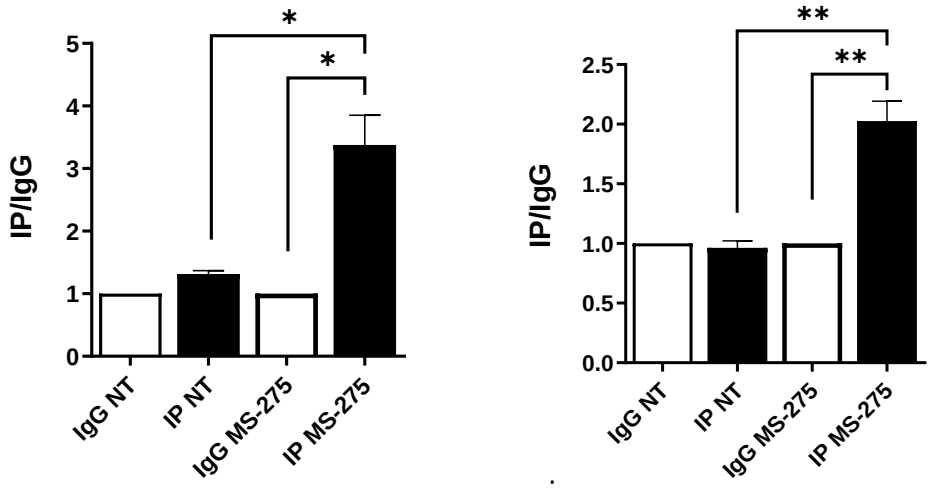

Figure 27 MS-275 promotes ACE and TMPRSS2 expression. Magnetic ChIP experiment showing the increase of H3 Acetylation on ACE and TMPRSS2 promoters upon treatment with 0,25 μM MS-275 for 48 hours. IP expression levels were folded to IgG of the same experimental condition. Bars represent the mean ± SEM of triplicate determinations in at least three independent experiments. P was calculated with respect to IgG MS-275 or IP-NT samples. Differences were considered significant at $p < 0.05$.

14. Myofibroblast transformation of MCs in visceral pleura from SARS-CoV-2-infected patients

Last, we wondered whether SARS-CoV-2 may directly infect pleura in COVID-19 patients along with infection's relative effects on the pleural membrane.
To answer this question, autoptic visceral pleura from COVID-19 patients was analysed and compared to visceral pleura from non-COVID-19 patients. Masson's trichrome staining revealed the onset of an intense fibrotic response in samples from COVID-19 patients (**Fig 28B**), with respect with non-COVID-19 patients (**Fig 28A**). When analysing pleura cellular components, while the MCs monolayer was maintained in the pleura of non-COVID-19 patients (**Fig 28C,D**), it appeared almost totally lost in COVID-19 patients (**Fig 28E,F**), highlighting the specificity of pleural disruption in this disease. Immunohistochemical labelling with WT1, a MC marker, showed positivity in spindle-like cells infiltrating the submesothelial stroma of COVID-19 patients (**Fig 28E**). Accordingly, staining with anti-cytokeratin AE1/AE3 antibody confirmed the mesothelial origin of these infiltrating cells (**Fig 28F**). The sub-mesothelial stroma in non-COVID-19 samples was devoid of WT1, (**Fig 28C**), or cytokeratin positive cells, (**Fig 28D**), highlighting a specific impact of SARS-CoV-2 infection in promoting the acquisition of invasive ability by MCs. Anti SARS-CoV-2 immunolabeling did not reveal specific stain in the rare MCs present in visceral pleura from COVID-19 patients. However, positivity was found in pneumocytes from the same patients, in agreement to previously published data (*344*). Interestingly, we also found evidence of ACE2 expression, the main SARS-CoV-2 plasma membrane receptor, in pleura MC (**Fig 28G**). These results demonstrate that SARS-CoV-2 infection causes the disruption of the monolayer of epithelial-like MCs, which in turn may invade the sub-mesothelial stroma promoting the onset of pleural fibrosis.

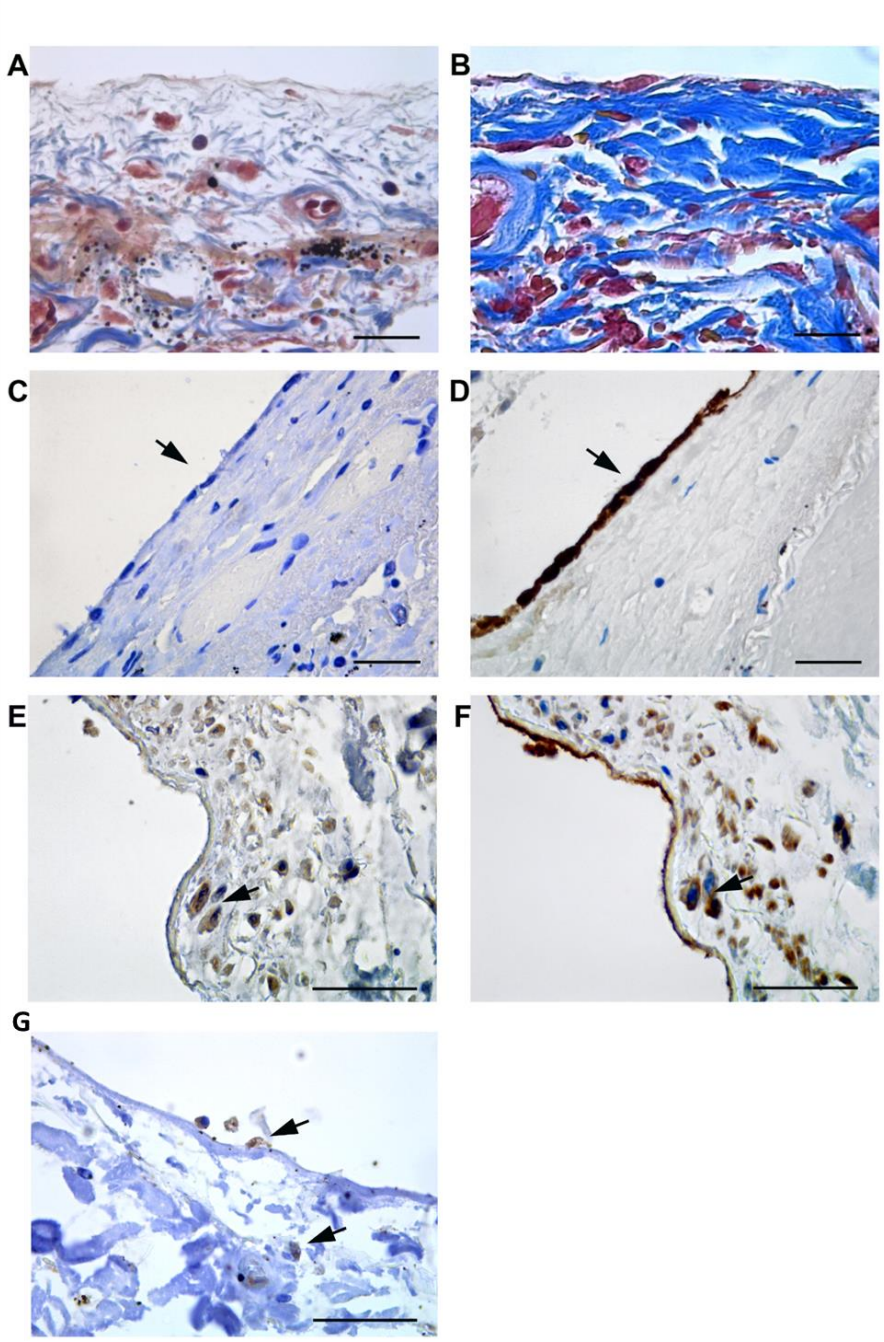

Figure 28 Fibrosis staining and immunohistochemical characterization of MSc in autoptic visceral pleura from COVID-19 patients compared to non COVID-19 patients.
(A) Masson's trichrome staining in tissue from non COVID-19 patient; **(B)** Masson's trichrome staining highlights the presence of collagen fibers (blue stain) in thickened submesothelial layer of visceral pleura from COVID-19 patients. **(C)** Visceral pleura from non COVID-19 patients show absence of staining (arrow) for WT1, a marker of reactive mesothelial cells. **(D)** Keratin AE1/AE3 staining, marker of mesothelial cells, shows a continuous monolyer of MCs in non COVID-19 patients. **(E,F)** Immunohistochemical labeling of WT1, shows positive submesothelial spindle cells in pleura from COVID-19 patients **(E, arrow),** and Keratin AE1/AE3 staining, performed on a consecutive section, show that the same cells **(F, arrow)** express both markers. (**G**) Labeling with a speficic antibody provides evidence of ACE2 expression (arrows) in MCs from visceral pleura of COVID-19 patients.
Scale bars = 30 μm

DISCUSSION

Peritoneal fibrotic damage depends on complex interactions between external stimuli, intrinsic properties of the peritoneal membrane, and subsequent activation of the local innate-adaptive immune system (*1*). In this context, we studied the MC response to viral infection focusing first on the role of TLR3, a sensor of virus-derived nucleic acids, in mediating changes in MC cell plasticity and the induction of an inflammatory response.

The effects of TLR3 stimulation have been so far scarcely studied in MCs. TLR3 stimulation has been demonstrated to induce matrix metalloproteinases/metalloproteinase inhibitors MMP9 and TIMP1 (*171*), playing a role in ECM remodeling. In another context such as pulmonary chronic inflammation, TLR3 mediated EMT and ECM remodeling in human small airway epithelial cells (*345*).

Treatment of MCs with Poly(I:C), a synthetic TLR3 agonist, promoted the induction of MMT-like features, such as the acquisition of a spindle-like shape, the downregulation of epithelial markers and upregulation of mesenchymal markers including Snail, the EMT master gene. Moreover, we observed the induction of pro-inflammatory cytokines/chemokines IL-1β, IL-6, TNFα, CXCL8 and CXCL10.

Since previous evidence from our laboratory demonstrated an effect of HDAC1/2 inhibition in reverting MMT state in biological contexts not related to viral infections ((*263*),(*340*)), we analysed the effect of MS-275/Entinostat, a pharmacological HDAC1/2 inhibitor after Poly(I:C) treatment. Using a wide range proteomic approach, we observed changing pathways in MS-275 treated MCs related to cytoskeleton remodelling and cellular plasticity. Thus, we validated the effective ability of MS-275 to revert the *bona fide MMT* induced by Poly(I:C) stimulation in MCs. Although Snail and Fibronectin gene expression levels resulted to be upregulated by MS-275 treatment, a previous study from our laboratory showed upregulated Snail expression coupled with functional inactivation upon MS-275 treatment in MCs (*263*). Moreover, the increased level of Fibronectin in MS-275 treated MCs was demonstrated to be dysfunctional in adhesion assays (Terri et al., Submitted).

On the track of proteomic analysis, we then focused on the analysis type-I inflammatory response after Poly(I:C) treatment. HDAC1/2 inhibition downregulated type-I IFN response activated by Poly(I:C). Mx1, IFIT1 and IFITM1, targets of IFN-β response, were strongly downregulated in MS-275 treated MCs. To clarify the molecular mechanisms underlying, we analysed STAT1 activation status using as a readout STAT1 tyrosine phosphorylation, which was found reduced in MS-275 treatment. We extended our analysis also on STAT3. MS-275 treatment resulted to downregulate STAT3 phosphorylation promoted by Poly(I:C). This result apparently is not coherent with increase of IL-6 (a STAT3 inducer) observed in the presence of MS-275. Entinostat was previously related to STAT3 activation as it promotes its acetylation status (*346*). When analysing other inflammatory cytokine/chemokine expression, while IL-6 and CXCL8 levels increased, TNFα was decreased upon Poly(I:C)/MS-275 treatment.

Thus, HDAC1/2 inhibition clearly downregulated Type-I IFN response induced by stimuli mimicking infections in MCs, while promoting at least in part pro-inflammatory cytokine expression.
Once demonstrated a role of Poly(I:C) in inducing MMT, inflammatory cytokine/chemokine production in MCs and its regulation by MS-275, we analysed the direct effect of a viral pathogen.
Since COVID-19 pathogenesis has lungs as primary targets, we analysed whether SARS-CoV-2 may infect pleural MCs, which are anatomically contiguous to alveolar epithelial cells. Despite the conceivable MCs participation in COVID-19 pathogenesis, so far only indirect evidence has been reported. We analysed 4 autoptic samples of COVID-19 patients comparing them with 4 non-COVID-19 ones. Even thought we did not find direct evidence of primary infection in the lungs of COVID-19 patients, we could observe a specific alteration of pleura characterized by disruption of the MC monolayer and invasion of the sub-mesothelial stroma by spindle-like MCs. No evidence so far pointed to a direct role of pleura MCs in the COVID-19 pathogenesis. This although around 10% of patients develop pleural effusions, have higher incidence of severe/critical illness, mortality rate and longer hospital stay time compared to their counterparts without pleural effusion ((*347*),(*348*),(*349*)). In this study, the observation of MCs loss with disruption of the MCs monolayer in biopsies of visceral pleura from autopsies of COVID-19 patients led to hypothesize a direct or cell-mediated cytopathic effect of the virus. In particular, WT1- and cytokeratin-positive cells with a fibroblastoid morphology (having undergone bona fide MMT) were found in the sub-mesothelial stroma. Events linked with MCs plasticity may influence the fibrotic process in different ways. MMT in particular, has been demonstrated as a common mechanism of fibrosis in serosal membranes exposed to biomechanical, inflammatory and infectious stimuli ((*98*),(*111*),(*350*),(*351*)).
We, then, analysed the effect of SARS-CoV-2 infection in a pleural cell line, the MeT5A cells, aimed to underlying molecular mechanisms implicated in the pleura brutal disruption observed in COVID-19 patients. In the in vitro analysis, we demonstrated that MeT5A cells express the main entry factors implicated in SARS-CoV-2 infection, i.e. ACE2, TMPRRS2, ADAM17 and NRP1. Cleavage of ACE2 has been demonstrated to impact on viral entry (*293*). While it was already known that MCs express high levels of NRP1, a co-receptor of VEGFR with pro-fibrotic activity, the expression of ACE2, TMPRSS2 and ADAM17 was reported for the first time by our study ((*308*),(*352*)).
By means of multiple approaches, we demonstrated that MCs sustain SARS-CoV-2 infection. Our observations provide a first evidence of SARS-CoV-2 infection, replication and inflammatory onset in pleural MCs (*172*).
Moreover, with respect to the cellular response to infection, we found an induction of IFN-α and IFN-β mRNA upon treatment with SARS-CoV-2. While the induction of a rapid IFN response is an indirect proof of MC infection, it also witnesses the ability of these cells to effectively clear SARS-CoV-2 infection at later time points.
It is known that cytokine production has both a pathogenic and a prognostic role in SARS-CoV-2 infection. Cytokine storm is responsible for multiorgan pathology and eventually death, and inflammatory cytokine signatures may predict COVID-19 severity and patient survival ((*353*),(*354*)).
The analysis of cytokines secreted by SARS-CoV-2-infected MCs highlighted a predominance of anti-inflammatory (i.e. IL-10, sTNF-Rs) over pro-inflammatory (IL-1β, TNFα, IL-6) responses.

Indeed, while inflammatory cytokine production was negligible (IL-1β, TNFα) or not significantly increased (IL-6), the production of IL-10 and of TNFRs was significantly enhanced upon viral infection. Of note, increased expression of sTNF-Rs has been previously reported in septic pleural effusions (*355*). The increase of interferons (IFNα, IFNβ, IFNγ, IL-28 and IL-29) corresponds to an increase of cytokines with anti-inflammatory/immunomodulatory activity (IL-10, IL-11 and IL-20). During SARS-CoV-2 infection, anti-inflammatory mediators are secreted at the same time with pro-inflammatory mediators, and in particular, IL-10 and IL-6 expression both correlate with disease severity (*356*). However, IL-10 appears to have a "double edge" activity during inflammation: this cytokine is a key negative regulator of T cell mediated responses, but is also endowed with pro-inflammatory effects, including stimulation of IFNβ production (*357*).
Moreover, MCs produced significantly increased levels of IL-2, IL-12 and IL-27, which may both activate NK and Th1 lymphocytes and promote antigen presentation. The production of MMPs by MCs is potentially relevant for induction of the pleura fibrotic response observed during SARS-CoV-2 infection.
It is conceivable that due to the considerable extension of pleura surface (2000 cm2 in an average adult male), the serous fluid recycling and the high vascularization of this organ, the predominant production of cytokines with anti-inflammatory activity by MCs may have a systemic effect of homeostatic dampening of the inflammatory response during infection. On the other hand, pleura may contribute to macrophage/lymphocyte activation and, through the secretion of mediators of ECM remodelling such as MMPs, play a role in lung fibrosis. Lineage tracing of WT1-positive MCs in a context of fibrotic lung disease provided evidence of MMT induction in vivo (*358*).
We next analysed the effect of HDAC1/2 inhibition in our SARS-CoV-2 model of viral infection. We found that HDAC1/2 inhibition promoted SARS-CoV-2 infection in MeT5A.
This result was in accordance with the downregulation of type-I IFN previously observed in response of Poly(I:C) in MCs treated with MS-275. IFN response is particularly important in SARS-CoV-2 infection, as it has been demonstrated that an optimal IFN production and controlled inflammation can reduce COVID-19 pathogenesis ((*359*),(*360*)). Indeed, IFN gene target were reduced in cells infected by SARS-CoV-2 in the presence of MS-275. In this experiment, we did not observe a clear upregulation on type-I INF response probably due to the different kinetic of viral infection (72 h) with respect to smaller time points of viral infection (shown in **Fig22C**). Moreover, we provided another mechanism, since we found that HDAC1/2 inhibition strongly upregulates ACE2 and TMPRSS2 expression, which causes a viral infection and/or spreading increase. Interestingly, a previous study reports that HDAC6 activity promotes ACE2 and NRP1 expression (*336*).
Mechanistically, we found increased histone acetylation promoted by MS-275 favouring chromatin remodelling in the region of ACE2 promoter. Studies have identified ACE2 as a human interferon-stimulated gene (ISG) ((*361*),(*362*),(*363*)), meaning that SARS-CoV-2 could exploit species-specific interferon-driven upregulation of ACE2 to enhance infection (*361*). These results have been so far only analysed in MeT5A and deserve further study in other cell lines already know to be a target for SARS-CoV-2.
Among potential therapeutical approaches tested during the COVID-19 pandemic, anticancer drugs with effects in epigenetic regulation, including HDAC inhibitors, have been used ((*333*),(*364*)). HDAC inhibition has been indicated as a potential therapeutical strategy to restore the deregulated immune type-I response during severe COVID-19 (*333*), particularly focusing on selective HDAC6 inhibitors. The

data indicated that HDAC6 inhibition participated in downmodulate the SARS-CoV-2 directed expression of pro-inflammatory cytokines and Type-I IFN response in monocytes (*333*). Epigenetic target inhibition of HDACs also limited the expression of SARS-CoV-2 associated receptor ACE2 and NRP1 in diverse cell lines (HK-2, Huh-7, HUVEC, Caco-2, and BEAS-2B) (*336*).

To sum up, here we provide evidence that MCs react to viral stimulation inducing MMT, fibrosis, type-I IFN response and pro-inflammatory cytokine/chemokine response as we first demonstrated in Poly(I:C) stimulation model and then partially validated in a SARS-CoV-2 infection model. Our study also indicates that HDAC1/2 pharmacological inhibition in MCs may have different effects. It reverted the MMT-like state while having not univocal effect in the expression of inflammatory cytokines/chemokines. Moreover, it dampened the Interferon response, which was linked to STAT1 reduced tyrosine phosphorylation. At the same time, it was demonstrated to promote the expression of SARS-CoV-2 receptors ACE2 and TMPRRS.

Entinostat is currently used alone or in combination therapy in different clinical trials for cancer therapies such as metastatic melanoma, breast cancer, Hodgkin lymphoma, myelodysplastic syndromes (MDS), acute myeloid leukaemia (AML) or acute lymphocytic leukaemia (ALL) ((*360*),(*365*)). Thus, our results raise a concern about the use of MS-275 or related inhibitors in immunocompromised patients where it may further potentiate the spread of SARS-CoV-2 infection.

CONCLUSIONS

In this doctoral thesis, we provide evidence that:

1. Primary human MCs from PD patients express a specific subset of TLRs, composed by TLR1, TLR2, TLR3 and TLR5, which are further induced upon treatment with Poly(I:C), a TLR3 specific ligand;
2. Poly(I:C) stimulation induces molecular and morphological changes related to MMT induction;
3. Poly(I:C) stimulation induces expression of pro-inflammatory cytokines and chemokines;
4. Proteomic analysis of MCs stimulated with MS-275, an HDAC1/2 inhibitor, reveals changes in expression pathways related to cell plasticity, inflammatory and interferon response;
5. Treatment with MS-275 in MCs stimulated with Poly(I:C) partially reverts the mesenchymal-like status favouring the acquisition of an epithelial-like phenotype;
6. Treatment with MS-275 inhibits STAT1 activity and Type-I IFN response;
7. Treatment with MS-275 differently modulates pro-inflammatory cytokine/chemokine in response to Poly(I:C) stimulation;
8. MeT5A cells express SARS-CoV-2 receptors/coreceptors ACE2, TMPRSS2, NRP1 and ADAM17;
9. MeT5A cells are permissive to SARS-CoV-2 infection;
10. SARS-CoV-2 infection result in a rapid Type I IFN response followed by upregulation of many inflammatory cytokines and chemokines involved in inflammation and in the modulation of the immune response in MeT5A cells;
11. Treatment with MS-275 potentiates SARS-CoV-2 infection in MeT5A cells;
12. Treatment with MS-275 induces ACE2 and TMPRRS2 expression, while limiting Type-I IFN response in MeT5A cells;
13. Treatment with MS-275 promotes H3 acetylation on ACE2 and TMPRRS2 promoters;
14. In COVID-19 autoptic pleura samples, MCs monolayer loss and the presence of mesenchymal like MCs in the submesothelial stroma were found, but no signs of direct pleura MC infection by SARS-CoV-2.

BIBLIOGRAPHY

1. M. Terri *et al.*, Mechanisms of Peritoneal Fibrosis: Focus on Immune Cells-Peritoneal Stroma Interactions. *Front Immunol* **12**, 607204 (2021).
2. O. N. Shilova, E. S. Shilov, A. Lieber, S. M. Deyev, Disassembling a cancer puzzle: Cell junctions and plasma membrane as targets for anticancer therapy. *J Control Release* **286**, 125-136 (2018).
3. M. Lopez-Cabrera, Mesenchymal conversion of mesothelial cells is a key event in the pathophysiology of the peritoneum during peritoneal dialysis. *Advances in Medicine* **2014**, 17 (2014).
4. R. R. Patel, K. Planche, Applied peritoneal anatomy. *Clin Radiol* **68**, 509-520 (2013).
5. J. Morelle, O. Devuyst, Water and solute transport across the peritoneal membrane. *Curr Opin Nephrol Hypertens* **24**, 434-443 (2015).
6. N. Di Paolo, G. Sacchi, Atlas of peritoneal histology. *Perit Dial Int* **20 Suppl 3**, S5-96 (2000).
7. R. Strippoli *et al.*, Molecular Mechanisms Underlying Peritoneal EMT and Fibrosis. *Stem Cells Int* **2016**, 3543678 (2016).
8. J. O. van Baal *et al.*, The histophysiology and pathophysiology of the peritoneum. *Tissue Cell* **49**, 95-105 (2017).
9. S. E. Herrick, S. E. Mutsaers, Mesothelial progenitor cells and their potential in tissue engineering. *Int J Biochem Cell Biol* **36**, 621-642 (2004).
10. S. E. Mutsaers, The mesothelial cell. *Int J Biochem Cell Biol* **36**, 9-16 (2004).
11. A. Isaza-Restrepo, J. S. Martin-Saavedra, J. L. Velez-Leal, F. Vargas-Barato, R. Riveros-Duenas, The Peritoneum: Beyond the Tissue - A Review. *Front Physiol* **9**, 738 (2018).
12. A. M. Albanese *et al.*, Peritoneal surface area: measurements of 40 structures covered by peritoneum: correlation between total peritoneal surface area and the surface calculated by formulas. *Surg Radiol Anat* **31**, 369-377 (2009).
13. S. C. Blackburn, M. P. Stanton, Anatomy and physiology of the peritoneum. *Semin Pediatr Surg* **23**, 326-330 (2014).
14. J. A. Nagy, R. W. Jackman, Anatomy and Physiology of the Peritoneal Membrane. Seminars in Dialysis *Basic Science and Dialysis* (1998).
15. M. Gulyas, A. Hjerpe, Proteoglycans and WT1 as markers for distinguishing adenocarcinoma, epithelioid mesothelioma, and benign mesothelium. *J Pathol* **199**, 479-487 (2003).
16. B. Wilm, R. Munoz-Chapuli, The Role of WT1 in Embryonic Development and Normal Organ Homeostasis. *Methods Mol Biol* **1467**, 23-39 (2016).
17. S. Karki *et al.*, Wilms' tumor 1 (Wt1) regulates pleural mesothelial cell plasticity and transition into myofibroblasts in idiopathic pulmonary fibrosis. *FASEB journal : official publication of the Federation of American Societies for Experimental Biology* **28**, 1122-1131 (2014).
18. M. Yanez-Mo *et al.*, Peritoneal dialysis and epithelial-to-mesenchymal transition of mesothelial cells. *N Engl J Med* **348**, 403-413 (2003).
19. A. H. Yang, J. Y. Chen, J. K. Lin, Myofibroblastic conversion of mesothelial cells. *Kidney Int* **63**, 1530-1539 (2003).
20. R. Strippoli *et al.*, Caveolin-1 deficiency induces a MEK-ERK1/2-Snail-1-dependent epithelial-mesenchymal transition and fibrosis during peritoneal dialysis. *EMBO Mol Med* **7**, 102-123 (2015).
21. L. S. Aroeira *et al.*, Epithelial to mesenchymal transition and peritoneal membrane failure in peritoneal dialysis patients: pathologic significance and potential therapeutic interventions. *J Am Soc Nephrol* **18**, 2004-2013 (2007).
22. S. E. Mutsaers, Mesothelial cells: their structure, function and role in serosal repair. *Respirology* **7**, 171-191 (2002).
23. S. E. Mutsaers, D. Whitaker, J. M. Papadimitriou, Changes in the concentration of microvilli on the free surface of healing mesothelium are associated with alterations in surface membrane charge. *J Pathol* **180**, 333-339 (1996).

24. S. Yung, T. M. Chan, Pathophysiological changes to the peritoneal membrane during PD-related peritonitis: the role of mesothelial cells. *Mediators Inflamm* **2012**, 484167 (2012).
25. A. Breborowicz *et al.*, Role of peritoneal mesothelial cells and fibroblasts in the synthesis of hyaluronan during peritoneal dialysis. *Perit Dial Int* **18**, 382-386 (1998).
26. S. E. Mutsaers *et al.*, Mesothelial cells in tissue repair and fibrosis. *Front Pharmacol* **6**, 113 (2015).
27. A. Aguilera, Loureiro, J., Gónzales-Mateo, G., Selgas, R., and López-Cabrera, M. (2013), vol. The latest in peritoneal dialysis, pp. (CAP.2, 22-37).
28. S. Citi, M. Cordenonsi, Tight junction proteins. *Biochim Biophys Acta* **1448**, 1-11 (1998).
29. L. Gonzalez-Mariscal, R. Tapia, D. Chamorro, Crosstalk of tight junction components with signaling pathways. *Biochim Biophys Acta* **1778**, 729-756 (2008).
30. S. Lamouille, J. Xu, R. Derynck, Molecular mechanisms of epithelial-mesenchymal transition. *Nat Rev Mol Cell Biol* **15**, 178-196 (2014).
31. C. Retana *et al.*, Alterations of intercellular junctions in peritoneal mesothelial cells from patients undergoing dialysis: effect of retinoic Acid. *Perit Dial Int* **35**, 275-287 (2015).
32. A. K. Rajasekaran, M. Hojo, T. Huima, E. Rodriguez-Boulan, Catenins and zonula occludens-1 form a complex during early stages in the assembly of tight junctions. *J Cell Biol* **132**, 451-463 (1996).
33. C. M. Niessen, Tight junctions/adherens junctions: basic structure and function. *J Invest Dermatol* **127**, 2525-2532 (2007).
34. H. Peinado, E. Ballestar, M. Esteller, A. Cano, Snail mediates E-cadherin repression by the recruitment of the Sin3A/histone deacetylase 1 (HDAC1)/HDAC2 complex. *Mol Cell Biol* **24**, 306-319 (2004).
35. A. Hartsock, W. J. Nelson, Adherens and tight junctions: structure, function and connections to the actin cytoskeleton. *Biochim Biophys Acta* **1778**, 660-669 (2008).
36. N. A. Gloushankova, S. N. Rubtsova, I. Y. Zhitnyak, Cadherin-mediated cell-cell interactions in normal and cancer cells. *Tissue Barriers* **5**, e1356900 (2017).
37. M. Simionescu, N. Simionescu, Organization of cell junctions in the peritoneal mesothelium. *J Cell Biol* **74**, 98-110 (1977).
38. Y. Takada, X. Ye, S. Simon, The integrins. *Genome Biol* **8**, 215 (2007).
39. M. H. Ginsberg, A. Partridge, S. J. Shattil, Integrin regulation. *Curr Opin Cell Biol* **17**, 509-516 (2005).
40. M. A. Arnaout, B. Mahalingam, J. P. Xiong, Integrin structure, allostery, and bidirectional signaling. *Annu Rev Cell Dev Biol* **21**, 381-410 (2005).
41. D. R. Critchley, Cytoskeletal proteins talin and vinculin in integrin-mediated adhesion. *Biochem Soc Trans* **32**, 831-836 (2004).
42. D. R. Critchley, Genetic, biochemical and structural approaches to talin function. *Biochem Soc Trans* **33**, 1308-1312 (2005).
43. O. Devuyst, B. Rippe, Water transport across the peritoneal membrane. *Kidney Int* **85**, 750-758 (2014).
44. S. E. Mutsaers, C. M. Prele, S. Pengelly, S. E. Herrick, Mesothelial cells and peritoneal homeostasis. *Fertil Steril* **106**, 1018-1024 (2016).
45. R. W. Hamilton, Principles of dialysis: diffusion, convection, and dialysis machines. 1999.
46. J. Himmelfarb, T. A. Ikizler, Hemodialysis. *N Engl J Med* **363**, 1833-1845 (2010).
47. J. Perl, J. M. Bargman, Peritoneal dialysis: from bench to bedside and bedside to bench. *Am J Physiol Renal Physiol* **311**, F999-F1004 (2016).
48. https://www.niddk.nih.gov. (National institute of Health).
49. S. Pastan, J. Bailey, Dialysis therapy. *N Engl J Med* **338**, 1428-1437 (1998).
50. N. Nakamura-Taira, Y. Muranaka, M. Miwa, S. Kin, K. Hirai, Views of Japanese patients on the advantages and disadvantages of hemodialysis and peritoneal dialysis. *Int Urol Nephrol* **45**, 1145-1158 (2013).
51. K. M. Ansel, R. B. Harris, J. G. Cyster, CXCL13 is required for B1 cell homing, natural antibody production, and body cavity immunity. *Immunity* **16**, 67-76 (2002).
52. M. B. Buechler, S. J. Turley, Neutrophils Follow Stromal Omens to Limit Peritoneal Inflammation. *Immunity* **52**, 578-580 (2020).

53. A. Douvdevani *et al.*, Human peritoneal mesothelial cells synthesize IL-1 alpha and beta. *Kidney Int* **46**, 993-1001 (1994).
54. N. Topley, R. K. Mackenzie, J. D. Williams, Macrophages and mesothelial cells in bacterial peritonitis. *Immunobiology* **195**, 563-573 (1996).
55. M. J. Hausmann, B. Rogachev, M. Weiler, C. Chaimovitz, A. Douvdevani, Accessory role of human peritoneal mesothelial cells in antigen presentation and T-cell growth. *Kidney Int* **57**, 476-486 (2000).
56. M. G. Betjes *et al.*, Interleukin-8 production by human peritoneal mesothelial cells in response to tumor necrosis factor-alpha, interleukin-1, and medium conditioned by macrophages cocultured with Staphylococcus epidermidis. *J Infect Dis* **168**, 1202-1210 (1993).
57. N. Topley *et al.*, Human peritoneal mesothelial cells synthesize interleukin-6: induction by IL-1 beta and TNF alpha. *Kidney Int* **43**, 226-233 (1993).
58. N. Topley *et al.*, Human peritoneal mesothelial cells synthesize interleukin-8. Synergistic induction by interleukin-1 beta and tumor necrosis factor-alpha. *Am J Pathol* **142**, 1876-1886 (1993).
59. L. Lanfrancone *et al.*, Human peritoneal mesothelial cells produce many cytokines (granulocyte colony-stimulating factor [CSF], granulocyte-monocyte-CSF, macrophage-CSF, interleukin-1 [IL-1], and IL-6) and are activated and stimulated to grow by IL-1. *Blood* **80**, 2835-2842 (1992).
60. N. Jonjic *et al.*, Expression of adhesion molecules and chemotactic cytokines in cultured human mesothelial cells. *J Exp Med* **176**, 1165-1174 (1992).
61. T. Liberek, N. Topley, W. Luttmann, J. D. Williams, Adherence of neutrophils to human peritoneal mesothelial cells: role of intercellular adhesion molecule-1. *J Am Soc Nephrol* **7**, 208-217 (1996).
62. P. Kinnaert, J. P. De Wilde, B. Bournonville, C. Husson, I. Salmon, Direct activation of human peritoneal mesothelial cells by heat-killed microorganisms. *Ann Surg* **224**, 749-754; discussion 754-745 (1996).
63. H. A. Mutsaers, E. G. Stribos, G. Glorieux, R. Vanholder, P. Olinga, Chronic Kidney Disease and Fibrosis: The Role of Uremic Retention Solutes. *Front Med (Lausanne)* **2**, 60 (2015).
64. J. W. Dobbie, T. Pavlina, J. Lloyd, R. C. Johnson, Phosphatidylcholine synthesis by peritoneal mesothelium: its implications for peritoneal dialysis. *Am J Kidney Dis* **12**, 31-36 (1988).
65. P. Heldin, H. Pertoft, Synthesis and assembly of the hyaluronan-containing coats around normal human mesothelial cells. *Exp Cell Res* **208**, 422-429 (1993).
66. S. P. Evanko, M. I. Tammi, R. H. Tammi, T. N. Wight, Hyaluronan-dependent pericellular matrix. *Adv Drug Deliv Rev* **59**, 1351-1365 (2007).
67. K. Kramer, N. Senninger, H. Herbst, W. Probst, Effective prevention of adhesions with hyaluronate. *Arch Surg* **137**, 278-282 (2002).
68. S. Yung, G. J. Thomas, M. Davies, Induction of hyaluronan metabolism after mechanical injury of human peritoneal mesothelial cells in vitro. *Kidney Int* **58**, 1953-1962 (2000).
69. B. Tingstedt, K. Isaksson, E. Andersson, R. Andersson, Prevention of abdominal adhesions--present state and what's beyond the horizon? *Eur Surg Res* **39**, 259-268 (2007).
70. J. P. Thiery, H. Acloque, R. Y. Huang, M. A. Nieto, Epithelial-mesenchymal transitions in development and disease. *Cell* **139**, 871-890 (2009).
71. R. Kalluri, R. A. Weinberg, The basics of epithelial-mesenchymal transition. *J Clin Invest* **119**, 1420-1428 (2009).
72. Q. Yao *et al.*, The role of the TGF/Smad signaling pathway in peritoneal fibrosis induced by peritoneal dialysis solutions. *Nephron Exp Nephrol* **109**, e71-78 (2008).
73. J. W. Wu *et al.*, Crystal structure of a phosphorylated Smad2. Recognition of phosphoserine by the MH2 domain and insights on Smad function in TGF-beta signaling. *Mol Cell* **8**, 1277-1289 (2001).
74. C. H. Heldin, K. Miyazono, P. ten Dijke, TGF-beta signalling from cell membrane to nucleus through SMAD proteins. *Nature* **390**, 465-471 (1997).
75. Y. Shi, J. Massague, Mechanisms of TGF-beta signaling from cell membrane to the nucleus. *Cell* **113**, 685-700 (2003).
76. J. Xu, S. Lamouille, R. Derynck, TGF-beta-induced epithelial to mesenchymal transition. *Cell Res* **19**, 156-172 (2009).

77. R. Weiskirchen, S. K. Meurer, BMP-7 counteracting TGF-beta1 activities in organ fibrosis. *Front Biosci (Landmark Ed)* **18**, 1407-1434 (2013).
78. J. Loureiro *et al.*, BMP-7 blocks mesenchymal conversion of mesothelial cells and prevents peritoneal damage induced by dialysis fluid exposure. *Nephrol Dial Transplant* **25**, 1098-1108 (2010).
79. M. A. Yu *et al.*, HGF and BMP-7 ameliorate high glucose-induced epithelial-to-mesenchymal transition of peritoneal mesothelium. *J Am Soc Nephrol* **20**, 567-581 (2009).
80. E. F. Wagner, A. R. Nebreda, Signal integration by JNK and p38 MAPK pathways in cancer development. *Nat Rev Cancer* **9**, 537-549 (2009).
81. T. Gui, Y. Sun, A. Shimokado, Y. Muragaki, The Roles of Mitogen-Activated Protein Kinase Pathways in TGF-beta-Induced Epithelial-Mesenchymal Transition. *J Signal Transduct* **2012**, 289243 (2012).
82. R. Strippoli *et al.*, Epithelial-to-mesenchymal transition of peritoneal mesothelial cells is regulated by an ERK/NF-kappaB/Snail1 pathway. *Dis Model Mech* **1**, 264-274 (2008).
83. C. Hough, M. Radu, J. J. Dore, Tgf-beta induced Erk phosphorylation of smad linker region regulates smad signaling. *PLoS One* **7**, e42513 (2012).
84. R. Strippoli *et al.*, Caveolin-1 deficiency induces a MEK-ERK1/2-Snail-1-dependent epithelial-mesenchymal transition and fibrosis during peritoneal dialysis. *Embo Molecular Medicine* **7**, 102-123 (2015).
85. R. Strippoli *et al.*, p38 maintains E-cadherin expression by modulating TAK1-NF-kappa B during epithelial-to-mesenchymal transition. *J Cell Sci* **123**, 4321-4331 (2010).
86. R. Strippoli *et al.*, Inhibition of transforming growth factor-activated kinase 1 (TAK1) blocks and reverses epithelial to mesenchymal transition of mesothelial cells. *PLoS One* **7**, e31492 (2012).
87. N. A. Bhowmick *et al.*, Transforming growth factor-beta1 mediates epithelial to mesenchymal transdifferentiation through a RhoA-dependent mechanism. *Mol Biol Cell* **12**, 27-36 (2001).
88. P. Patel *et al.*, Smad3-dependent and -independent pathways are involved in peritoneal membrane injury. *Kidney Int* **77**, 319-328 (2010).
89. A. Santos, D. Lagares, Matrix Stiffness: the Conductor of Organ Fibrosis. *Curr Rheumatol Rep* **20**, 2 (2018).
90. R. G. Wells, Tissue mechanics and fibrosis. *Biochim Biophys Acta* **1832**, 884-890 (2013).
91. M. J. Paszek *et al.*, Tensional homeostasis and the malignant phenotype. *Cancer Cell* **8**, 241-254 (2005).
92. A. C. Shieh, Biomechanical forces shape the tumor microenvironment. *Ann Biomed Eng* **39**, 1379-1389 (2011).
93. M. Najafi, B. Farhood, K. Mortezaee, Extracellular matrix (ECM) stiffness and degradation as cancer drivers. *J Cell Biochem* **120**, 2782-2790 (2019).
94. D. J. Tschumperlin, F. Boudreault, F. Liu, Recent advances and new opportunities in lung mechanobiology. *J Biomech* **43**, 99-107 (2010).
95. R. L. Heise, V. Stober, C. Cheluvaraju, J. W. Hollingsworth, S. Garantziotis, Mechanical stretch induces epithelial-mesenchymal transition in alveolar epithelia via hyaluronan activation of innate immunity. *J Biol Chem* **286**, 17435-17444 (2011).
96. N. F. Jufri, A. Mohamedali, A. Avolio, M. S. Baker, Mechanical stretch: physiological and pathological implications for human vascular endothelial cells. *Vasc Cell* **7**, 8 (2015).
97. Z. He, R. Potter, X. Li, M. Flessner, Stretch of human mesothelial cells increases cytokine expression. *Adv Perit Dial* **28**, 2-9 (2012).
98. R. Strippoli *et al.*, Caveolin1 and YAP drive mechanically induced mesothelial to mesenchymal transition and fibrosis. *Cell Death Dis* **11**, 647 (2020).
99. P. Sandoval *et al.*, Mesothelial-to-mesenchymal transition in the pathogenesis of post-surgical peritoneal adhesions. *J Pathol* **239**, 48-59 (2016).
100. J. M. Tsai *et al.*, Surgical adhesions in mice are derived from mesothelial cells and can be targeted by antibodies against mesothelial markers. *Sci Transl Med* **10**, (2018).
101. R. G. Parton, M. A. del Pozo, Caveolae as plasma membrane sensors, protectors and organizers. *Nat Rev Mol Cell Biol* **14**, 98-112 (2013).

102. P. J. Wipff, D. B. Rifkin, J. J. Meister, B. Hinz, Myofibroblast contraction activates latent TGF-beta1 from the extracellular matrix. *J Cell Biol* **179**, 1311-1323 (2007).
103. S. Dupont *et al.*, Role of YAP/TAZ in mechanotransduction. *Nature* **474**, 179-183 (2011).
104. S. Piccolo, S. Dupont, M. Cordenonsi, The biology of YAP/TAZ: hippo signaling and beyond. *Physiol Rev* **94**, 1287-1312 (2014).
105. R. Mehrotra, O. Devuyst, S. J. Davies, D. W. Johnson, The Current State of Peritoneal Dialysis. *J Am Soc Nephrol* **27**, 3238-3252 (2016).
106. C. Goodlad *et al.*, Measurement of innate immune response biomarkers in peritoneal dialysis effluent using a rapid diagnostic point-of-care device as a diagnostic indicator of peritonitis. *Kidney Int* **97**, 1253-1259 (2020).
107. C. Aufricht *et al.*, Biomarker research to improve clinical outcomes of peritoneal dialysis: consensus of the European Training and Research in Peritoneal Dialysis (EuTRiPD) network. *Kidney Int* **92**, 824-835 (2017).
108. J. S. Roh, D. H. Sohn, Damage-Associated Molecular Patterns in Inflammatory Diseases. *Immune Netw* **18**, e27 (2018).
109. O. Takeuchi, S. Akira, Pattern recognition receptors and inflammation. *Cell* **140**, 805-820 (2010).
110. A. C. Raby *et al.*, Toll-Like Receptors 2 and 4 Are Potential Therapeutic Targets in Peritoneal Dialysis-Associated Fibrosis. *J Am Soc Nephrol* **28**, 461-478 (2017).
111. A. C. Raby *et al.*, Targeting Toll-like receptors with soluble Toll-like receptor 2 prevents peritoneal dialysis solution-induced fibrosis. *Kidney Int* **94**, 346-362 (2018).
112. C. Higuchi, H. Nishimura, T. Sanaka, Biocompatibility of peritoneal dialysis fluid and influence of compositions on peritoneal fibrosis. *Ther Apher Dial* **10**, 372-379 (2006).
113. E. Garcia-Lopez, B. Lindholm, S. Davies, An update on peritoneal dialysis solutions. *Nat Rev Nephrol* **8**, 224-233 (2012).
114. T. Ito, N. Yorioka, M. Yamamoto, K. Kataoka, M. Yamakido, Effect of glucose on intercellular junctions of cultured human peritoneal mesothelial cells. *J Am Soc Nephrol* **11**, 1969-1979 (2000).
115. A. S. De Vriese, A. Flyvbjerg, S. Mortier, R. G. Tilton, N. H. Lameire, Inhibition of the interaction of AGE-RAGE prevents hyperglycemia-induced fibrosis of the peritoneal membrane. *J Am Soc Nephrol* **14**, 2109-2118 (2003).
116. S. Mortier, D. Faict, C. G. Schalkwijk, N. H. Lameire, A. S. De Vriese, Long-term exposure to new peritoneal dialysis solutions: Effects on the peritoneal membrane. *Kidney Int* **66**, 1257-1265 (2004).
117. J. Witowski *et al.*, Effect of glucose degradation products on human peritoneal mesothelial cell function. *J Am Soc Nephrol* **11**, 729-739 (2000).
118. T. Linden, A. Cohen, R. Deppisch, P. Kjellstrand, A. Wieslander, 3,4-Dideoxyglucosone-3-ene (3,4-DGE): a cytotoxic glucose degradation product in fluids for peritoneal dialysis. *Kidney Int* **62**, 697-703 (2002).
119. Y. Tomino, Mechanisms and interventions in peritoneal fibrosis. *Clin Exp Nephrol* **16**, 109-114 (2012).
120. R. Inagi *et al.*, Glucose degradation product methylglyoxal enhances the production of vascular endothelial growth factor in peritoneal cells: role in the functional and morphological alterations of peritoneal membranes in peritoneal dialysis. *FEBS Lett* **463**, 260-264 (1999).
121. M. S. Park, H. A. Lee, W. S. Chu, D. H. Yang, S. D. Hwang, Peritoneal accumulation of AGE and peritoneal membrane permeability. *Perit Dial Int* **20**, 452-460 (2000).
122. S. Ogata *et al.*, Effect of lactate and bicarbonate on human peritoneal mesothelial cells, fibroblasts and vascular endothelial cells, and the role of basic fibroblast growth factor. *Nephrol Dial Transplant* **19**, 2831-2837 (2004).
123. A. B. Saxena, Recent advances in the management of peritoneal dialysis patients. *F1000Prime Rep* **7**, 57 (2015).
124. D. W. Johnson *et al.*, Effects of biocompatible versus standard fluid on peritoneal dialysis outcomes. *J Am Soc Nephrol* **23**, 1097-1107 (2012).

125. J. P. Rougier, S. Guia, J. Hagege, G. Nguyen, P. M. Ronco, PAI-1 secretion and matrix deposition in human peritoneal mesothelial cell cultures: transcriptional regulation by TGF-beta 1. *Kidney Int* **54**, 87-98 (1998).
126. A. C. Raby, M. O. Labeta, Preventing Peritoneal Dialysis-Associated Fibrosis by Therapeutic Blunting of Peritoneal Toll-Like Receptor Activity. *Front Physiol* **9**, 1692 (2018).
127. G. Garosi, N. Di Paolo, Morphological aspects of peritoneal sclerosis. *J Nephrol* **14 Suppl 4**, S30-38 (2001).
128. A. M. Sherif *et al.*, Comparison between the pathology of encapsulating sclerosis and simple sclerosis of the peritoneal membrane in chronic peritoneal dialysis. *Ther Apher Dial* **12**, 33-41 (2008).
129. G. Baroni, A. Schuinski, T. P. de Moraes, F. Meyer, R. Pecoits-Filho, Inflammation and the peritoneal membrane: causes and impact on structure and function during peritoneal dialysis. *Mediators Inflamm* **2012**, 912595 (2012).
130. C. J. Danford, S. C. Lin, M. P. Smith, J. L. Wolf, Encapsulating peritoneal sclerosis. *World J Gastroenterol* **24**, 3101-3111 (2018).
131. A. Aguilera, Loureiro, J., Gónzales-Mateo, G., Selgas, R., and López-Cabrera, M. (2013), vol. The latest in peritoneal dialysis

pp. (CAP.2, 22-37).
132. J. Uitto, D. Kouba, Cytokine modulation of extracellular matrix gene expression: relevance to fibrotic skin diseases. *J Dermatol Sci* **24 Suppl 1**, S60-69 (2000).
133. M. Zeisberg, R. Kalluri, Fibroblasts emerge via epithelial-mesenchymal transition in chronic kidney fibrosis. *Front Biosci* **13**, 6991-6998 (2008).
134. M. Zeisberg, R. Kalluri, Reversal of experimental renal fibrosis by BMP7 provides insights into novel therapeutic strategies for chronic kidney disease. *Pediatr Nephrol* **23**, 1395-1398 (2008).
135. E. L. George, E. N. Georges-Labouesse, R. S. Patel-King, H. Rayburn, R. O. Hynes, Defects in mesoderm, neural tube and vascular development in mouse embryos lacking fibronectin. *Development* **119**, 1079-1091 (1993).
136. E. N. Georges-Labouesse, E. L. George, H. Rayburn, R. O. Hynes, Mesodermal development in mouse embryos mutant for fibronectin. *Dev Dyn* **207**, 145-156 (1996).
137. S. Astrof, R. O. Hynes, Fibronectins in vascular morphogenesis. *Angiogenesis* **12**, 165-175 (2009).
138. L. A. Davidson, R. Keller, D. W. DeSimone, Assembly and remodeling of the fibrillar fibronectin extracellular matrix during gastrulation and neurulation in Xenopus laevis. *Dev Dyn* **231**, 888-895 (2004).
139. M. Larsen, C. Wei, K. M. Yamada, Cell and fibronectin dynamics during branching morphogenesis. *J Cell Sci* **119**, 3376-3384 (2006).
140. A. Varadaraj *et al.*, TGF-beta triggers rapid fibrillogenesis via a novel TbetaRII-dependent fibronectin-trafficking mechanism. *Mol Biol Cell* **28**, 1195-1207 (2017).
141. R. O. Hynes, Integrins: bidirectional, allosteric signaling machines. *Cell* **110**, 673-687 (2002).
142. Z. Sun, S. S. Guo, R. Fassler, Integrin-mediated mechanotransduction. *J Cell Biol* **215**, 445-456 (2016).
143. Z. Li, H. Lee, C. Zhu, Molecular mechanisms of mechanotransduction in integrin-mediated cell-matrix adhesion. *Exp Cell Res* **349**, 85-94 (2016).
144. A. D. Doyle, S. S. Nazari, K. M. Yamada, Cell-extracellular matrix dynamics. *Phys Biol* **19**, (2022).
145. E. H. Danen, A. Sonnenberg, Integrins in regulation of tissue development and function. *J Pathol* **201**, 632-641 (2003).
146. J. T. Yang, R. O. Hynes, Fibronectin receptor functions in embryonic cells deficient in alpha 5 beta 1 integrin can be replaced by alpha V integrins. *Mol Biol Cell* **7**, 1737-1748 (1996).
147. S. Filippov *et al.*, MT1-matrix metalloproteinase directs arterial wall invasion and neointima formation by vascular smooth muscle cells. *J Exp Med* **202**, 663-671 (2005).
148. E. Marchina, S. Barlati, Degradation of human plasma and extracellular matrix fibronectin by tissue type plasminogen activator and urokinase. *Int J Biochem Cell Biol* **28**, 1141-1150 (1996).

149. E. Ohuchi *et al.*, Membrane type 1 matrix metalloproteinase digests interstitial collagens and other extracellular matrix macromolecules. *J Biol Chem* **272**, 2446-2451 (1997).
150. T. M. Odrljin, C. G. Haidaris, N. B. Lerner, P. J. Simpson-Haidaris, Integrin alphavbeta3-mediated endocytosis of immobilized fibrinogen by A549 lung alveolar epithelial cells. *Am J Respir Cell Mol Biol* **24**, 12-21 (2001).
151. T. S. Panetti, S. A. Wilcox, C. Horzempa, P. J. McKeown-Longo, Alpha v beta 5 integrin receptor-mediated endocytosis of vitronectin is protein kinase C-dependent. *J Biol Chem* **270**, 18593-18597 (1995).
152. J. Sottile, J. Chandler, Fibronectin matrix turnover occurs through a caveolin-1-dependent process. *Mol Biol Cell* **16**, 757-768 (2005).
153. F. Shi, J. Sottile, Caveolin-1-dependent beta1 integrin endocytosis is a critical regulator of fibronectin turnover. *J Cell Sci* **121**, 2360-2371 (2008).
154. F. Shi, J. Sottile, MT1-MMP regulates the turnover and endocytosis of extracellular matrix fibronectin. *J Cell Sci* **124**, 4039-4050 (2011).
155. H. Sato *et al.*, A matrix metalloproteinase expressed on the surface of invasive tumour cells. *Nature* **370**, 61-65 (1994).
156. C. Frantz, K. M. Stewart, V. M. Weaver, The extracellular matrix at a glance. *J Cell Sci* **123**, 4195-4200 (2010).
157. M. Lopez-Cabrera *et al.*, Ex vivo analysis of dialysis effluent-derived mesothelial cells as an approach to unveiling the mechanism of peritoneal membrane failure. *Perit Dial Int* **26**, 26-34 (2006).
158. F. Verrecchia, A. Mauviel, Transforming growth factor-beta signaling through the Smad pathway: role in extracellular matrix gene expression and regulation. *J Invest Dermatol* **118**, 211-215 (2002).
159. D. A. Fishman *et al.*, Metastatic dissemination of human ovarian epithelial carcinoma is promoted by alpha2beta1-integrin-mediated interaction with type I collagen. *Invasion Metastasis* **18**, 15-26 (1998).
160. K. E. Kadler, C. Baldock, J. Bella, R. P. Boot-Handford, Collagens at a glance. *J Cell Sci* **120**, 1955-1958 (2007).
161. V. Iorio, L. D. Troughton, K. J. Hamill, Laminins: Roles and Utility in Wound Repair. *Adv Wound Care (New Rochelle)* **4**, 250-263 (2015).
162. N. Cui, M. Hu, R. A. Khalil, Biochemical and Biological Attributes of Matrix Metalloproteinases. *Prog Mol Biol Transl Sci* **147**, 1-73 (2017).
163. J. Liu, R. A. Khalil, Matrix Metalloproteinase Inhibitors as Investigational and Therapeutic Tools in Unrestrained Tissue Remodeling and Pathological Disorders. *Prog Mol Biol Transl Sci* **148**, 355-420 (2017).
164. H. Nagase, R. Visse, G. Murphy, Structure and function of matrix metalloproteinases and TIMPs. *Cardiovasc Res* **69**, 562-573 (2006).
165. C. Amalinei, I. D. Caruntu, R. A. Balan, Biology of metalloproteinases. *Rom J Morphol Embryol* **48**, 323-334 (2007).
166. G. Murphy, H. Nagase, Progress in matrix metalloproteinase research. *Mol Aspects Med* **29**, 290-308 (2008).
167. R. Visse, H. Nagase, Matrix metalloproteinases and tissue inhibitors of metalloproteinases: structure, function, and biochemistry. *Circ Res* **92**, 827-839 (2003).
168. M. Whittaker, C. D. Floyd, P. Brown, A. J. Gearing, Design and therapeutic application of matrix metalloproteinase inhibitors. *Chem Rev* **99**, 2735-2776 (1999).
169. F. Mannello, V. Medda, Nuclear localization of matrix metalloproteinases. *Prog Histochem Cytochem* **47**, 27-58 (2012).
170. T. Klein, R. Bischoff, Physiology and pathophysiology of matrix metalloproteases. *Amino Acids* **41**, 271-290 (2011).
171. M. Merkle *et al.*, Effect of activation of viral receptors on the gelatinases MMP-2 and MMP-9 in human mesothelial cells. *Matrix Biol* **29**, 202-208 (2010).

172. G. Matusali *et al.*, Pleural Mesothelial Cells Modulate the Inflammatory/Profibrotic Response During SARS-CoV-2 Infection. *Front Mol Biosci* **8**, 752616 (2021).
173. C. A. Janeway, Jr., R. Medzhitov, Innate immune recognition. *Annu Rev Immunol* **20**, 197-216 (2002).
174. S. Akira, S. Uematsu, O. Takeuchi, Pathogen recognition and innate immunity. *Cell* **124**, 783-801 (2006).
175. X. Cai, Y. H. Chiu, Z. J. Chen, The cGAS-cGAMP-STING pathway of cytosolic DNA sensing and signaling. *Mol Cell* **54**, 289-296 (2014).
176. I. Botos, D. M. Segal, D. R. Davies, The structural biology of Toll-like receptors. *Structure* **19**, 447-459 (2011).
177. T. Kawai, S. Akira, The role of pattern-recognition receptors in innate immunity: update on Toll-like receptors. *Nat Immunol* **11**, 373-384 (2010).
178. T. Celhar, R. Magalhaes, A. M. Fairhurst, TLR7 and TLR9 in SLE: when sensing self goes wrong. *Immunol Res* **53**, 58-77 (2012).
179. T. Regan *et al.*, Identification of TLR10 as a key mediator of the inflammatory response to Listeria monocytogenes in intestinal epithelial cells and macrophages. *J Immunol* **191**, 6084-6092 (2013).
180. S. M. Lee *et al.*, Toll-like receptor 10 is involved in induction of innate immune responses to influenza virus infection. *Proc Natl Acad Sci U S A* **111**, 3793-3798 (2014).
181. A. L. Blasius, B. Beutler, Intracellular toll-like receptors. *Immunity* **32**, 305-315 (2010).
182. S. Y. Zhang *et al.*, TLR3 deficiency in patients with herpes simplex encephalitis. *Science* **317**, 1522-1527 (2007).
183. J. J. Bernard *et al.*, Ultraviolet radiation damages self noncoding RNA and is detected by TLR3. *Nat Med* **18**, 1286-1290 (2012).
184. N. Takemura *et al.*, Blockade of TLR3 protects mice from lethal radiation-induced gastrointestinal syndrome. *Nat Commun* **5**, 3492 (2014).
185. G. Mancuso *et al.*, Bacterial recognition by TLR7 in the lysosomes of conventional dendritic cells. *Nat Immunol* **10**, 587-594 (2009).
186. C. Guiducci *et al.*, RNA recognition by human TLR8 can lead to autoimmune inflammation. *J Exp Med* **210**, 2903-2919 (2013).
187. H. Tanji, U. Ohto, T. Shibata, K. Miyake, T. Shimizu, Structural reorganization of the Toll-like receptor 8 dimer induced by agonistic ligands. *Science* **339**, 1426-1429 (2013).
188. A. Hidmark, A. von Saint Paul, A. H. Dalpke, Cutting edge: TLR13 is a receptor for bacterial RNA. *J Immunol* **189**, 2717-2721 (2012).
189. X. D. Li, Z. J. Chen, Sequence specific detection of bacterial 23S ribosomal RNA by TLR13. *Elife* **1**, e00102 (2012).
190. M. Oldenburg *et al.*, TLR13 recognizes bacterial 23S rRNA devoid of erythromycin resistance-forming modification. *Science* **337**, 1111-1115 (2012).
191. Z. Shi *et al.*, A novel Toll-like receptor that recognizes vesicular stomatitis virus. *J Biol Chem* **286**, 4517-4524 (2011).
192. C. Coban *et al.*, Immunogenicity of whole-parasite vaccines against Plasmodium falciparum involves malarial hemozoin and host TLR9. *Cell Host Microbe* **7**, 50-61 (2010).
193. R. Mathur *et al.*, A mouse model of Salmonella typhi infection. *Cell* **151**, 590-602 (2012).
194. F. Yarovinsky *et al.*, TLR11 activation of dendritic cells by a protozoan profilin-like protein. *Science* **308**, 1626-1629 (2005).
195. A. A. Koblansky *et al.*, Recognition of profilin by Toll-like receptor 12 is critical for host resistance to Toxoplasma gondii. *Immunity* **38**, 119-130 (2013).
196. W. A. Andrade *et al.*, Combined action of nucleic acid-sensing Toll-like receptors and TLR11/TLR12 heterodimers imparts resistance to Toxoplasma gondii in mice. *Cell Host Microbe* **13**, 42-53 (2013).
197. P. Broz, D. M. Monack, Newly described pattern recognition receptors team up against intracellular pathogens. *Nat Rev Immunol* **13**, 551-565 (2013).
198. S. C. Lin, Y. C. Lo, H. Wu, Helical assembly in the MyD88-IRAK4-IRAK2 complex in TLR/IL-1R signalling. *Nature* **465**, 885-890 (2010).

199. C. Kollewe *et al.*, Sequential autophosphorylation steps in the interleukin-1 receptor-associated kinase-1 regulate its availability as an adapter in interleukin-1 signaling. *J Biol Chem* **279**, 5227-5236 (2004).
200. Z. Jiang, J. Ninomiya-Tsuji, Y. Qian, K. Matsumoto, X. Li, Interleukin-1 (IL-1) receptor-associated kinase-dependent IL-1-induced signaling complexes phosphorylate TAK1 and TAB2 at the plasma membrane and activate TAK1 in the cytosol. *Mol Cell Biol* **22**, 7158-7167 (2002).
201. Z. J. Chen, Ubiquitination in signaling to and activation of IKK. *Immunol Rev* **246**, 95-106 (2012).
202. P. P. Roux, J. Blenis, ERK and p38 MAPK-activated protein kinases: a family of protein kinases with diverse biological functions. *Microbiol Mol Biol Rev* **68**, 320-344 (2004).
203. A. A. Ajibade *et al.*, TAK1 negatively regulates NF-kappaB and p38 MAP kinase activation in Gr-1+CD11b+ neutrophils. *Immunity* **36**, 43-54 (2012).
204. J. H. Shim *et al.*, TAK1, but not TAB1 or TAB2, plays an essential role in multiple signaling pathways in vivo. *Genes Dev* **19**, 2668-2681 (2005).
205. D. Ori *et al.*, Essential roles of K63-linked polyubiquitin-binding proteins TAB2 and TAB3 in B cell activation via MAPKs. *J Immunol* **190**, 4037-4045 (2013).
206. A. P. West *et al.*, TLR signalling augments macrophage bactericidal activity through mitochondrial ROS. *Nature* **472**, 476-480 (2011).
207. X. Jiang, Z. J. Chen, The role of ubiquitylation in immune defence and pathogen evasion. *Nat Rev Immunol* **12**, 35-48 (2011).
208. M. Chang, W. Jin, S. C. Sun, Peli1 facilitates TRIF-dependent Toll-like receptor signaling and proinflammatory cytokine production. *Nat Immunol* **10**, 1089-1095 (2009).
209. T. Kawasaki, N. Takemura, D. M. Standley, S. Akira, T. Kawai, The second messenger phosphatidylinositol-5-phosphate facilitates antiviral innate immune signaling. *Cell Host Microbe* **14**, 148-158 (2013).
210. H. Negishi *et al.*, Evidence for licensing of IFN-gamma-induced IFN regulatory factor 1 transcription factor by MyD88 in Toll-like receptor-dependent gene induction program. *Proc Natl Acad Sci U S A* **103**, 15136-15141 (2006).
211. A. Takaoka *et al.*, Integral role of IRF-5 in the gene induction programme activated by Toll-like receptors. *Nature* **434**, 243-249 (2005).
212. H. Tsujimura *et al.*, Toll-like receptor 9 signaling activates NF-kappaB through IFN regulatory factor-8/IFN consensus sequence binding protein in dendritic cells. *J Immunol* **172**, 6820-6827 (2004).
213. P. Tailor *et al.*, The feedback phase of type I interferon induction in dendritic cells requires interferon regulatory factor 8. *Immunity* **27**, 228-239 (2007).
214. M. Wornle *et al.*, Novel role of toll-like receptor 3, RIG-I and MDA5 in poly (I:C) RNA-induced mesothelial inflammation. *Mol Cell Biochem* **322**, 193-206 (2009).
215. M. Yamamoto *et al.*, Role of adaptor TRIF in the MyD88-independent toll-like receptor signaling pathway. *Science* **301**, 640-643 (2003).
216. S. Doyle *et al.*, IRF3 mediates a TLR3/TLR4-specific antiviral gene program. *Immunity* **17**, 251-263 (2002).
217. M. F. Tsan, B. Gao, Endogenous ligands of Toll-like receptors. *J Leukoc Biol* **76**, 514-519 (2004).
218. L. Yu, L. Wang, S. Chen, Endogenous toll-like receptor ligands and their biological significance. *J Cell Mol Med* **14**, 2592-2603 (2010).
219. Y. Okamura *et al.*, The extra domain A of fibronectin activates Toll-like receptor 4. *J Biol Chem* **276**, 10229-10233 (2001).
220. S. T. Smiley, J. A. King, W. W. Hancock, Fibrinogen stimulates macrophage chemokine secretion through toll-like receptor 4. *J Immunol* **167**, 2887-2894 (2001).
221. T. Vogl *et al.*, Mrp8 and Mrp14 are endogenous activators of Toll-like receptor 4, promoting lethal, endotoxin-induced shock. *Nat Med* **13**, 1042-1049 (2007).
222. K. Croce *et al.*, Myeloid-related protein-8/14 is critical for the biological response to vascular injury. *Circulation* **120**, 427-436 (2009).
223. K. Midwood *et al.*, Tenascin-C is an endogenous activator of Toll-like receptor 4 that is essential for maintaining inflammation in arthritic joint disease. *Nat Med* **15**, 774-780 (2009).

224. P. Zhang, C. J. Cox, K. M. Alvarez, M. W. Cunningham, Cutting edge: cardiac myosin activates innate immune responses through TLRs. *J Immunol* **183**, 27-31 (2009).
225. L. Apetoh *et al.*, Toll-like receptor 4-dependent contribution of the immune system to anticancer chemotherapy and radiotherapy. *Nat Med* **13**, 1050-1059 (2007).
226. G. Felsenfeld, A brief history of epigenetics. *Cold Spring Harb Perspect Biol* **6**, (2014).
227. C. H. Waddington, The epigenotype. . *Int J Epidemiol* **41**, 10-13 (1942).
228. C. H. Waddington, Towards a theoretical biology. *Nature* **218**, 525-527 (1968).
229. C. Dupont, D. R. Armant, C. A. Brenner, Epigenetics: definition, mechanisms and clinical perspective. *Semin Reprod Med* **27**, 351-357 (2009).
230. S. L. Berger, T. Kouzarides, R. Shiekhattar, A. Shilatifard, An operational definition of epigenetics. *Genes Dev* **23**, 781-783 (2009).
231. L. Sun, J. Fang, Epigenetic regulation of epithelial-mesenchymal transition. *Cell Mol Life Sci* **73**, 4493-4515 (2016).
232. K. J. Falkenberg, R. W. Johnstone, Histone deacetylases and their inhibitors in cancer, neurological diseases and immune disorders. *Nature Reviews Drug Discovery* **13**, 673-691 (2014).
233. W. L. Tam, R. A. Weinberg, The epigenetics of epithelial-mesenchymal plasticity in cancer. *Nat Med* **19**, 1438-1449 (2013).
234. Y. Lin, C. Dong, B. P. Zhou, Epigenetic regulation of EMT: the Snail story. *Curr Pharm Des* **20**, 1698-1705 (2014).
235. S. J. Serrano-Gomez, M. Maziveyi, S. K. Alahari, Regulation of epithelial-mesenchymal transition through epigenetic and post-translational modifications. *Mol Cancer* **15**, 18 (2016).
236. G. G. Wang, C. D. Allis, P. Chi, Chromatin remodeling and cancer, Part II: ATP-dependent chromatin remodeling. *Trends Mol Med* **13**, 373-380 (2007).
237. E. Sanchez-Tillo *et al.*, ZEB1 represses E-cadherin and induces an EMT by recruiting the SWI/SNF chromatin-remodeling protein BRG1. *Oncogene* **29**, 3490-3500 (2010).
238. J. Otani *et al.*, Structural basis for recognition of H3K4 methylation status by the DNA methyltransferase 3A ATRX-DNMT3-DNMT3L domain. *EMBO Rep* **10**, 1235-1241 (2009).
239. W. Bechtel *et al.*, Methylation determines fibroblast activation and fibrogenesis in the kidney. *Nat Med* **16**, 544-550 (2010).
240. K. H. Kim *et al.*, Effect of DNA demethylation in experimental encapsulating peritoneal sclerosis. *Ther Apher Dial* **18**, 628-636 (2014).
241. S. Thiagalingam *et al.*, Histone deacetylases: unique players in shaping the epigenetic histone code. *Ann N Y Acad Sci* **983**, 84-100 (2003).
242. Y. Shi *et al.*, Genetic or pharmacologic blockade of enhancer of zeste homolog 2 inhibits the progression of peritoneal fibrosis. *J Pathol* **250**, 79-94 (2020).
243. K. Maeda *et al.*, Inhibition of H3K9 methyltransferase G9a ameliorates methylglyoxal-induced peritoneal fibrosis. *PLoS One* **12**, e0173706 (2017).
244. R. Tamura *et al.*, Inhibition of the H3K4 methyltransferase SET7/9 ameliorates peritoneal fibrosis. *PLoS One* **13**, e0196844 (2018).
245. T. Irifuku *et al.*, Inhibition of H3K9 histone methyltransferase G9a attenuates renal fibrosis and retains klotho expression. *Kidney Int* **89**, 147-157 (2016).
246. K. Sasaki *et al.*, Inhibition of SET Domain-Containing Lysine Methyltransferase 7/9 Ameliorates Renal Fibrosis. *J Am Soc Nephrol* **27**, 203-215 (2016).
247. A. Eberharter, P. B. Becker, Histone acetylation: a switch between repressive and permissive chromatin. Second in review series on chromatin dynamics. *EMBO Rep* **3**, 224-229 (2002).
248. E. Borbone *et al.*, Histone deacetylase inhibitors induce thyroid cancer-specific apoptosis through proteasome-dependent inhibition of TRAIL degradation. *Oncogene* **29**, 105-116 (2010).
249. M. Dokmanovic, C. Clarke, P. A. Marks, Histone deacetylase inhibitors: overview and perspectives. *Mol Cancer Res* **5**, 981-989 (2007).
250. M. Haberland, R. L. Montgomery, E. N. Olson, The many roles of histone deacetylases in development and physiology: implications for disease and therapy. *Nat Rev Genet* **10**, 32-42 (2009).

251. Z. Yang *et al.*, Discovery of 1,2,4-oxadiazole-Containing hydroxamic acid derivatives as histone deacetylase inhibitors potential application in cancer therapy. *Eur J Med Chem* **178**, 116-130 (2019).
252. M. Pang *et al.*, Inhibition of histone deacetylase activity attenuates renal fibroblast activation and interstitial fibrosis in obstructive nephropathy. *Am J Physiol Renal Physiol* **297**, F996-F1005 (2009).
253. S. Yoon, G. Kang, G. H. Eom, HDAC Inhibitors: Therapeutic Potential in Fibrosis-Associated Human Diseases. *Int J Mol Sci* **20**, (2019).
254. N. Majdzadeh, B. E. Morrison, S. R. D'Mello, Class IIA HDACs in the regulation of neurodegeneration. *Front Biosci* **13**, 1072-1082 (2008).
255. X. Qiu, X. Xiao, N. Li, Y. Li, Histone deacetylases inhibitors (HDACis) as novel therapeutic application in various clinical diseases. *Prog Neuropsychopharmacol Biol Psychiatry* **72**, 60-72 (2017).
256. N. Khan *et al.*, Determination of the class and isoform selectivity of small-molecule histone deacetylase inhibitors. *Biochem J* **409**, 581-589 (2008).
257. T. Tatamiya, A. Saito, T. Sugawara, O. Nakanishi, Isozyme-selective activity of the HDAC inhibitor MS-275. *Cancer Research* **64**, 567-567 (2004).
258. M. Naldi *et al.*, Histone post-translational modifications by HPLC-ESI-MS after HT29 cell treatment with histone deacetylase inhibitors. *Proteomics* **9**, 5437-5445 (2009).
259. A. Saito *et al.*, A synthetic inhibitor of histone deacetylase, MS-27-275, with marked in vivo antitumor activity against human tumors. *Proc Natl Acad Sci U S A* **96**, 4592-4597 (1999).
260. P. Shah, Y. Gau, G. Sabnis, Histone deacetylase inhibitor entinostat reverses epithelial to mesenchymal transition of breast cancer cells by reversing the repression of E-cadherin. *Breast Cancer Res Treat* **143**, 99-111 (2014).
261. R. K. Srivastava, R. Kurzrock, S. Shankar, MS-275 sensitizes TRAIL-resistant breast cancer cells, inhibits angiogenesis and metastasis, and reverses epithelial-mesenchymal transition in vivo. *Mol Cancer Ther* **9**, 3254-3266 (2010).
262. T. Suzuki *et al.*, Synthesis and histone deacetylase inhibitory activity of new benzamide derivatives. *J Med Chem* **42**, 3001-3003 (1999).
263. L. Rossi *et al.*, HDAC1 inhibition by MS-275 in mesothelial cells limits cellular invasion and promotes MMT reversal. *Sci Rep* **8**, 8492 (2018).
264. N. Liu *et al.*, Blocking the class I histone deacetylase ameliorates renal fibrosis and inhibits renal fibroblast activation via modulating TGF-beta and EGFR signaling. *PLoS One* **8**, e54001 (2013).
265. S. Y. Choi *et al.*, Class I HDACs specifically regulate E-cadherin expression in human renal epithelial cells. *J Cell Mol Med* **20**, 2289-2298 (2016).
266. W. Lei *et al.*, Histone deacetylase 1 is required for transforming growth factor-beta1-induced epithelial-mesenchymal transition. *Int J Biochem Cell Biol* **42**, 1489-1497 (2010).
267. K. C. Park *et al.*, A new histone deacetylase inhibitor improves liver fibrosis in BDL rats through suppression of hepatic stellate cells. *Br J Pharmacol* **171**, 4820-4830 (2014).
268. F. Liu *et al.*, Histone-deacetylase inhibition reverses atrial arrhythmia inducibility and fibrosis in cardiac hypertrophy independent of angiotensin. *J Mol Cell Cardiol* **45**, 715-723 (2008).
269. W. Guo, B. Shan, R. C. Klingsberg, X. Qin, J. A. Lasky, Abrogation of TGF-beta1-induced fibroblast-myofibroblast differentiation by histone deacetylase inhibition. *Am J Physiol Lung Cell Mol Physiol* **297**, L864-870 (2009).
270. W. R. Coward, K. Watts, C. A. Feghali-Bostwick, A. Knox, L. Pang, Defective histone acetylation is responsible for the diminished expression of cyclooxygenase 2 in idiopathic pulmonary fibrosis. *Mol Cell Biol* **29**, 4325-4339 (2009).
271. L. Xu *et al.*, Histone deacetylase 6 inhibition counteracts the epithelial-mesenchymal transition of peritoneal mesothelial cells and prevents peritoneal fibrosis. *Oncotarget* **8**, 88730-88750 (2017).
272. K. Io *et al.*, SAHA Suppresses Peritoneal Fibrosis in Mice. *Perit Dial Int* **35**, 246-258 (2015).
273. I. M. Adcock, HDAC inhibitors as anti-inflammatory agents. *Br J Pharmacol* **150**, 829-831 (2007).
274. T. Ichiyama *et al.*, Sodium valproate inhibits production of TNF-alpha and IL-6 and activation of NF-kappaB. *Brain Res* **857**, 246-251 (2000).

275. F. Leoni *et al.*, The antitumor histone deacetylase inhibitor suberoylanilide hydroxamic acid exhibits antiinflammatory properties via suppression of cytokines. *Proc Natl Acad Sci U S A* **99**, 2995-3000 (2002).
276. F. Leoni *et al.*, The histone deacetylase inhibitor ITF2357 reduces production of pro-inflammatory cytokines in vitro and systemic inflammation in vivo. *Mol Med* **11**, 1-15 (2005).
277. Y. Choi *et al.*, Histone deacetylase inhibitor KBH-A42 inhibits cytokine production in RAW 264.7 macrophage cells and in vivo endotoxemia model. *Exp Mol Med* **40**, 574-581 (2008).
278. J. C. Ximenes *et al.*, Valproic acid: an anticonvulsant drug with potent antinociceptive and anti-inflammatory properties. *Naunyn Schmiedebergs Arch Pharmacol* **386**, 575-587 (2013).
279. I. Nusinzon, C. M. Horvath, Interferon-stimulated transcription and innate antiviral immunity require deacetylase activity and histone deacetylase 1. *Proc Natl Acad Sci U S A* **100**, 14742-14747 (2003).
280. V. M. Corman, D. Muth, D. Niemeyer, C. Drosten, Hosts and Sources of Endemic Human Coronaviruses. *Adv Virus Res* **100**, 163-188 (2018).
281. J. Cui, F. Li, Z. L. Shi, Origin and evolution of pathogenic coronaviruses. *Nat Rev Microbiol* **17**, 181-192 (2019).
282. J. T. Wu, K. Leung, G. M. Leung, Nowcasting and forecasting the potential domestic and international spread of the 2019-nCoV outbreak originating in Wuhan, China: a modelling study. *Lancet* **395**, 689-697 (2020).
283. D. S. Hui *et al.*, The continuing 2019-nCoV epidemic threat of novel coronaviruses to global health - The latest 2019 novel coronavirus outbreak in Wuhan, China. *Int J Infect Dis* **91**, 264-266 (2020).
284. B. Hu, H. Guo, P. Zhou, Z. L. Shi, Characteristics of SARS-CoV-2 and COVID-19. *Nat Rev Microbiol* **19**, 141-154 (2021).
285. S. M. Abate, S. Ahmed Ali, B. Mantfardo, B. Basu, Rate of Intensive Care Unit admission and outcomes among patients with coronavirus: A systematic review and Meta-analysis. *PLoS One* **15**, e0235653 (2020).
286. F. Zhou *et al.*, Clinical course and risk factors for mortality of adult inpatients with COVID-19 in Wuhan, China: a retrospective cohort study. *Lancet* **395**, 1054-1062 (2020).
287. L. Mutti *et al.*, Coronavirus Disease (Covid-19): What Are We Learning in a Country With High Mortality Rate? *Front Immunol* **11**, 1208 (2020).
288. D. Ji *et al.*, Prediction for Progression Risk in Patients With COVID-19 Pneumonia: The CALL Score. *Clin Infect Dis* **71**, 1393-1399 (2020).
289. F. M. K. Williams *et al.*, Self-Reported Symptoms of COVID-19, Including Symptoms Most Predictive of SARS-CoV-2 Infection, Are Heritable. *Twin Res Hum Genet* **23**, 316-321 (2020).
290. C. Lucas *et al.*, Longitudinal analyses reveal immunological misfiring in severe COVID-19. *Nature* **584**, 463-469 (2020).
291. Q. Zhang *et al.*, Inborn errors of type I IFN immunity in patients with life-threatening COVID-19. *Science* **370**, (2020).
292. P. Bastard *et al.*, Autoantibodies against type I IFNs in patients with life-threatening COVID-19. *Science* **370**, (2020).
293. M. Hoffmann *et al.*, SARS-CoV-2 Cell Entry Depends on ACE2 and TMPRSS2 and Is Blocked by a Clinically Proven Protease Inhibitor. *Cell* **181**, 271-280 e278 (2020).
294. S. Bindoli, M. Felicetti, P. Sfriso, A. Doria, The amount of cytokine-release defines different shades of Sars-Cov2 infection. *Exp Biol Med (Maywood)* **245**, 970-976 (2020).
295. R. Carsetti *et al.*, Different Innate and Adaptive Immune Responses to SARS-CoV-2 Infection of Asymptomatic, Mild, and Severe Cases. *Front Immunol* **11**, 610300 (2020).
296. R. A. Grant *et al.*, Circuits between infected macrophages and T cells in SARS-CoV-2 pneumonia. *Nature* **590**, 635-641 (2021).
297. A. J. Rodriguez-Morales *et al.*, Clinical, laboratory and imaging features of COVID-19: A systematic review and meta-analysis. *Travel Med Infect Dis* **34**, 101623 (2020).
298. Y. Xie *et al.*, Epidemiologic, clinical, and laboratory findings of the COVID-19 in the current pandemic: systematic review and meta-analysis. *BMC Infect Dis* **20**, 640 (2020).

299. F. Del Sole *et al.*, Features of severe COVID-19: A systematic review and meta-analysis. *Eur J Clin Invest* **50**, e13378 (2020).
300. C. Wu *et al.*, Risk Factors Associated With Acute Respiratory Distress Syndrome and Death in Patients With Coronavirus Disease 2019 Pneumonia in Wuhan, China. *JAMA Intern Med* **180**, 934-943 (2020).
301. H. K. Siddiqi, M. R. Mehra, COVID-19 illness in native and immunosuppressed states: A clinical-therapeutic staging proposal. *J Heart Lung Transplant* **39**, 405-407 (2020).
302. P. Shankar *et al.*, Organ Involvement in COVID-19: A Molecular Investigation of Autopsied Patients. *Microorganisms* **10**, (2022).
303. Z. Wu, J. M. McGoogan, Characteristics of and Important Lessons From the Coronavirus Disease 2019 (COVID-19) Outbreak in China: Summary of a Report of 72 314 Cases From the Chinese Center for Disease Control and Prevention. *JAMA* **323**, 1239-1242 (2020).
304. H. Yue *et al.*, Clinical characteristics of coronavirus disease 2019 in Gansu province, China. *Ann Palliat Med* **9**, 1404-1412 (2020).
305. M. Arentz *et al.*, Characteristics and Outcomes of 21 Critically Ill Patients With COVID-19 in Washington State. *JAMA* **323**, 1612-1614 (2020).
306. C. Ronco, P. Navalesi, J. L. Vincent, Coronavirus epidemic: preparing for extracorporeal organ support in intensive care. *Lancet Respir Med* **8**, 240-241 (2020).
307. A. Heurich *et al.*, TMPRSS2 and ADAM17 cleave ACE2 differentially and only proteolysis by TMPRSS2 augments entry driven by the severe acute respiratory syndrome coronavirus spike protein. *J Virol* **88**, 1293-1307 (2014).
308. L. Cantuti-Castelvetri *et al.*, Neuropilin-1 facilitates SARS-CoV-2 cell entry and infectivity. *Science* **370**, 856-860 (2020).
309. L. A. Teuwen, V. Geldhof, A. Pasut, P. Carmeliet, COVID-19: the vasculature unleashed. *Nat Rev Immunol* **20**, 389-391 (2020).
310. S. Tian *et al.*, Pulmonary Pathology of Early-Phase 2019 Novel Coronavirus (COVID-19) Pneumonia in Two Patients With Lung Cancer. *J Thorac Oncol* **15**, 700-704 (2020).
311. M. Ackermann *et al.*, Pulmonary Vascular Endothelialitis, Thrombosis, and Angiogenesis in Covid-19. *N Engl J Med* **383**, 120-128 (2020).
312. T. R. F. Smith *et al.*, Immunogenicity of a DNA vaccine candidate for COVID-19. *Nat Commun* **11**, 2601 (2020).
313. F. C. Zhu *et al.*, Safety, tolerability, and immunogenicity of a recombinant adenovirus type-5 vectored COVID-19 vaccine: a dose-escalation, open-label, non-randomised, first-in-human trial. *Lancet* **395**, 1845-1854 (2020).
314. Q. Gao *et al.*, Development of an inactivated vaccine candidate for SARS-CoV-2. *Science* **369**, 77-81 (2020).
315. S. Xia *et al.*, Effect of an Inactivated Vaccine Against SARS-CoV-2 on Safety and Immunogenicity Outcomes: Interim Analysis of 2 Randomized Clinical Trials. *JAMA* **324**, 951-960 (2020).
316. V. Monteil *et al.*, Inhibition of SARS-CoV-2 Infections in Engineered Human Tissues Using Clinical-Grade Soluble Human ACE2. *Cell* **181**, 905-913 e907 (2020).
317. X. Tian *et al.*, Potent binding of 2019 novel coronavirus spike protein by a SARS coronavirus-specific human monoclonal antibody. *Emerg Microbes Infect* **9**, 382-385 (2020).
318. S. Xia *et al.*, Inhibition of SARS-CoV-2 (previously 2019-nCoV) infection by a highly potent pan-coronavirus fusion inhibitor targeting its spike protein that harbors a high capacity to mediate membrane fusion. *Cell Res* **30**, 343-355 (2020).
319. M. Kawase, K. Shirato, L. van der Hoek, F. Taguchi, S. Matsuyama, Simultaneous treatment of human bronchial epithelial cells with serine and cysteine protease inhibitors prevents severe acute respiratory syndrome coronavirus entry. *J Virol* **86**, 6537-6545 (2012).
320. B. N. Williamson *et al.*, Clinical benefit of remdesivir in rhesus macaques infected with SARS-CoV-2. *Nature* **585**, 273-276 (2020).
321. C. Huang *et al.*, Clinical features of patients infected with 2019 novel coronavirus in Wuhan, China. *Lancet* **395**, 497-506 (2020).

322. P. Mehta *et al.*, COVID-19: consider cytokine storm syndromes and immunosuppression. *Lancet* **395**, 1033-1034 (2020).
323. L. J. Stockman, R. Bellamy, P. Garner, SARS: systematic review of treatment effects. *PLoS Med* **3**, e343 (2006).
324. E. Mantlo, N. Bukreyeva, J. Maruyama, S. Paessler, C. Huang, Antiviral activities of type I interferons to SARS-CoV-2 infection. *Antiviral Res* **179**, 104811 (2020).
325. Y. Wang *et al.*, Peritoneal M2 macrophage-derived extracellular vesicles as natural multitarget nanotherapeutics to attenuate cytokine storms after severe infections. *J Control Release* **349**, 118-132 (2022).
326. K. Duan *et al.*, Effectiveness of convalescent plasma therapy in severe COVID-19 patients. *Proc Natl Acad Sci U S A* **117**, 9490-9496 (2020).
327. C. Shen *et al.*, Treatment of 5 Critically Ill Patients With COVID-19 With Convalescent Plasma. *JAMA* **323**, 1582-1589 (2020).
328. C. Wang *et al.*, A human monoclonal antibody blocking SARS-CoV-2 infection. *Nat Commun* **11**, 2251 (2020).
329. Y. Wu *et al.*, A noncompeting pair of human neutralizing antibodies block COVID-19 virus binding to its receptor ACE2. *Science* **368**, 1274-1278 (2020).
330. S. J. Zost *et al.*, Potently neutralizing and protective human antibodies against SARS-CoV-2. *Nature* **584**, 443-449 (2020).
331. R. Shi *et al.*, A human neutralizing antibody targets the receptor-binding site of SARS-CoV-2. *Nature* **584**, 120-124 (2020).
332. P. Gougis *et al.*, Anticancer drugs and COVID-19 antiviral treatments in patients with cancer: What can we safely use? *Eur J Cancer* **136**, 1-3 (2020).
333. C. Ripamonti *et al.*, HDAC Inhibition as Potential Therapeutic Strategy to Restore the Deregulated Immune Response in Severe COVID-19. *Front Immunol* **13**, 841716 (2022).
334. A. Trezza, D. Iovinelli, A. Santucci, F. Prischi, O. Spiga, An integrated drug repurposing strategy for the rapid identification of potential SARS-CoV-2 viral inhibitors. *Sci Rep* **10**, 13866 (2020).
335. S. K. Singh, U. Poddar, R. Mishra, A. Srivastava, S. K. Yachha, Ascitic fluid infection in children with liver disease: time to change empirical antibiotic policy. *Hepatol Int* **14**, 138-144 (2020).
336. M. L. Saiz *et al.*, Epigenetic targeting of the ACE2 and NRP1 viral receptors limits SARS-CoV-2 infectivity. *Clin Epigenetics* **13**, 187 (2021).
337. W. S. Fortson *et al.*, Histone deacetylase inhibitors, valproic acid and trichostatin-A induce apoptosis and affect acetylation status of p53 in ERG-positive prostate cancer cells. *Int J Oncol* **39**, 111-119 (2011).
338. B. Hanley, S. B. Lucas, E. Youd, B. Swift, M. Osborn, Autopsy in suspected COVID-19 cases. *J Clin Pathol* **73**, 239-242 (2020).
339. C. Battistelli *et al.*, The Snail repressor recruits EZH2 to specific genomic sites through the enrollment of the lncRNA HOTAIR in epithelial-to-mesenchymal transition. *Oncogene* **36**, 942-955 (2017).
340. G. Bontempi *et al.*, Restoration of WT1/miR-769-5p axis by HDAC1 inhibition promotes MMT reversal in mesenchymal-like mesothelial cells. *Cell Death Dis* **13**, 965 (2022).
341. F. A. Murphy, A. Schinwald, C. A. Poland, K. Donaldson, The mechanism of pleural inflammation by long carbon nanotubes: interaction of long fibres with macrophages stimulates them to amplify pro-inflammatory responses in mesothelial cells. *Part Fibre Toxicol* **9**, 8 (2012).
342. S. J. Woo, Y. Kim, H. Jung, J. J. Lee, J. Y. Hong, Tuberculous Fibrosis Enhances Tumorigenic Potential via the NOX4-Autophagy Axis. *Cancers (Basel)* **13**, (2021).
343. S. Fujino, A. Yokoyama, N. Kohno, K. Hiwada, Interleukin 6 is an autocrine growth factor for normal human pleural mesothelial cells. *Am J Respir Cell Mol Biol* **14**, 508-515 (1996).
344. L. Falasca *et al.*, Postmortem Findings in Italian Patients With COVID-19: A Descriptive Full Autopsy Study of Cases With and Without Comorbidities. *J Infect Dis* **222**, 1807-1815 (2020).

345. B. Tian *et al.*, NF-kappaB Mediates Mesenchymal Transition, Remodeling, and Pulmonary Fibrosis in Response to Chronic Inflammation by Viral RNA Patterns. *Am J Respir Cell Mol Biol* **56**, 506-520 (2017).
346. L. Shen *et al.*, Class I histone deacetylase inhibitor entinostat suppresses regulatory T cells and enhances immunotherapies in renal and prostate cancer models. *PLoS One* **7**, e30815 (2012).
347. Z. Luo *et al.*, Association between chest CT features and clinical course of Coronavirus Disease 2019. *Respir Med* **168**, 105989 (2020).
348. P. Mo *et al.*, Clinical Characteristics of Refractory Coronavirus Disease 2019 in Wuhan, China. *Clin Infect Dis* **73**, e4208-e4213 (2021).
349. N. Zhan *et al.*, Clinical characteristics of COVID-19 complicated with pleural effusion. *BMC Infect Dis* **21**, 176 (2021).
350. V. Ruiz-Carpio *et al.*, Genomic reprograming analysis of the Mesothelial to Mesenchymal Transition identifies biomarkers in peritoneal dialysis patients. *Sci Rep* **7**, 44941 (2017).
351. S. Namvar *et al.*, Functional molecules in mesothelial-to-mesenchymal transition revealed by transcriptome analyses. *J Pathol* **245**, 491-501 (2018).
352. M. L. Perez-Lozano *et al.*, Functional relevance of the switch of VEGF receptors/co-receptors during peritoneal dialysis-induced mesothelial to mesenchymal transition. *PLoS One* **8**, e60776 (2013).
353. D. M. Del Valle *et al.*, An inflammatory cytokine signature predicts COVID-19 severity and survival. *Nat Med* **26**, 1636-1643 (2020).
354. N. Mangalmurti, C. A. Hunter, Cytokine Storms: Understanding COVID-19. *Immunity* **53**, 19-25 (2020).
355. C. Marie *et al.*, Cytokines and soluble cytokine receptors in pleural effusions from septic and nonseptic patients. *Am J Respir Crit Care Med* **156**, 1515-1522 (1997).
356. H. Han *et al.*, Profiling serum cytokines in COVID-19 patients reveals IL-6 and IL-10 are disease severity predictors. *Emerg Microbes Infect* **9**, 1123-1130 (2020).
357. L. Lu, H. Zhang, D. J. Dauphars, Y. W. He, A Potential Role of Interleukin 10 in COVID-19 Pathogenesis. *Trends Immunol* **42**, 3-5 (2021).
358. V. Sontake *et al.*, Wilms' tumor 1 drives fibroproliferation and myofibroblast transformation in severe fibrotic lung disease. *JCI Insight* **3**, (2018).
359. S. R. Dyavar *et al.*, Role of toll-like receptor 7/8 pathways in regulation of interferon response and inflammatory mediators during SARS-CoV2 infection and potential therapeutic options. *Biomed Pharmacother* **141**, 111794 (2021).
360. S. Feng, D. D. De Carvalho, Clinical advances in targeting epigenetics for cancer therapy. *The FEBS Journal* **289**, 1214-1239 (2022).
361. C. G. K. Ziegler *et al.*, SARS-CoV-2 Receptor ACE2 Is an Interferon-Stimulated Gene in Human Airway Epithelial Cells and Is Detected in Specific Cell Subsets across Tissues. *Cell* **181**, 1016-1035 e1019 (2020).
362. G. Oliveto *et al.*, The non-functional ACE2 isoform, but not the SARS-CoV-2 receptor, is induced as an interferon-stimulated gene, in SARS-CoV-2 infected adults. *Cytokine* **158**, 155997 (2022).
363. H. K. Lee, O. Jung, L. Hennighausen, JAK inhibitors dampen activation of interferon-stimulated transcription of ACE2 isoforms in human airway epithelial cells. *Commun Biol* **4**, 654 (2021).
364. K. El Bairi *et al.*, Repurposing anticancer drugs for the management of COVID-19. *Eur J Cancer* **141**, 40-61 (2020).
365. R. M. Connolly, M. A. Rudek, R. Piekarz, Entinostat: a promising treatment option for patients with advanced breast cancer. *Future Oncol* **13**, 1137-1148 (2017).

Ringraziamenti

Un ringraziamento speciale al mio tutor, il prof. Raffaele Strippoli, per avermi offerto l'opportunità di lavorare nel suo laboratorio facendomi sentire fin da subito parte della squadra. Credo che nella ricerca sia molto importante sentirsi parte di un gruppo dinamico e coinvolgente sia dal punto di vista scientifico che umano per favorire la collaborazione e la cooperazione per lo sviluppo della conoscenza scientifica.

Vorrei, inoltre, ringraziare il prof. Marco Tripodi per la grande opportunità di lavorare nel suo gruppo di ricerca e per il costante stimolo a lavorare per espandere le frontiere della conoscenza.

E che gruppo!

Michela, Giulio: questo percorso di dottorato non sarebbe stato lo stesso senza di voi. Per tutte le giornate in laboratorio e le serate al bar. Per i momenti seri e la follia. Per i momenti di condivisione, quelli di scienza e tutte le risate, che poi quanto so' belle quelle vere in compagnia.

Siete persone preziose, grazie.

A mia madre, Daniela, va il ringraziamento più grande. A lei che mi ha visto cadere, rialzarmi e lottare per inseguire un sogno che piano piano è diventato una meta concreta. A lei che ha creduto in me da sempre, festeggiando con me ogni singolo traguardo.

A mio fratello, Claudio, che mi ha aiutato a capire quanto sia importante concedersi un momento di pausa ogni tanto, perché nella vita non possiamo sempre correre. Ogni tanto bisogna anche andare piano e godersi il viaggio.

Ai miei nonni, a zia Cri e zio Gianni, a Marta e Ale un enorme grazie per esserci stati. Ognuno a suo modo, con ottimi consigli, abbracci, risate o un semplice piatto caldo per poter cenare alla fine di una giornata faticosa. Grazie.

E poi ci sono gli Amici, quelli con la A maiuscola.

A tutte le persone vecchie e a quelle nuove. A tutti quelli che sono entrati nella mia vita e l'hanno resa quella che è oggi: bella, folle e piena. A tutte quelle persone che 'non ti aspetti' e a quelle che sono un riferimento da molto tempo ormai. Per tutte le risate, i pianti, i confronti e le follie fatte insieme. Grazie.